Optimal Process Analyzer Selection and Positioning for Plant-Wide Monitoring

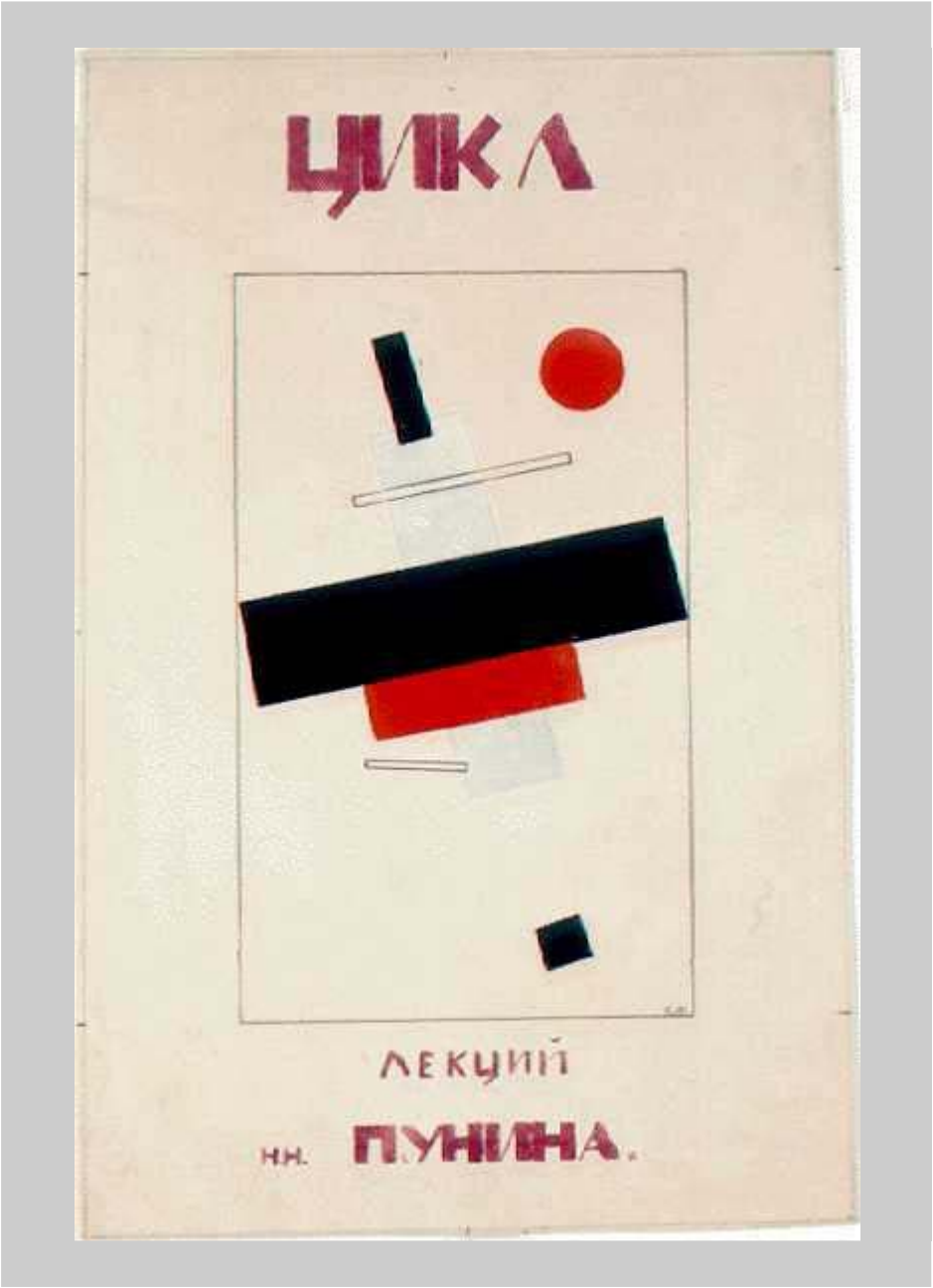

Frans van den Berg

Optimal Process Analyzer Selection and Positioning for Plant-Wide Monitoring

ACADEMISCH PROEFSCHRIFT

ter verkrijgen van de graad van doctor
aan de Universiteit van Amsterdam
op gezag van de Rector Magnificus
prof. dr. J.J.M. Franse
ten overstaan van een door het college voor promoties ingestelde
commissie, in het openbaar te verdedigen in de Aula der Universiteit
op donderdag 11 oktober 2001, te 10.00 uur

door

Franciscus (Frans) Winfried Jozef van den Berg

geboren te Breda

Promotor: prof. dr. A.K. Smilde
Co-promotor: dr. H.C.J. Hoefsloot, UHD

Faculteit der Natuurwetenschappen, Wiskunde en Informatica

Promotiecommissie:
prof. dr. A. Bliek
prof. dr. P.D. Iedema
dr. ir. B.J. Kip
prof. dr. J.F. MacGregor
prof. dr. P.J. Schoenmakers
prof. dr. S. Verduyn Lunel

The work presented in this thesis was conducted at the Department of Chemical Engineering, Process Analysis and Chemometrics, University of Amsterdam, The Netherlands. This work was financially supported by Nederlandse Organisatie voor Wetenschappelijk Onderzoek (NWO), The Netherlands.

Contents

1. Selection and Positioning: Introduction

Theory of Process Analytical Chemistry

1.1 Introduction - How do plant managers make decisions regarding which process analyzers to buy and install for monitoring and controlling their processes? Should it be on-line, at-line or off-line instruments? Slow but accurate process GC's or fast but relatively imprecise NIR spectrometers? Often such decisions are made ad-hoc and based on limited research, because extensive development and long 'try-out' periods are considered as too expensive. However, there exists theory that can guide this decision-making: the Theory of Process Analytical Chemistry.

Process analytical chemistry is a rapidly growing field. For a large part this is due to the activities of the CPAC in Seattle (Washington, USA [1]), but other research groups have also focused their activities on performing process analytical measurements. The field is rapidly coming of age as indicated by special review articles devoted to process analytical chemistry. Moreover, at international analytical chemistry conferences, process analytical chemistry always deserves specialized sessions; there are even international conferences solely devoted to the subject.

A considerable number of process analytical chemistry papers discuss issues like calibration and standardization of process analyzers; building interfaces and equipment for on-line, in-line and in-situ monitoring; or sensor development for performing process analytical measurements. The reported figures of merit in these papers are often limited to precision (e.g. the root-mean squared error of prediction, RMSEP) and analysis time. However, precision and analysis time do not tell the whole story. Is a method that is more robust but also less precise than an alternative method to be preferred? What is an acceptable degree of precision given a certain process? Where in the process should one extract the sample or place the analyzer interface?

All the questions above are very important for the practical use of process analyzers. Answers to these questions can be found if process analytical measurements are formulated in one unifying theoretical framework. In

the chemical engineering literature the problem of optimal sensor location has attracted attention [2], but this work only takes into account some instrument specifications. In this thesis, a framework is presented which accounts for all instrument specifications. This framework is based on the measurability theory developed by Van der Grinten [3], [4]. The measurability theory has been expanded to include the problems mentioned above. In this introduction the theory will be explained using a case study. An in-depth explanation is given in earlier papers [5]-[7].

1.2 Case Study - A simulated case study is used for illustrative purposes. In this case study, the goal is to monitor conversion at the end of a styrene polymerization reactor. This example closely resembles industrial practice, dealing with a highly relevant reaction of sufficient complexity. Hence, it is a good example for illustrating our method. All calculations were validated using real experiments, reported elsewhere [7], [Chap. 4].
The example concerns the free radical polymerization of styrene. A simplified step-wise reaction scheme is given in Box 1.1. The reaction is performed in a tubular reactor (of one-meter length) as shown in Figure 1.1. The figure also shows some details on experimental conditions. The reactor tube is fed with a mixture of styrene monomer and initiator. The initiator concentration in the reactor feed shows small, unknown fluctuations around its nominal value. These fluctuations are considered as process disturbances and their influence on degree of conversion at the end of the reactor - how much styrene monomer has reacted to polystyrene - has to be monitored.

Initialization **I** → 2 **I•** + $\mathbf{N_2}$
Chain initialization **I•** + **M** → **I-M•**
Propagation **I-M•** + **M** → **I-M-M**
Termination **I-M-…-M-I•** + **•M-…-I** → **I-M-…-M-I**

Box 1.1

Four types of process analyzers are available for this monitoring task. Both a Size Exclusion Chromatograph (XSEC) [8] and a Near-Infrared

(NIR) spectrometer can be operated close to the reactor (*at-line*). The alternative is a Short-Wave Near-Infrared (SW-NIR) spectrometer, operated in *on-line* or *in-line* mode.

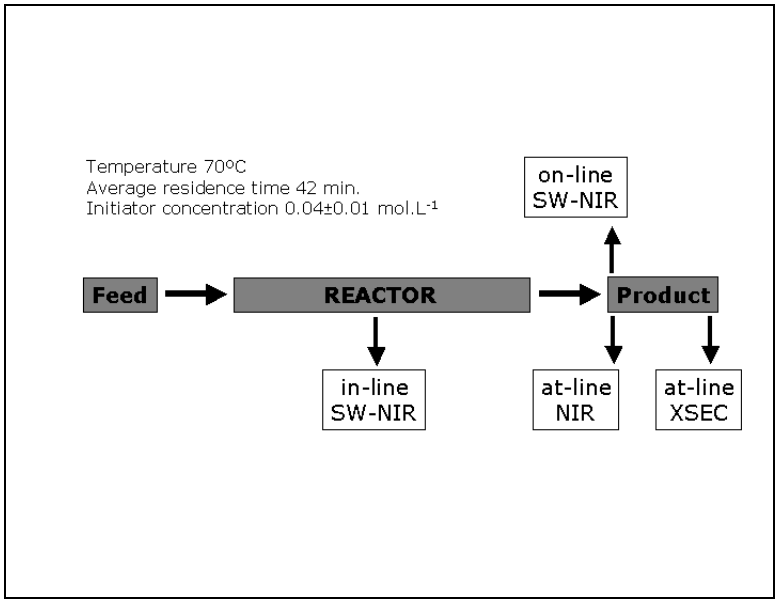

Figure 1.1 Schematic drawing of the styrene polymerization reactor.

1.3 Post-Analysis Signal Reconstruction - The process analyzer measures the conversion (the 'process signal') at the end of the reactor. Due to the limitations of the process analyzer, continuous and perfect knowledge of this process signal is not possible: every analyzer has a limited precision and analysis time. Hence, we always have to do with a 'reconstructed signal': the process signal we can reconstruct using the measurements of our process analyzer.

The central theme of the Theory of Process Analytical Chemistry is signal reconstruction. Suppose that we would have a perfect instrument that would measure the conversion instantaneously without any error. The result is then the gray line in Figure 1.2. This represents the true process variation: the variation of degree of conversion in time that we are interested in.

Unfortunately, we do not have perfect instruments. Our instrument has a limited precision (indicated by a standard deviation σ_i) and we expect our measurements to be spread around the true value, e.g. $\pm 3\sigma_i$. This confidence interval is shown in Figure 1.2a by the gray markers.

We can reconstruct the signal in the best possible way by connecting all these measurements. This 'connection line' is the black line and this is the best reconstruction we can get *post-analysis*, that is, after collecting the last measurement results. If there is no systematic error in the measurements, the value of σ_i is an indication of the error we make in sampling the true signal. Obviously, the poorer the precision of the process analyzer, the greater the error in our reconstructed signal.

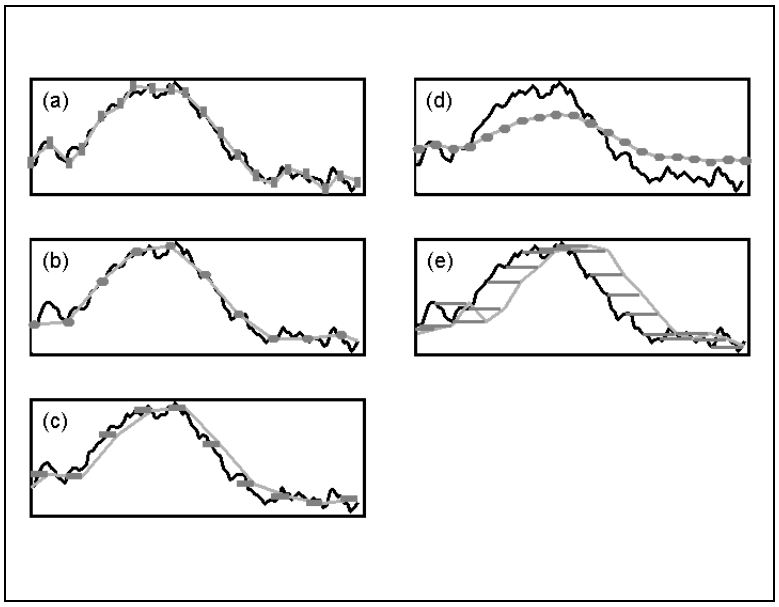

Figure 1.2 The effect of different instrument imperfections on signal reconstruction: a) precision σ_i, b) sampling frequency T_f, c) sampling time T_g, d) response correlation T_i, e) delay time T_d.

There are other contributions to the imperfection of process analyzers. Process measurements can only be performed at a limited frequency expressed as the sampling rate: the time in-between taking successive samples (indicated by T_f). Figure 1.2b shows the consequence of this limited sampling frequency. Likewise, the sampling itself is not instantaneous. It takes some time to collect ('grab') the sample from the process (indicated by T_g) and during this time, process variation is averaged. This is shown in Figure 1.2c. There might also be response correlation. This is carry-over in the detector response from one measurement to another (indicated by T_i, the mean correlation time). The effect of this is shown in Figure 1.2d. Finally, the process analyzer can have a significant analysis time, T_d. This causes a delay in the availability of the result and its effect is illustrated in Figure 1.2e. Of course, *post-*

analysis this delay can be counteracted by shifting the whole reconstructed signal to the left with a shift equal to the analysis time T_d.
In reality, all these imperfections are present to some degree and affect the quality of the reconstructed signal. Moreover, we want to reconstruct the signal *real-time*, while the process runs. Hence, we cannot interpolate and shift the reconstructed signal anymore, because at time *t* the measurement at time $t+T_d$ is not yet available. The optimal process analyzer reconstructs the process signal *real-time* and minimizes the distortion of the true process signal.

1.4 Real-time Signal Reconstruction - The problems of real-time signal reconstruction are visualized in Figure 1.3, where an off-line XSEC is used to measure the conversion. XSEC is an analytical technique based on Size Exclusion Chromatography where conversion (X) of a product is determined from the polymer and monomer peak areas in the exclusion chromatogram. Realistic values for this measurement are $T_i=T_g=0$, $T_d=T_f=20$ minutes with a precision of 0.17% conversion [8].

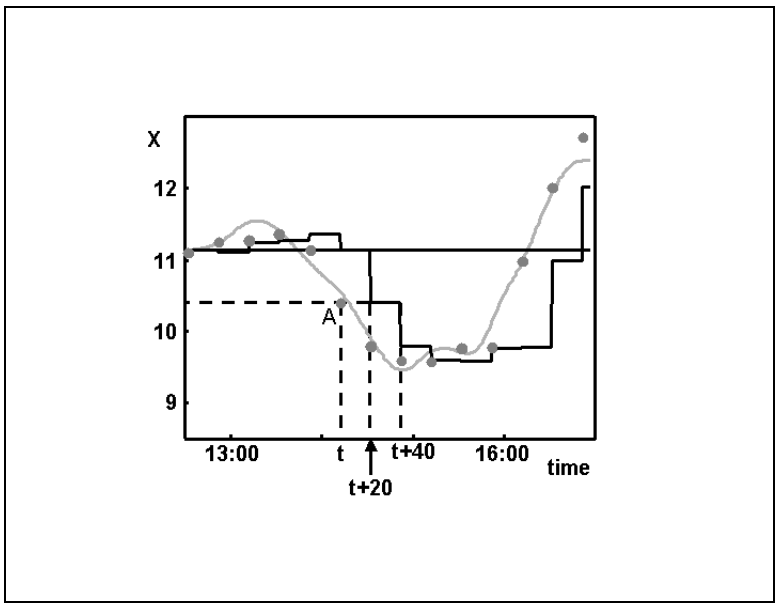

Figure 1.3 Real-time signal reconstructions of the degree of conversion: at-line XSEC.

Suppose that a sample is taken at time *t* minutes. Again, in practice the gray line (real process variation) is not known, but for the sake of argument the line is drawn in the figure. The analysis result of this sample becomes available at time *t*+20 minutes and has the value A, indicated by

a gray dot at time point t. This value A is not exactly the process value at time t because of the limited precision of the XSEC measurement. At time point *t*+20 minutes another sample is taken from which the result becomes available at *t*+40 minutes. The best guess for the process value in-between time points *t*+20 and *t*+40 minutes is the measured value A. This is indicated in the figure by the black bar in-between time points *t*+20 and *t*+40 minutes. In this way a real-time reconstruction of the process values can be obtained and the black line indicates this.
Clearly, the reconstruction of the signal in real-time analysis is poorer than a post-analysis reconstruction. This is the price we pay for monitoring in real-time. To compare the quality of signal reconstructions using different process analyzers, we need to have a measure of such a quality.

1.5 Quality of Signal Reconstruction - We can express the quality of signal reconstruction in a simple number, the measurability. Suppose we know the true process value $x_{\text{true}}(n)$ at time point n (in reality this true value is never known, but conceptually $x_{\text{true}}(n)$ exists). Then the variation in $x_{\text{true}}(n)$ can be expressed as a variance σ^2_{true} around its target value μ, which is the nominal operating point of the process. When the measurements are performed at time points n=1,...,N, this variance σ^2_{true} can be calculated as:

$$\sigma^2_{true} = \frac{1}{N}\sum_{n=1}^{N}\left[x_{true}(n) - \mu\right]^2 \qquad (1.1)$$

where $x_{\text{true}}(n)$ is the true process value (conversion in our example) at time point n. If the reconstructed signal value at a time point n is written as $x_{\text{rec}}(n)$, then the reconstruction error is $x_{\text{true}}(n)$- $x_{\text{rec}}(n)$. The average squared error over time interval N is thus:

$$\sigma^2_{error} = \frac{1}{N}\sum_{n=1}^{N}\left[x_{true}(n) - x_{rec}(n)\right]^2 \qquad (1.2)$$

and we want to minimize this σ^2_{error}. In theoretical studies, integrals are used to calculate σ^2_{error} and σ^2_{true} instead of summations, but the principle remains the same.

It is easier to work with relative errors because σ^2_{error} as such is a meaningless number. Hence, we define *M* as

$$M = \frac{\sigma^2_{true} - \sigma^2_{error}}{\sigma^2_{true}} \qquad (1.3)$$

and this value *M*, called measurability factor, is always smaller than one. A value of one means that σ^2_{error}=0 and we are perfectly able to monitor the process signal. This will never happen in practice. A low value of M means that σ^2_{error} is relatively high and the measurements do not add much to the knowledge of the variation in the process variable. A value in-between 0.5 and 1 is considered acceptable [3].

1.6 Measurability of Conversion in the Example - Now we can apply the simple concept of measurability to determine objectively the performance of different process analyzers. In all cases the process analyzers are used to measure conversion in our polymerization example. The at-line XSEC, at-line NIR and on-line SW-NIR perform measurements at the outlet of the reactor, whereas the in-line SW-NIR performs its measurements somewhere along the reactor tube. The specifications and measurability factors of the different process analyzers are given in Table 1.1.

	$T_f=T_d$	σ_i	M
At-line XSEC*)	20 min	0.17%	M_{XSEC} = 0.44
At-line NIR	10 min	0.45%	M_{NIR} = 0.72
On-line SW-NIR	30 sec	0.63%	$M_{O\text{-}SWN}$ = 0.95
In-line SW-NIR	30 sec	0.63%	$M_{I\text{-}SWN}$ = 0.98

Table 1.1

*) All process analyzers are assumed to work with $T_i=T_g=0$ and $T_f=T_d$ for simplicity.

From an instrumental performance point of view the four process analyzers in our example differ only in analysis time T_d and precision σ_i. The XSEC - despite its high precision - is clearly to slow to monitor the degree of conversion of the present reaction in real-time (samples indicated by gray markers in Figure 1.3). The result is a poor signal reconstruction (black line). The measurability factor (M_{XSEC} = 0.44) is too low for practical purposes and the main reason is that the analysis time (T_d) and (thus) the sampling rate (T_g) are too long, causing serious delays in reconstruction.

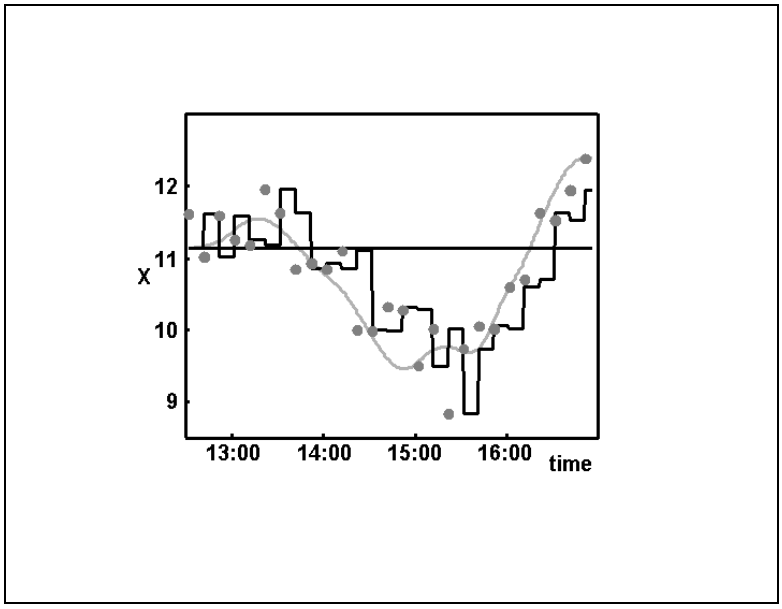

Figure 1.4 Real-time signal reconstructions of the degree of conversion: at-line NIR.

At-line NIR gives a considerable improvement compared to the at-line XSEC. Figure 1.4 shows that the at-line NIR is faster than the at-line XSEC, but the precision of the at-line NIR is worse. This results in a measurability of 0.72 (M_{NIR} = 0.72). The on-line SW-NIR gives a much reduced analysis time without compromising too much on precision ($M_{O\text{-}SWN}$ = 0.95).

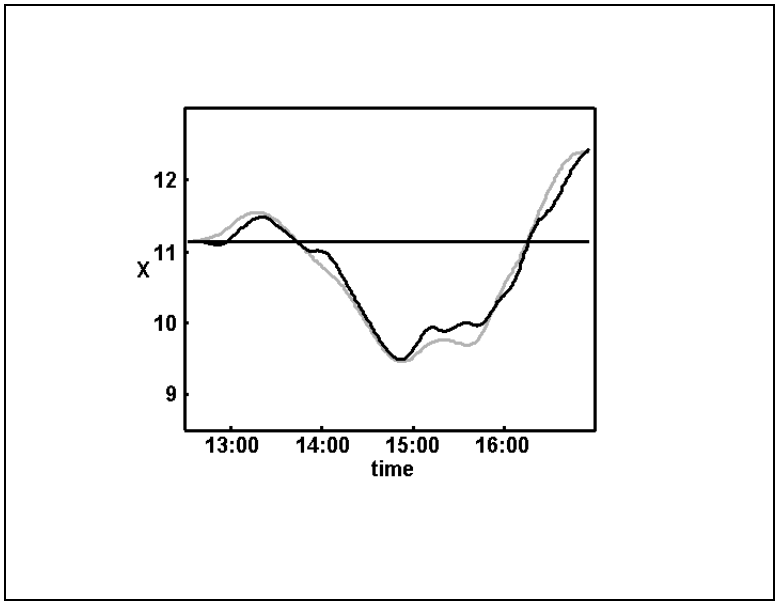

Figure 1.5 Real-time signal reconstructions of the degree of conversion: in-line SW-NIR.

The in-line SW-NIR process analyzer is positioned near the end of the reactor tube, which turns out to be the optimal location. The measurement results of the SW-NIR at this position are used to predict the degree of conversion in the reactor product (Figure 1.5). This prediction is made with the use of a process model. Calculating the optimal location and predicting conversion at the end of the reactor will be explained later. In-line SW-NIR performs slightly better than on-line SW-NIR, although the differences are small ($M_{I\text{-}SWN}$=0.98).
Eq. 1.3 uses the true process variation and reconstructed signal. In practice, we do not know this true process variation and have to calculate the *M* value in a different way.

1.7 Calculating Measurability in the Design Phase - Fortunately, for calculating the measurability index we do not need to know the true process variation nor do we need to perform the actual measurements. All we need to have is a process model and knowledge about the behavior of realistic disturbances. Using this it is possible to calculate *theoretical* measurabilities. This is based an advanced method of error propagation.

Suppose that for a two-step analytical method it is known that step one has a precision of σ_1^2 and step two has a precision of σ_2^2. Then error propagation shows that the total analysis has a precision of $\sigma_1^2 + \sigma_2^2$

assuming that the two steps are independent. This assessment can be made without actually performing the experiments. The only requirements are that i) we have to know the individual contributions (σ_1^2 and σ_2^2) and ii) we have to know a model ($\sigma_{tot}^2 = \sigma_1^2 + \sigma_2^2$). Theoretical measurabilities are calculated by error propagation using a process model.

The process model is based on the reaction mechanism shown in Box 1.1. The kinetics of these reactions are known and, hence, the whole polymerization process can be summarized as mass balances in the form of differential equations related to these reactions.

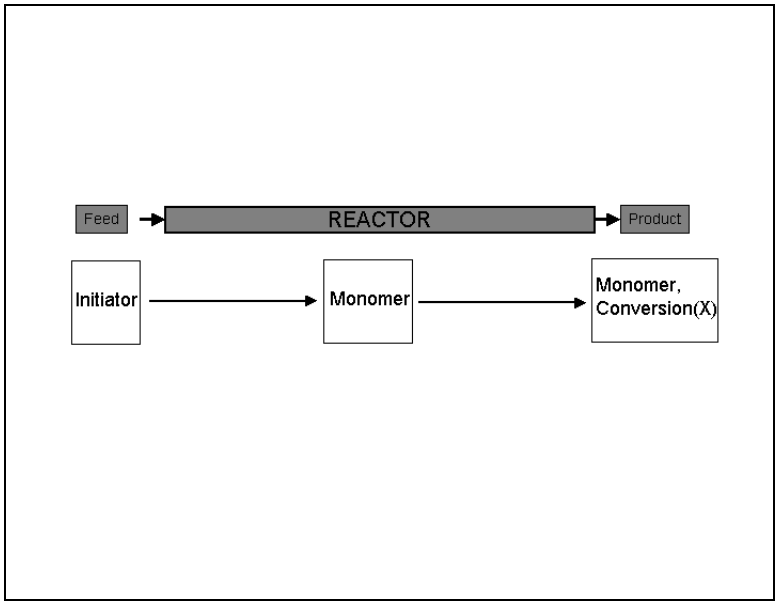

Figure 1.6 Illustration of the way that fluctuations in initiator (feed) cause variation in monomer concentrations and degree of conversion.

We want to monitor conversion at the outlet of the reactor. The disturbance in our example is uncertainty in the initiator concentration in the reactor feed. This external process uncertainty can be represented with variance σ_{AIBN}^2. We can propagate the variance of the initiator concentration through the reactor, as shown in Figure 1.6. Fluctuations in initiator concentration travel through the reactor as fluctuations in the monomer concentrations (governed by the reaction kinetics) and result in fluctuations in the monomer concentration and, hence, the conversion X at the end of the reactor. Assuming a certain σ_{AIBN}^2, the expected fluctuation of X can be calculated, which results in $\sigma_{X,true}^2$. This $\sigma_{X,true}^2$ is the

variation we can expect to be present at the outlet of the reactor. It is this variation that we want to monitor with our instrument(s).

Similar to the situation for process uncertainty σ^2_{AIBN}, we can compute an expected performance of the process analyzer in measuring the conversion at the outlet by adding equations for the analyzer to the process model. Using appropriate values for the five instrument specifications T_i, T_g, T_f, T_d and σ_i (see Figure 1.2 and Table 1.1), a theoretical performance of the process analyzer can be determined. It is the task of process analytical chemists and instrument vendors to supply realistic values of such specifications (e.g. a $\sigma_i = RMSEP$ of 0.63% for the SW-NIR). Thus, we have i) the individual contributions T_i, T_g, T_f, T_d, σ_i and ii) a model relating these contributions to the error of estimating the conversion. Next, we can perform error propagation to obtain the expected variance $\sigma^2_{X,error}$ of the estimation error of the conversion. The theoretical measurability is now:

$$M_{theor} = \frac{\sigma^2_{X,true} - \sigma^2_{X,error}}{\sigma^2_{X,true}} \qquad (1.4)$$

which is a similar definition as 1.3.

Figure 1.7 shows the theoretical measurability factors of equation 1.4 for in-line SW-NIR at different locations in the reactor tube (σ^2_{AIBN} = 0.1x10^{-3} mol^2.L^{-2}). The theoretical process analyzer characteristics are those for the in-line SW-NIR instrument: $T_i = T_g$, $T_f = T_d$ = 30sec and σ_i= 0.63%.

Performing the in-line SW-NIR measurement close to the reactor entrance would reduce the time needed to observe the process disturbances (because these initiator disturbances enter at the inlet), but the change in monomer concentration due to the disturbance in the initiator concentration is not very strong at the inlet. Performing the SW-NIR measurement at the reactor exit would result in a much larger signal (the disturbance has traveled through the system and the change in monomer concentration is attenuated), but then the disturbance is detected late. From Figure 1.7 we learn that in-line SW-NIR measurements in the first

part of the reactor tube yield insufficient information to predict the conversion. In-line SW-NIR in the second half of the reactor tube is much better suited for estimating the conversion in the reactor product. The best compromise for predicting the conversion at the exit is found close to the exit. For this optimum location, the in-line SW-NIR results of Figure 1.5 were calculated.

The theory as explained above was tested with a real reactor. The results are reported elsewhere in this thesis and show a good agreement between the theoretical and practical measurabilities.

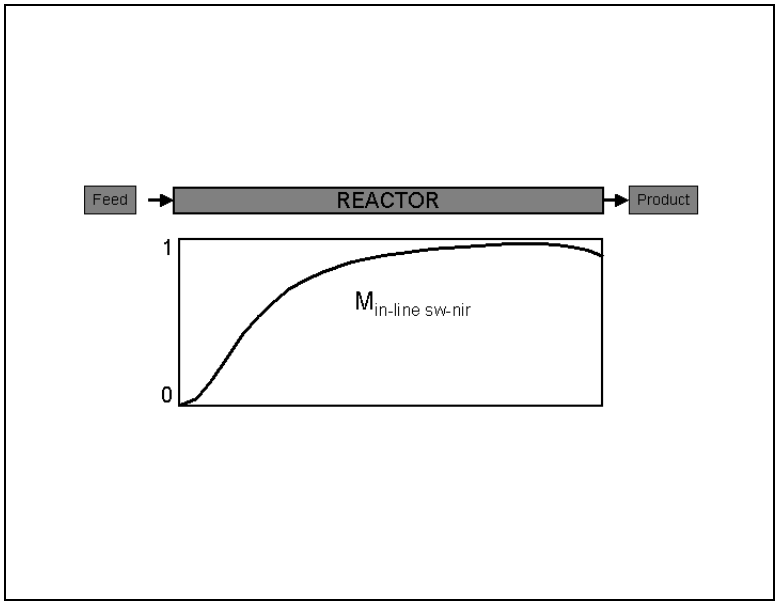

Figure 1.7 The measurability factor for the SW-NIR analyzer as a function of the position along the reactor tube.

1.8 Extensions of the method - The measurability index can be readily extended to include more than one process variable. Suppose that not only the conversion but also the molar mass distribution (e.g. M_n and M_w) of the polymer are important. Polymer chain growth has a direct relation with styrene monomer conversion. By estimating the conversion from process analytical measurements we can also infer the M_n and M_w of the polystyrene product using a process model of our reactor system. Again, error propagation can be used, but now resulting in an uncertainty covariance matrix σ_{error} of size 3x3 for conversion, M_n and M_w. For the external process disturbances, the variation of the three process variables in the product stream is expressed in a covariance matrix Σ_{true}, also of size

3x3. The matrices Σ_{true} and Σ_{error} are natural extensions of σ_z^2 and $\sigma_{z,error}^2$, respectively. The measurability definition 1.4 can thus be generalized to

$$M_{theor} = \frac{tr(\mathbf{\Sigma}_{true}) - tr(\mathbf{\Sigma}_{error})}{tr(\mathbf{\Sigma}_{true})} \qquad (1.5)$$

where tr(.) means the trace of a matrix: the sum of its diagonal elements. This trace of Σ_{true} and Σ_{error} comes down to summing all variances of true and estimated conversion, M_n and M_w, respectively. It is also possible to extent the approach to accommodate several measurements performed simultaneously, e.g., using an in-line SW-NIR along the reactor and a NIR at the end.

The measurability index constructed can be used to calculate the performance of competing process analyzer configurations already in the design phase of a process. Naturally, it can also be used for an existing process. Hence, the answer to the question posed in the beginning: plant managers can make a selection regarding which process analyzers to use by calculating their measurabilities!

1.9 Problems and Future Outlook - In this introduction we have presented a rudimentary overview of the theory of process analytical chemistry. For calculating the measurability index a fundamental model of the process has to be available. If a fundamental model is available, then this model contains estimated constants (e.g. kinetic constants). Such estimates carry some uncertainty and the consequences of this uncertainty on the calculated measurability have to be established.

The theory as presented in this thesis works for continuous processes. An extension of the theory of process analytical chemistry for batch processes is also pursued.

If the fundamental model is incomplete, then experiments can be run and so-called gray models can be built. These are hybrid models containing fundamental and empirical parts. The use of such models for calculating measurability indexes is still under investigation.

1.10 Thesis Summary – This thesis deals with optimal process analyzer selection and positioning for plant-wide monitoring. This part of the text – **chapter 1** – gives a more popular overview, while the remaining parts go into detail on different aspects of the subject. The first choice a *process analytical chemist* (with the help of chemical engineers) has to make is: which of the often-large number of process variables are we going to measure? What constituent, at what position in the system should be sampled to attain the maximum amount of information on the process state in 'real time'? The answer to this question is found in the science of *process dynamics*, the subject of **chapter 2**. In this chapter simulations are used to define a number of *deterministic* selection criteria for optimal sensor selection and positioning. Besides the dynamics of a process, external disturbances and measurement characteristics are important in analyzer selection and positioning. In **chapter 3** simulations are used to define a so-called *stochastic* selection criterion: the *measurability factor*. With this factor different instruments, at different positions, can be compared at a quantitative level. In defining the measurability factor the so-called *process analyzer dynamics* – formulating an abstract definition of sampling and analysis equipment – are introduced based on five criteria: precision, sampling frequency, sampling time, response correlation and delay time.

To verify the theory on process analyzer selection and positioning a lab-scale tubular reactor for bulk polymerization of styrene to polystyrene was constructed. On-line and in-line spectroscopic methods can be compared in the setup. The results of these experiments – presented in **chapter 4** – confirm the link between theory and (laboratory) experiments. The last part of this thesis – **chapter 5** – deals with styrene batch processes. In these systems the question changes: at which point on the batch trajectory should we perform a measurement to get the best estimate of the process state. In this chapter it is shown how the measurability factor can be used to answer this question. The chapter also gives some practical implications on the use of state observers for batch processes, using data from lab-scale experiments.

2. Selection and Positioning: Deterministic Grounds

Selection of Optimal Sensor Position in a Tubular Reactor using Robust Degree of Observability Criteria

Abstract – Robust selection criteria for the optimal location for in-process concentration or temperature sensors along the length of a tubular reactor for the partial oxidation of benzene to maleic anhydride are developed. A model of the reactor is constructed by rewriting the Pde's describing the mass and heat balances into a set of Ode's through the method of lines on a grid defined over the reactor length. The linearized model is described as a continuous, time invariant state-space model where the state is formed by temperature and concentration profiles on the grid-points. The best sensor location for the reactor is found by specifying scalar measures on the observability Gramian integral from the linear least squares state estimation problem. New robust criteria for a degree of observability are specified. The scores on these criteria are determined by the amount of signal received by a sensor for a specific system configuration. These new selection criteria are compared with known measures for degree of observability for the optimal sensor location problem from the literature.

2.1 Introduction - The implementation and operation of in-process measurements – either compositional/analytical or physical in nature – can be quite expensive. The cost of purchasing and maintenance often form an obstacle for the number of sensors that can be implemented for monitoring and/or control purposes. These costs naturally lead to the following question: what is the best location to place the limited number of sensors available (typically one) in a process? Stated differently, what type of sensor on what position delivers the information best suited to monitor the system under observation?

In this chapter we investigate the optimal sensor position for the purpose of state estimation of a unit operation. As an example we will use a computer simulation model of a fixed bed tubular reactor for the catalytic partial oxidation of benzene to produce maleic anhydride. The state of this system is formed by the concentration and temperature profiles over the reactor tube, which has to be determined from measuring one of these variables. We will examine both the position of the sensor along the reactor tube, as well as compare four different types of measurements. The measurements used are two process analyzers (for reactant and product) and two temperature measurements (fluid and solid phase). The present study will be limited to the hypothetical case of continuous, error free and immediate response signal transducers. Selection of the best configuration of in-process sensors with the purpose of monitoring a process by estimating the state of the system is done by defining a degree of observability.

State observability is an established definition for systems represented in the well-known state-space notation. The state of a dynamic system at any time may be (loosely) defined as the collection of information which is both necessary and sufficient to determine the future behavior of the system, assuming that all future inputs are also known. The state-space consists of all those values, which the state may take on [9]. Observability defines whether the state can be observed given a certain output. In this work the outputs are the sensor responses acquired through measurements.

The systems theoretical definition of observability is binary in nature: a system is either state observable or state unobservable. A consequence of

this definition is that unobservability is a 'singular' condition, in the sense that if a system is unobservable, any small perturbation of the systems elements might cause it to become observable. As a consequence, most simulation models with physical constants are completely observable [9]. This makes the yes/no definition impracticable when comparing different system configurations. If we want to study e.g. different sensor locations in one unit operation we need a degree of observability for comparison.

Many authors have looked for possible expressions for a degree of state observability and its dual, the state controllability (see e.g. [10]-[15]). All these criteria are scalar functions of the observability Gramian integral (the unscaled Fisher information matrix), or the observability matrix in case of a discrete time system. The interpretation of these criteria for state controllability is straightforward. The energy required by the control action for disturbance reduction must be minimized, and the degree of controllability criterion should show a minimum for the configuration that optimizes this performance. For a degree of observability the explanation is less obvious. A possible interpretation is that the best sensor position is the one that gives maximum signal response on the sensor when changes due to input disturbances in the system – thus the state vector specifying the system – occur. The scalar degree of observability criteria must again indicate the best configuration by some minimum or maximum value.

The most frequently encountered criteria for a degree of observability are those introduced by Müller and Weber [11]. They define measures that are dominated by those elements in the state vector that show only minimal changes for disturbances and thus are difficult to estimate from the measurements. For the tubular reactor in our study this leads to impractical solutions for the optimal sensor location problem. By utilizing the idea of maximal measurement response or maximal 'energy' collected by a particular choice of sensor we will derive alternative measures for degree of observability. With these supplementary criteria we hope to come to so-called 'robust' selection procedures for sensor placement. The central idea for optimal sensor location with these new criteria is to monitor only major changes in the state variables for the system under observation. This concept resembles the theory previously developed by others for complete state versus input-output controllability [16], [17].

The chapter is organized as follows. The next section gives a short description of the tubular reactor simulation model. The third section explains the theoretical meaning of observability as defined in systems theory and introduces the different scalar measures for a degree of observability. In the fourth section we present the result for the optimal sensor location problem for the tubular reactor, and the last section is used to discuss these results.

2.2 Tubular Reactor Model - The theory developed in this chapter is illustrated in combination with a simulation model of a fixed bed tubular reactor for the production of maleic anhydride by partial oxidation of benzene. Most of the information used in this computer model can be found in the papers by Wohlfahrt and Emig [18] and Ramirez and Calderbank [19]. Some essential data not included in these two sources were assessed from general literature.
Three exothermic, irreversible gas phase reactions take place on a solid V_2O_5-MoO_3-P_2O_5 catalyst particles packed in a one-inch diameter tube

$$C_6H_6 + 4\ O_2 \xrightarrow[k_1]{} C_4H_2O_3 + CO + CO_2 + 2\ H_2O \qquad (2.1)$$

$$C_6H_6 + 6\ O_2 \xrightarrow[k_2]{} 3\ CO + 3\ CO_2 + 3\ H_2O \qquad (2.2)$$

$$C_4H_2O_3 + 2\ O_2 \xrightarrow[k_3]{} 2\ CO + 2\ CO_2 + H_2O \qquad (2.3)$$

Reaction (2.1) is the desired path for the formation of maleic anhydride – the product – from benzene. Reactions (2.2) and (2.3) represent the undesired oxidation (burning) of reactant and product, respectively. The feed stream to the reactor is air mixed with approximately 0.009 $mol.s^{-1}$ benzene. Because of the oxygen excess in the feed all reactions are assumed to be pseudo first order for the limiting reactant. The Arrhenius equation for the reaction rates in formula (2.1)-(2.3) is given by equation (2.4). The frequency factors, activation energies and the reaction heat used are shown in Table 2.1.

$$k_i(t,z) = A_i e^{\frac{-E_i}{RT_s(t,z)}} \qquad (2.4)$$

Reaction	A_i (s^{-1})	E_i ($J.mol^{-1}$)	ΔH_i ($J.mol^{-1}$)
(1)	86760	71711.7	-1490×10^3
(2)	37260	71711.7	-2322×10^3
(3)	149.4	36026.3	-832×10^3

Table 2.1

The two mass balances used in the model are molar flow benzene F_B ($mol.s^{-1}$) and molar flow maleic anhydride F_{MA} ($mol.s^{-1}$) in the fluid phase stream. The partial differential equations are given by (2.5) and (2.6). The parameters for these two equations are shown in Table 2.2 (t (s) denotes time; z (m) indicates axial position in the reactor; total length is 3.2 m).

$$\frac{\partial F_B(t,z)}{\partial t} = -v\frac{\partial F_B(t,z)}{\partial z} + D_{eff}\frac{\partial^2 F_B(t,z)}{\partial z^2} - k_1(t,z)F_B(t,z) - k_2(t,z)F_B(t,z) \quad (2.5)$$

$$\frac{\partial F_{MA}(t,z)}{\partial t} = -v\frac{\partial F_{MA}(t,z)}{\partial z} + D_{eff}\frac{\partial^2 F_{MA}(t,z)}{\partial z^2} + k_1(t,z)F_B(t,z) - k_3(t,z)F_{MA}(t,z) \quad (2.6)$$

Two heat balances are included in the simulation, namely the temperature of the fluid phase T_f (K) (the gas flow) and the temperature of the stagnant solid phase catalyst T_s (K). The corresponding (partial) differential equations are shown in (2.7) and (2.8); the parameters are given in Table 2.2.

$$\frac{\partial T_f(t,z)}{\partial t} = -v\frac{\partial T_f(t,z)}{\partial z} + k_{eff}\frac{\partial^2 T_f(t,z)}{\partial z^2} - U_{f-w}(T_f(t,z) - T_w) - U_{s-f}(T_s(t,z) - T_f(t,z)) \quad (2.7)$$

$$\frac{dT_s(t,z)}{dt} = -U_{s-f}(T_s(t,z) - T_f(t,z)) + c_s\Delta H_1 k_1(t,z)F_B(t,z) + c_s\Delta H_2 k_2(t,z)F_B(t,z) + c_s\Delta H_3 k_3(t,z)F_{MA}(t,z) \quad (2.8)$$

Parameter	value (unit)
linear gas velocity v	2.48 ($m.s^{-1}$)
Effective mass diffusion coefficient D_{eff}	$3.17x10^{-3}$ ($m^2.s^{-1}$)
Effective heat diffusion coefficient k_{eff}	$3.17x10^{-2}$ ($m^2.s^{-1}$)
Effective heat transfer coefficient fluid phase-wall temp. U_{f-w}	10.6 (s^{-1})
wall temperature T_w	733 (K)
Effective heat transfer coefficient solid-fluid phase U_{s-f}	84.0 (s^{-1})
solid phase heat balance constant c_s	0.729 ($s.K.J^{-1}$)

Table 2.2

We would like to emphasize that our aim was not to make a detailed study of the reactor setup used in the simulations. Many aspects (for example pressure drop, radial diffusion, etc.) are not included in the model. Their impact on the subject of our study – optimal sensor location – is assumed to be of less importance.

Figure 2.1 shows the steady-state concentration and temperature profiles over the reactor tube for three different benzene feeds. The boundary conditions used in the calculations are $F_B(t,0)$ = [feed] $mol.s^{-1}$, $F_{MA}(t,0)$ = 0 $mol.s^{-1}$ and $T_f(t,0)$ = 733 K. Diffusion effects at the entrance and exit are neglected.

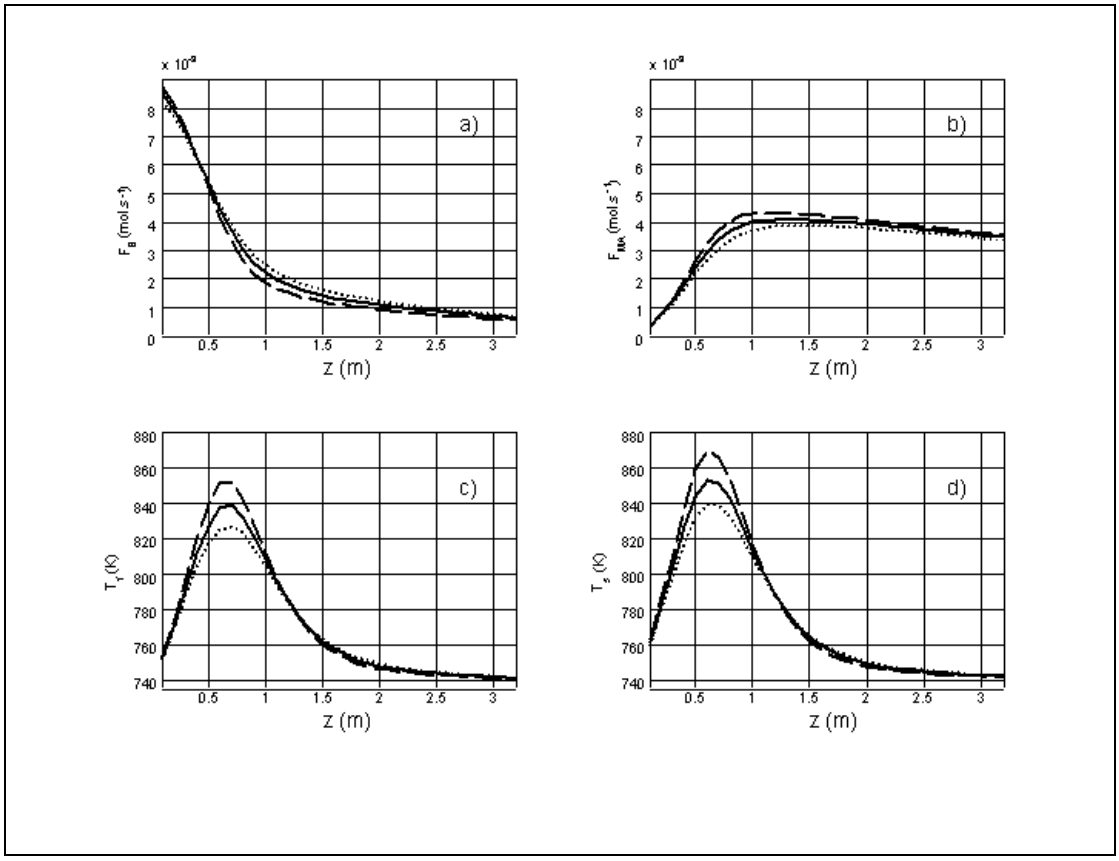

Figure 2.1 a) molar flow benzene b) molar flow maleic anhydride c) fluid phase temperature d) solid phase temperature; benzene feed 0.00900 (-), 0.00873 (..) and 0.00927 mol.s^{-1} (--)

The systems theoretical definitions for observability that are used in the remainder of this chapter require a linear, finite dimensional state-space reactor model. The first step is to divide the reactor length into *m* equidistant segments indicated by z_i (where z_0 is the reactor entrance which is not included in the dynamic simulation model). The distance between two successive grid points is Δz meters. For every grid-point z_i we define four (partial) differential equations from formula (2.5)-(2.8). In the next step the first and second order differential terms in partial the differential equations on every gird-point z_i are approximated by second order upwind and central difference terms according (2.9) and (2.10), respectively (where *f* is F_B, F_{MA} or T_f).

$$\frac{\partial f(t,z_i)}{\partial z_i} = \frac{3f(t,z_i) - 4f(t,z_i) + f(t,z_i)}{2\Delta z} + O(\Delta z^2) \qquad (2.9)$$

$$\frac{\partial^2 f(t,z_i)}{\partial z_i^2} = \frac{f(t,z_i) - 2f(t,z_i) + f(t,z_i)}{\Delta z^2} + O(\Delta z^2) \qquad (2.10)$$

After these modifications the original reactor model is transformed into a set of n = 4 x m ordinary differential equations, two mass and two heat balances on all m grid-point over the reactor length ('Method Of Lines' approximation).

The last step is to linearize all non-linear terms in the reactor model (more precisely, the cross products of the Arrhenius equation and molar fractions in equations (2.5), (2.6) and (2.8)). This is done by a first order Taylor-series approximation.

After these two modifications we have transformed the original reactor model (2.5)-(2.8) into n linear time invariant ordinary differential equations. They can then be reorganized into state-space notation as shown in the next equation (see e.g. [9])

$$\frac{d\mathbf{x}(t)}{dt} = \mathbf{A}\mathbf{x}(t) + \mathbf{B}\mathbf{u}(t) \qquad (2.11a)$$

In this formula state vector **x** (n x 1) contains four variables for all m grid points. The state vector is organized in an alternating fashion **x** = [$F_B(t,z_1)$, $F_{MA}(t,z_1)$, $T_f(t,z_1)$, $T_s(t,z_1)$, $F_B(t,z_2)$, ... , $T_s(t,z_m)$]'. The other components of (2.11a) are the band diagonal system or dynamic coefficients matrix **A** (n x n) with appropriate constants connecting the n linear differential equations for successive grid points, the input coupling coefficients or control matrix **B** (n x p) and the input vector **u** (p x 1). In our reactor model p is one because benzene concentration in the feed stream is the only variable to manipulate. Because we use derivative variables the boundary conditions for equation (2.11a) simplify to $\mathbf{x}(t_0)$ = **0**.

In Figure 2.2 the (complex) eigenvalues of the system matrix **A** are plotted for a grid size of m = 32 (Δz = 0.1 m). These eigenvalues are the poles of the system and the reciprocal values of their real parts are time constants of the natural frequencies of the process. In the plot we see

that all eigenvalues have negative real parts. This means that the system is asymptotically stable.

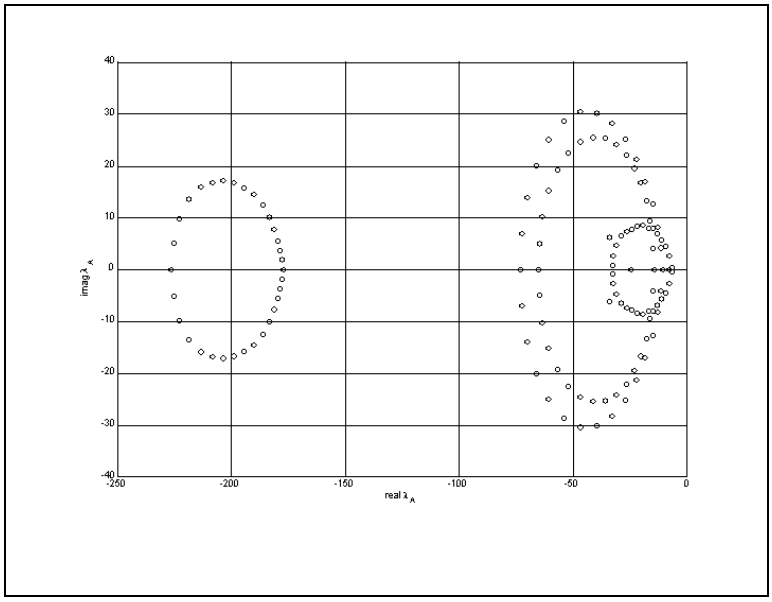

Figure 2.2 eigenvalues system matrix A for grid-size m = 32 (n = 128)

The second conclusion we draw from Figure 2.2 is that four clusters of eigenvalues can be distinguished, corresponding with the four differential equations (2.5)-(2.8) of the original reactor model. Although there is a strong connection between these four equations and the four clusters there is no simple one-on-one relation because of the coupling between the equations. The cluster with the fastest dynamic response (left side of the plot) is closely connected to the solid phase temperature balance. The 'slower system poles' (real part near zero) could suggest neglecting the former. However, all balances are fully connected and fixing one of the balances on a steady-state value would influence the overall dynamic behavior of the simulation model. For complete state estimation we keep all sources of dynamics in the model.

The eigenvalues in Figure 2.2 also warn us that state estimation will be a difficult task. This situation is comparable with the one encountered in many control applications: some small disturbances of the system might be very hard to control. From a systems theoretical point of view a particular configuration might even be state uncontrollable, but by focusing the control action on the dominant effects in the system the overall controller performance can be very efficient [16]. Comparable

reasoning holds for the optimal sensor position problem for the reactor state determination in this study: focusing the selection criteria on the dominating effects instead of the minor phenomena that are hardest to observe leads to different results.

To simulate measurements on the reactor the system in (2.11a) is expanded with a measurement equation

$$\mathbf{y}(t) = \mathbf{C}\mathbf{x}(t) \tag{2.11b}$$

The output or measurement sensitivity matrix **C** (q x n) selects the elements of the state vectors that can be observed, and **y** (q x 1) contains the measurement results. Simulating for instance a fluid phase temperature sensor on the kth grid point along the reactor length can be done by placing an element one on the proper place (in this case position 4 x (k-1) + 3) in a all-zero row vector **C**. Other measurements can be introduced by adding new rows to **C**.
The sensor response $\mathbf{y}(t_1)$ for time t_1 can by found from the solution of the system in equation (2.11)

$$\mathbf{y}(t_1) = \mathbf{C}e^{\mathbf{A}(t_1-t_0)}\mathbf{x}(t_0) + \int_{t_0}^{t_1} \mathbf{C}e^{\mathbf{A}(t-t_0)}\mathbf{B}\mathbf{u}(t)dt \tag{2.12}$$

In this equation $\mathbf{x}(t_0)$ is the known state at time t_0 and $\mathbf{u}(t)$ is the known input signal on the time trajectory $t_0 \le t \le t_1$. On the right hand side of (2.12) we recognize the first term as the natural response of the system and the second term as the input part or forced response.

2.3 Theory - Observability concerns the extent to which the state of a linear system influences the outputs [9]. In this chapter the state vector $\mathbf{x}(t)$ contains the concentration and temperature profiles on the grid-points over the reactor tube, and the output is the signal received from measurements as formulated in equation (2.11). To determine whether a system is state observable on the time trajectory t_0 to t_1 (for any $t_1 > t_0$)

we define the positive (semi) definite observability Gramian $\mathbf{W}_o(t_1,t_0)$ (n x n) in equation (2.13). The role of the observability Gramian matrix in state determination is explained in Appendix 2.A.

$$\mathbf{W}_o(t_1,t_0)=\int_{t_0}^{t_1} e^{\mathbf{A}'(t-t_0)}\mathbf{C}'\mathbf{C}e^{\mathbf{A}(t-t_0)}dt \qquad (2.13)$$

A state $\mathbf{x}(t_0)$ is unobservable if it belongs to the null space of this symmetric observability Gramian. Consequently, (2.11) is completely observable if and only if $\mathbf{W}_o(t_1,t_0)$ is of full rank n (nonsingular). This rank determination is the mathematical solution to the question of (binary) observability: a system is either observable (rank($\mathbf{W}_o(t_1,t_0)$) = n) or unobservable (rank($\mathbf{W}_o(t_1,t_0)$) < n).

Closely related to state observability – determine $\mathbf{x}(t_0)$ from measurements $\mathbf{y}(t)$, $t_0 \le t \le t_1$; estimating a state in the past – is state construction (also known as state reconstruction or determinability) which is the ability to estimate the state vector $\mathbf{x}(t_1)$ based on measurements $\mathbf{y}(t)$, $t_0 \le t \le t_1$ (estimating the present state from past measurements). It can be shown that for linear, continuous time invariant systems state observation and construction are equivalent [16], [20].

An analytical solution for the Gramian matrix in equation (2.13) can be found by solving the corresponding Lyapunov equation (2.14) for the special case of a stable system on the time trajectory $t_0 = 0$ and $t_1 = \infty$ (see e.g. Ogata [21]). Since the definition of observability for continuous systems is valid for any $t_1 > t_0$, we will use equation (2.14) to compute the observability Gramian's in the remainder this study.

$$\mathbf{A}'\mathbf{W}_o(\infty,0)+\mathbf{W}_o(\infty,0)\mathbf{A}+\mathbf{C}'\mathbf{C}\equiv\mathbf{A}'\mathbf{W}_o+\mathbf{W}_o\mathbf{A}+\mathbf{C}'\mathbf{C}=0 \qquad (2.14)$$

From the state observability test by establishing the rank of $\mathbf{W}_o$, as formulated above, there can be no comparison between different configurations, meaning for our study different sensors on different positions. The only distinction possible by the original definition is between systems that are completely state observable and systems that are

unobservable. It is not possible to determine a ranking in the set of observable systems. What is needed is a degree or quality of observability, preferably some scalar function of the observability Gramian.

Many authors have formulated measures to establish the degree of observability based on the matrix $\mathbf{W}_o$. The approach most frequently used is the one formulated by Müller and Weber. They define a series of imbedded means on the symmetric Gramian ($s \leq 0$)

$$m_s = (\Lambda(\mathbf{W}_0)) = \left(\sum_{i=1}^{n} \frac{1}{n} \lambda_i^s \right)^{\frac{1}{s}} \tag{2.15}$$

In this equation $\Lambda(\mathbf{W}_o)$ is a n-dimensional diagonal matrix with the eigenvalues of the observability Gramian as its elements. Higher scores for the criteria formulated in equation (2.15) correspond with better degree of observability for the system under investigation. Three cases of the series in (2.15) are of special interest

$$\mu_1 = \lim_{s \to -\infty} m_s(\mathbf{W}_0) = \lambda_{\min}(\mathbf{W}_o) \tag{2.16}$$

$$\mu_2 = m_{-1}(\mathbf{W}_0) = \frac{n}{trace(\mathbf{W}_o^{-1})} \tag{2.17}$$

$$\mu_3 = \lim_{s \to 0} m_s(\mathbf{W}_0) = \sqrt[n]{\det(\mathbf{W}_0)} \tag{2.18}$$

As stated previously, the series (2.15) are imbedded – meaning $\mu_1 \leq \mu_2 \leq \mu_3$ – for one particular system (one particular sensor position). The interpretation when comparing degrees of observability for different configurations is less obvious. In terms of the observability Gramian the comparison of the costs can be formulated as '$\mathbf{W}_{oA} > \mathbf{W}_{oB}$' when system A is better observable than system B. This matrix inequality is equivalent to n scalar conditions of which (2.16)-(2.18) are possible candidates. There is however no guarantee that all n criteria will select the same optimal sensor position, a situation encountered in e.g. [14]. An example in

Appendix 2.B illustrates the situation where the criteria (2.16)-(2.18) led to contradictory conclusions for the optimal sensor location problem.
Another criterion for degree of observability is proposed by Dochain *et*. *al*. [15]. They use the condition number of the observability Gramian to select the best observable system

$$\gamma(\mathbf{W}_0) = \frac{\sigma_{\max}(\mathbf{W}_o)}{\sigma_{\min}(\mathbf{W}_o)} \tag{2.19}$$

where the σ's are the singular values of a matrix. Smaller condition numbers indicate better observable systems leading to improved state estimations.

All the preceding criteria for degree of observability place strong emphasis on smallest eigenvalues (or singular values) of the Gramian $\mathbf{W}_o$. The reason for selecting these measures is that if a system is near singular, inversion of the Gramian (see Appendix 2.A) or errors introduced by this inversion are dominated by the smallest eigenvalues. This effect is illustrated by the example in Appendix 2.B, where it is shown that using the definitions (2.16)-(2.19) the selection for optimal sensor location is dominated by the smallest eigenvalue of the original system. This corresponds with dynamic phenomena related to those state vector elements that are the most difficult to determine. When monitoring a process we are primarily interested in detecting principal changes in the system (observed by changes in the state vector elements). For the reactor under study this means that we are interested in the significant changes taking place in the hot-spot region z = 0.4-0.7 m (see Figure 2.1) and not in trivial alterations in the last part of the reactor tube. For this purpose we would like to introduce two 'robust' selection criteria for optimal sensor location. They are based on the idea of maximizing the signal received by a sensor for a system disrupted from steady state. We also formulate an alternative interpretation of criterion (2.16) and use this for comparison with the new robust selection criteria.

The first measure is the spectral 'norm' defined as (since Gramian's are by definition symmetric positive (semi) definite, eigenvalues and singular values are equivalent)

$$\rho(\mathbf{W}_0) = \sigma_{\max}(\mathbf{W}_o) \tag{2.20}$$

The set of eigenvalues of $\mathbf{W}_o$ are called the spectrum of the matrix, and the largest one the spectral radius. It is not a norm for general matrices because the triangular inequality does not generally hold. However, for the special case of symmetric positive definite matrices the spectral radius is a matrix norm (the induced 2-norm; see e.g. [17]). It can be interpreted as an indicator of the geometric size of a matrix. Taking into consideration the position of the observability Gramian in state determination, as explained in Appendix 2.A, this means that larger values for spectral norm (2.20) correspond with a better ('larger') $\mathbf{W}_o$.
The second criterion we propose is the trace of the observability Gramian

$$trace(\mathbf{W}_0) = \sum_{i=1}^{n} \sigma_i(\mathbf{W}_o) \tag{2.21}$$

Trace can be interpreted as a (weighted) size criterion of the singular values for the matrix under investigation. A larger value for (2.21) means that a certain configuration of the state-space model (2.11) is better equipped for state estimation. Maximization of equation (2.21) bears close resemblance to the A-optimality criterion in experimental design theory [22].
The third criterion – near singularity (2.22) – is a alternative interpretation of equation (2.16). It is used to illustrate the difference between the robust sensor selection measures presented above and the criteria proposed in literature.

$$NS(\mathbf{W}_0) = \sigma_{\min}(\mathbf{W}_o) \tag{2.22}$$

Equation (2.A3) in Appendix 2.A tells us that if the observability matrix $\mathbf{W}_o$ is singular the system under investigation is unobservable. However, as mentioned in the introduction most physical systems are always observable. Let us assume that the Gramian $\mathbf{W}_o$ is nonsingular and the sum $\mathbf{W}_o + \mathbf{E}$ is singular. One particular choice of $\mathbf{E}$ that satisfies this assumption is $\mathbf{E} = -\mathbf{u}_{min}\sigma_{min}(\mathbf{W}_o)\mathbf{u}'_{min}$, where $\mathbf{W}_o = \mathbf{U}\Sigma\mathbf{U}'$ is the singular value decomposition of $\mathbf{W}_o$. Thus, the smallest singular value tells us how near a matrix is to being rank deficient [17]. The configuration with the highest value for this near singularity criterion is furthest from being unobservable. The near singularity measure (2.22), as well as the criteria (2.16)-(2.18), are closely related to D- and E-optimal experimental design methods [22].

2.4 Results - In this paragraph the three criteria (2.20)-(2.22) for optimal sensor location are computed for the tubular reactor model described earlier. A state-space model of the form (2.11a) is constructed with a maze size of m = 32 equidistant grid points (Δz = 0.1 m). This results in an intrinsically stable system since all eigenvalues of the **A**-matrix have negative real parts (see Figure 2.2). In this model one sensor on one grid point is selected through equation (2.11b). For this system $\mathbf{W}_o$ from equation (2.14) is computed [23]. From this matrix the different norms (2.20)-(2.22) for optimal sensor location are calculated. This procedure is repeated for every element in the state vector (n times), selecting the corresponding measurements (benzene, maleic anhydride, fluid phase and solid phase temperature) through equation (2.11b). The results are shown in Figure 2.3.

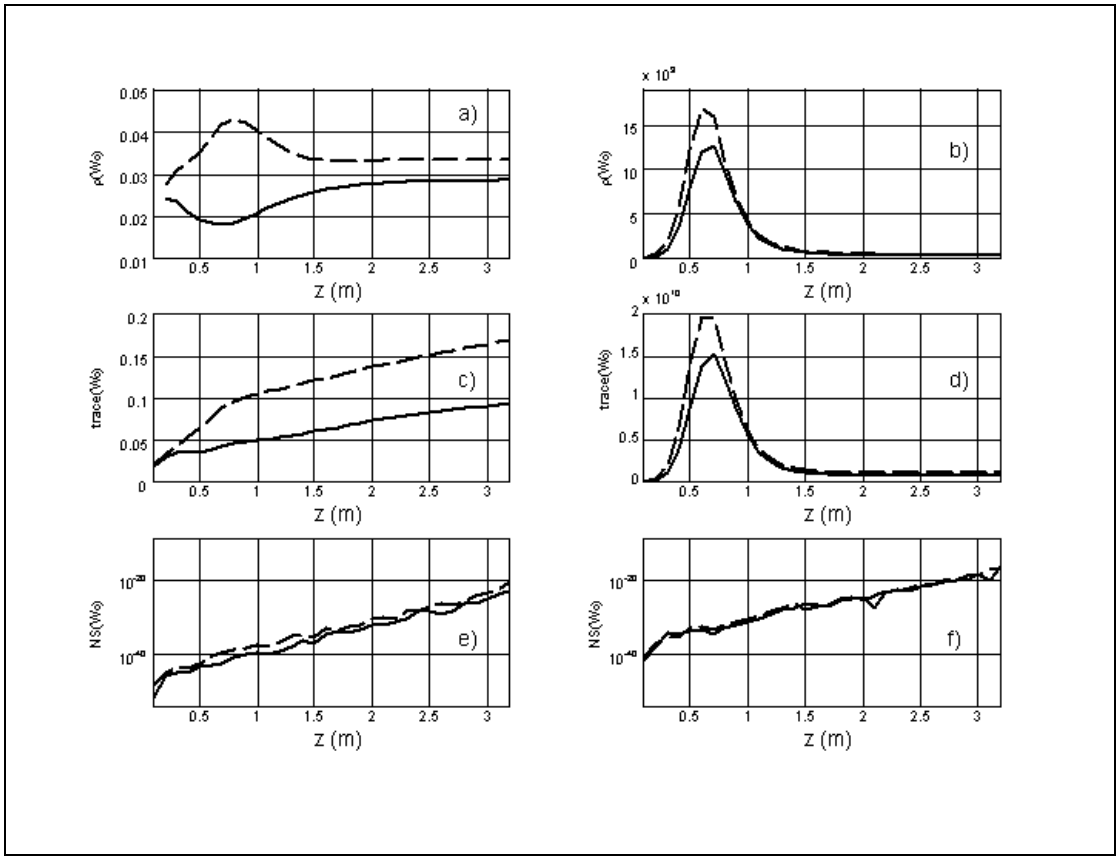

Figure 2.3 a) $\rho(W_o)$, c) trace(W_o) and e) NS(W_o) : benzene (-) and maleic anhydride (--) measurements; b) $\rho(W_o)$, d) trace(W_o) and f) NS(W_o) : fluid (-) and solid (--) temperature sensors

Interpreting the results for spectral radius (2.20) (Figures 2.3a-b) we see that the best sensor position for maleic anhydride concentration (the product of interest), fluid or solid phase temperature is on the hot-spot in the reactor tube (see Figures 2.1c-d). For benzene (the reactant) the optimal sensor position is after the hot-spot. This observation agrees with the 'negative feed-back' as observed in Figure 2.1 and the reaction rate parameters in Table 2.1. The increase (or decrease) of benzene concentration in the feed stream has little or no effect on the benzene concentration profile over the reactor range z = 0.4-0.7 m. These findings are also in good agreement with the results presented by other authors studying the subject of optimal sensor location in tubular reactors [2], [24], [26].

The results also indicate that for the case of continuous error free measurements temperature sensors are preferred over concentration sensors for state estimation. Looking at Figure 2.1 these results also

corresponds with engineering intuition. Small variations in the benzene feed show noticeable effects in the temperature curves in the region z = 0.4-0.9 m.

Using equation (2.21) – the trace of the observability Gramian (Figure 2.3c-d) – as selection criterion the best sensor position for concentration measurements is found down stream at the reactor outlet. For temperature the optimal position is still at the hot-spot of the reactor tube. From the results in Figure 2.3 and the definition for trace in (2.21) we concluded that the spectrum of the Gramian for temperature measurements is dominated by the spectral radius. For concentration measurements trace as optimal sensor position selection criterion forms an intermediate between spectral (2.20) norm and near singularity (2.22) (see below).

For the near singularity criterion (2.22) the results indicate two things (Figure 2.3e-f; notice the logarithmic y-scale; equations (2.17)-(2.19) for degree of observability give similar results). First of all, the size of the smallest singular values tells us that all the observability Gramian's are very close to being singular. The algorithms used in these calculations have great difficulty computing these small numbers. This causes the noisy appearance of the curves, but the overall trend is clear. The second conclusion from these last results is that for measurements placed at the beginning of the reactor the observability Gramian is much closer to being singular than for sensors at the end of the reactor. To interpret this result we have to go back to the original reactor model. Looking at the differential equations (2.5)-(2.8) and the parameters of the simulation model in Table 2.2 we see that the fluid phase travels down stream (from reactor entrance to exit) with a velocity v = 2.48 m.s^{-1}. The only possible method of transporting information upstream (from exit to entrance) is by the small mass and thermal diffusion coefficients opposing the down stream flow. If we look again at Figure 2.1c-d, we observe that the last part of the temperature profiles (beyond z = 2 m) hardly change when manipulating the benzene feed. If complete state observability is required from for instance a maleic anhydride measurement on the first grid point

it is very hard to detect minuscule changes in the reactor temperature down stream, and very hard in this context means a near singular observability matrix. This confirms that calculating the degree of observability by near singularity (2.22) – aimed at complete state observability – is dominated by those state vector elements that are the most difficult to estimate, which clearly leads to undesirable solutions for the optimal sensor location problem for our reactor model. The same conclusion holds for the degree of observability criteria (2.16)-(2.19) retrieved from literature.

2. 5 Conclusions - In this chapter we introduce new and robust selection criteria for optimal sensor location for state estimation of a tubular reactor model. The two criteria we propose are scalar measures calculated from the observability Gramian for the system configuration under investigation. The spectral norm (2.20) focuses on maximizing the energy received by the sensor. The trace (2.21) is an average measure of the estimation performance. For comparison we use the near singularity criterion (2.22), a measure indicating how far a system is from being unobservable. This criterion focuses on complete state observability. For the tubular reactor simulation used as an example in this chapter the last criterion was of little use. Its outcome for the optimal sensor location problem is dominated by the minuscule changes in components and temperature profiles in the last part of the reactor tube for disturbances in the benzene feed. The same conclusion holds for measures for degree of observability (2.17)-(2.19) proposed in literature.
When one is interested in monitoring major changes in the state variables through state estimation (e.g. alterations in the temperature profile near the hot-spot to avoid possible damage) the robust spectral norm is a more suitable selection criterion than near singularity (or the criteria proposed in literature) for optimal sensor positioning. This distinction between complete state versus important disturbances for degree observability criteria resembles the differentiation made by e.g. Rosenbrock [16] and Skogestadt and Postlethwaite [17] between (complete) state and input/output controllability.

In this study we assumed the hypothetical case of continuous, error free and immediate sensor responses, while disregarding uncertainty in the process model. Although these are deviations from real in-process measurements, the methods developed in this chapter can serve as early screening tools for the possibilities of in-process measurements implementation, avoiding the necessity of specifying the performance characteristics of real sensors. This aspect distinguishes our approach from other solutions to the optimal sensor location popular in literature [24]-[32]. In these publications the error covariance matrix from a state estimation Kalman filter is minimized by varying the sensor position. Implementing a Kalman filter however, requires knowledge (or at least assumptions) about the measurement dynamics and process uncertainty, which again directly influence the sensor location problem. Research on including sensor performance in the optimal location selection criteria is presented in later chapters of this thesis.

2.A Appendix - In this appendix we illustrate the role of the observability Gramian – also known as the unscaled Fisher information matrix – in state vector determination. In the formal statistical definition the information matrix represents the information obtained from a sample of values from a known probability distribution. It is a scaled version of the Gramian matrix when the measurement errors in $\mathbf{y}(t)$ have a joint Gaussian distribution. The information matrix is a quantitative statistical characterization of the 'information' that is in the data $\mathbf{y}(t)$ used for estimating $\mathbf{x}(t)$. The Gramian primarily serves as a qualitative algebraic characterization of the uniqueness of a solution [32], [33].

Consider the following problem: we want to determine a state vector $\mathbf{x}(t_0)$ from the observations $\mathbf{y}(t)$, $t_0 \le t \le t_1$, through equation (2.A1)

$$\mathbf{y}(t) = \mathbf{C}e^{\mathbf{A}(t-t_0)}\mathbf{x}(t_0) \qquad (2.A1)$$

In (2.A1) we recognize the natural response of a system as given by equation (2.12). If we wish to determine $\mathbf{x}(t_0)$, the solution can be found through the normal equations for (2.A1)

$$e^{\mathbf{A}'(t-t_0)}\mathbf{C}'\mathbf{y}(t) = e^{\mathbf{A}'(t-t_0)}\mathbf{C}'\mathbf{C}e^{\mathbf{A}(t-t_0)}\mathbf{x}(t_0) \qquad (2.A2)$$

Integrating over the entire measured time trajectory $\mathbf{y}(t)$ we find the following solution for $\mathbf{x}(t_0)$

$$\mathbf{x}(t_0) = \left(\int_{t_0}^{t_1} e^{\mathbf{A}'(t-t_0)}\mathbf{C}'\mathbf{C}e^{\mathbf{A}(t-t_0)}dt \right)^{-1} \int_{t_0}^{t_1} e^{\mathbf{A}'(t-t_0)}\mathbf{C}'\mathbf{y}(t)dt = \mathbf{W}_o(t_1,t_0)^{-1} \int_{t_0}^{t_1} e^{\mathbf{A}'(t-t_0)}\mathbf{C}'\mathbf{y}(t)dt \qquad (2.A3)$$

We recognize the term in brackets as the observability Gramian of the system, equation (2.13). From equation (2.A3) we notice that the solution is only possible if the inverse of $\mathbf{W}_o(t_1,t_0)$ exists. This is the same as stating that the Gramian has to be full rank, which immediately leads to the original (binary) definition of observability.

For classical parameter estimation the inverse of the scaled information matrix (scaled by a function of the known distribution of the errors assumed to be present in the sensor responses $\mathbf{y}(t)$) is equal to the estimation covariance matrix of $\mathbf{x}(t_0)$. This covariance or 'estimation error' matrix obviously should be minimized to optimize the estimation procedure. This corresponds to maximizing a scaled observability Gramian. For classical estimation, using a proper experimental design will guarantee an optimal information matrix in the corresponding regression models [22].

The objective of this study is optimal sensor location. The only parameter to investigate is the sensor type and position as specified by the output or measurement matrix **C**. From (2.A3) we concluded that the 'size' or 'norm' of the observability Gramian $\mathbf{W}_o(t_1,t_0)$ be can used to judge the performance of experiments for different configurations.

From a theoretically point of view, by assuming continuous, error free and immediate response measurement we have to assume finite arithmetic

precision. If we would assume infinite precise computations all systems in (2.A3) would give equal outcomes.

2.B Appendix - The system in (2.B1) serves as an example to study the different criteria for degree of observability

$$\dot{\mathbf{x}}(t) = \mathbf{A}\mathbf{x}(t) = \begin{bmatrix} -1 & 1 & 1.5 \\ 1 & -2 & 1 \\ 0 & 1 & -3 \end{bmatrix} \cdot \begin{bmatrix} x_1(t) \\ x_2(t) \\ x_3(t) \end{bmatrix} \qquad \text{(2.B1a)}$$

The eigenvalues **A** are λ_1 = -0.06, λ_2 = -2.56 and λ_3 = -3.38, thus (2.B1) is stable. Three different models are formed from three different measurement vectors

$$y_i(t) = \mathbf{c}_i \mathbf{x}(t) \qquad \text{(2.B1b)}$$

$$\mathbf{c}_1 = \begin{bmatrix} 1 & 0 & 0 \end{bmatrix} \qquad \mathbf{c}_2 = \begin{bmatrix} 0 & 1 & 0 \end{bmatrix} \qquad \mathbf{c}_3 = \begin{bmatrix} 0 & 0 & 1 \end{bmatrix} \qquad \text{(2.B1c)}$$

The squared responses calculated from equation (2.12) for a unit impulse disturbance at t = 0 for these three systems are shown in Figure 2.B1. The maximum signal response ('energy') for these three observable configurations is clearly number one, measuring the first element in the state vector.

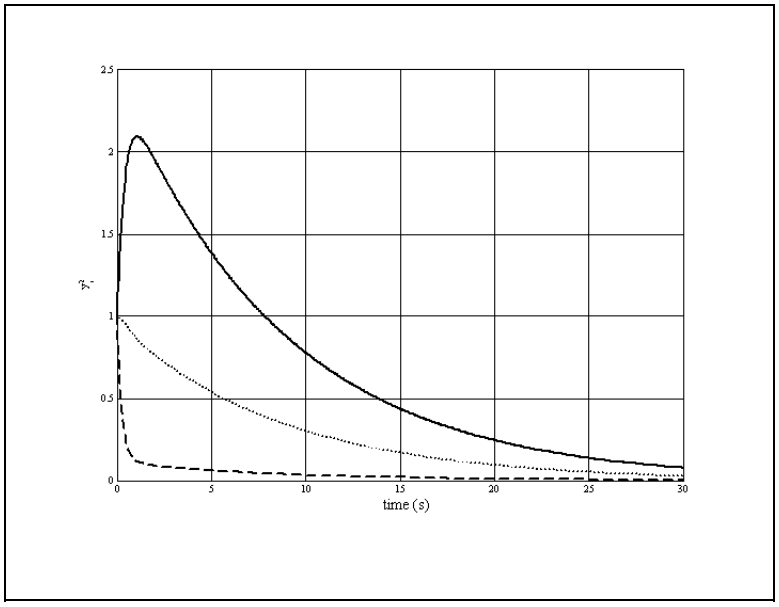

Figure 2.B1 squared impulse response for system (2.B1): y_1 (-), y_2 (..) and y_3 (--)

The Gramian's from equation (2.14) plus the corresponding eigenvalues for these three systems are

$$\mathbf{W}_{o1} = \begin{bmatrix} 3.03 & 2.53 & 2.28 \\ 2.53 & 2.28 & 2.03 \\ 2.28 & 2.03 & 1.82 \end{bmatrix} \qquad \lambda_{\mathbf{W}_{o1}} = \begin{bmatrix} 7.00 \\ 0.12 \\ 8 \cdot 10^{-4} \end{bmatrix} \tag{2.B2a}$$

$$\mathbf{W}_{o2} = \begin{bmatrix} 1.02 & 1.02 & 0.85 \\ 1.02 & 1.19 & 0.86 \\ 0.85 & 0.86 & 0.71 \end{bmatrix} \qquad \lambda_{\mathbf{W}_{o2}} = \begin{bmatrix} 2.82 \\ 0.10 \\ 1 \cdot 10^{-4} \end{bmatrix} \tag{2.B2b}$$

$$\mathbf{W}_{o3} = \begin{bmatrix} 0.11 & 0.11 & 0.10 \\ 0.11 & 0.12 & 0.13 \\ 0.10 & 0.13 & 0.26 \end{bmatrix} \qquad \lambda_{\mathbf{W}_{o3}} = \begin{bmatrix} 0.41 \\ 0.08 \\ 26 \cdot 10^{-4} \end{bmatrix} \tag{2.B2c}$$

The matrices (2.B2) all have positive distinct eigenvalues, thus the observability Gramian's are positive definite. None of the differences between the Gramian's in (2.B2) are however positive definite, e.g. the difference between the first and the third system is

$$\mathbf{W}_{o1} - \mathbf{W}_{o3} = \begin{bmatrix} 2.92 & 2.42 & 2.17 \\ 2.42 & 2.16 & 1.90 \\ 2.17 & 1.90 & 1.55 \end{bmatrix} \qquad \lambda_{\mathbf{W}_{o1}-\mathbf{W}_{o3}} = \begin{bmatrix} 6.63 \\ 0.10 \\ -0.09 \end{bmatrix} \tag{2.B3}$$

The criteria for degree of observability for the three configurations of (2.B1) from equations (2.16)-(2.22) of the theoretical section are shown in Table 2.B1. From these results we observe that for this (synthetic) example there is no clear overall winner. Even for the criteria μ_1-μ_3 proposed by Müller and Weber there is no agreement (despite the imbedding for every individual system). The two robust selection criteria – ρ and trace – indicate measuring state one as the optimal position for state determination.

criterion*)	Equation	W_{o1}	W_{o2}	W_{o3}
μ_1	(16)	0.0008	0.0001	<u>0.0026</u>
μ_2	(17)	0.0024	0.0002	<u>0.0076</u>
μ_3	(18)	<u>0.0871</u>	0.0280	0.0444
γ	(19)	8851	36510	<u>157</u>
ρ	(20)	<u>7.00</u>	2.82	0.41
Trace	(21)	<u>7.12</u>	2.92	0.50
NS (= μ_1)	(22)	0.0008	0.0001	<u>0.0026</u>

Table 2.B1

*) Underlined result is the 'winning' configuration for this particular criterion based on the explanation from the theoretical section.

3. Selection and Positioning: Stochastic Grounds

Process analyzer location and performance assessment for optimal process monitoring in a tubular reactor

Abstract – The influence of process analyzer location and performance on plant-wide process monitoring is investigated. Process analyzer performance is evaluated using five uncertainty contributions to the estimation error: measurement error/uncertainty, analysis frequency, sample size/grab error, analyzer memory effect/response correlation and delay time. Both the choice of location and the performance characteristics of different process analyzers can be evaluated using a measurability factor *M*, ranging from zero to one, where one indicates perfect monitoring capabilities. Due to the unifying nature of the measurability factor, this factor can be used to make a rational decision between very different process analyzers. This allows for finding optimal process analyzer configurations for existing processes or for processes in the design phase. We use a tubular reactor simulation model for the partial oxidation of benzene to maleic anhydride to demonstrate the use of the measurability factor.

3.1 Introduction - An ever-increasing number of process analyzers is implemented in chemical industry. At the same time the diversity in techniques suitable for harsh process conditions – e.g. Chromatography, (Near)Infrared-, Raman- or (low field) nuclear magnetic resonance spectroscopy, mass spectrometry, flow injection analysis, ultrasonic analysis, to name just a few - grows steadily [34]. The implementation and operation of analytical in-process[1] measurements is, however, still relatively expensive. The cost of purchase and maintenance often limits the number of analyzers that can be implemented for monitoring and/or control purposes. This naturally leads to the following three questions: what is the best location to place the limited amount of analytical instruments available, what is the best choice among the wide selection of process analyzers to monitor the process under observation and what is the added value of process analyzers as compared to more conventional, interferential measuring devices like temperature-, pressure-, flow-sensors?

In order to assess the performance of a process analyzer we identify five contributions to characterize the process analyzer, the *analyzer dynamics*. The first contribution is the uncertainty or error encountered in every real world measurement. The second contribution is the analysis frequency of the instrument, which determines the signal reconstruction capabilities. The third contribution is the uncertainty build-up introduced by collection a sample of sufficient size, the so-called grab error. The fourth contribution is memory effect or correlation between successive measurements. This phenomenon is often observed in 'physical' measurements like ion-selective electrodes, pH or conductivity, where responses are correlated over time. The fifth contribution is the delay time: the time passed between taking a sample and retrieving the analysis result. Separation based composition analyzers, e.g. require some time to analyze the sample before the result becomes available. These five contributions are used to characterize a process analyzer; describing the way an in-process measurement observes process variables

[1] The expression 'in-process' is an idiom for all off-line, at-line, on-line, in-line and non-invasive measurement techniques suited for 'real-time' monitoring and/or controlling of a process.

and presents them to e.g. the controllers. Additional instrumental characteristics could be considered, but the five mentioned above form a good representation of most analyzers.

In this chapter we model non-ideal measurements for estimating the entire state of a fixed bed tubular reactor simulation model for the catalytic partial oxidation of benzene to maleic anhydride. The state of this system is formed by the concentration and temperature profiles over the reactor tube. These state elements have to be determined from measuring one of the variables at one particular position. The optimal analyzer type and position are selected by minimizing the theoretical state estimation error in a Kalman filter. Using state estimation error as a criterion for optimization requires knowledge of the uncertainty in both the system and measurements. Many authors discussed the optimal sensor location problem using this same optimization criterion [24]-[32]. These authors however all work with relative simple sensors (typically temperatures), at the most dealing with measurement uncertainty and sample frequency in the optimization.

For process analyzers this is insufficient. The time delay introduced when performing an accurate Gas Chromatographic concentration measurement, e.g. might be competing with a fast but less accurate spectroscopic determination. These measurement - accuracy, sample frequency, delay time, etc. - characteristics must be incorporated to fairly assess the performance of different in-process applications. We do this by incorporating all dynamics (both plant and analyzer) in one system model, creating a so-called *standard plant* [36]. We explicitly model uncertainty caused by stochastic process disturbances and analyzer characteristics, showing their impact on optimal measurement type and location from a set of realizable configurations[2]. An alternative can be found in a deterministic analyzer selection criterion (focusing on the system dynamics, not using the stochastic process uncertainty) of optimal analyzer location based on the idea of *degree of observability* from system theory [5], [Chap. 1].

[2] If we use the word the 'optimal' in this chapter we mean the best choice from the set of all possible process analyzers. The true 'optimal analyzer' would be infinitely fast and infinitely precise which are impossible specifications for practical and real measurements.

In the 1960's P.M.E.M. van der Grinten developed ideas to quantify the performance of measurements and control actions by approximate first order dynamics and uncertainties [3], [37]. A short explanation of the theory developed by van der Grinten is given in Appendix 3.A. He introduced two scalar values called 'meetbaarheidsfactor' (measurability factor) and 'regelbaarheidsfactor' (controllability factor) that quantify how well a signal can be measured and how well a disturbance can be suppressed. The ideas only found limited application outside of the Dutch engineering community, possibly due to the language barrier ([38]; p.445). Only a few sources on this theory in the English language are available [3], [4], [39], [40].

The original theory of van der Grinten focuses on univariate, (simplified) first order descriptions of a process and a measurement and a fixed location. In this chapter we extend the five key ideas on measurement uncertainty and dynamics of van der Grinten to state estimation problems and define a measurability factor *M* for the multivariate case, that is for the whole system. Moreover, we also consider the location of the analyzer in the optimization of the system's measurability.

Process analyzer location and performance assessment as presented in this chapter can be seen as related to other research areas such as sensor failure and data reconciliation (see e.g. [41]). In this chapter we will however not address these important issues. Although an ever-increasing number of in-process analytical measurements is being installed, the implementation cost involved still not allows them to be treated like more regular sensors. In nearly all situations analyzers are used for key-information on process variables, and information 'redundancy' from these measurements is not really an issue yet. This justifies our focus on the specific instrument characteristics for process analyzers selection and positioning.

The remainder of the chapter is organized as follows. In the next section we develop the theory on different sources of analyzer dynamics and show their implementation in the Kalman filter. The third section contains a short description of the reactor simulation model used as an example. In the fourth section we present the result for the optimal process analyzer configuration problem (both instrument characteristics and location) for

the tubular reactor, and the last section is used to formulate conclusion based on the results.

3.2 Theory - *Process model* - In this chapter we model non-ideal measurements of a dynamic process and subsequently estimate the entire state of this system. The position of an analyzer for process monitoring or control in this chapter is shown in Figure 3.1. The process is influenced by a deterministic input (possibly modified by a regulator) and stochastic disturbances. This results in a certain process output. The analyzer measures one of the variables in the process and together with a filter tries to find the best estimate of the present state of the process. The estimated value is then used to adjust the regulator to achieve a desired process output.

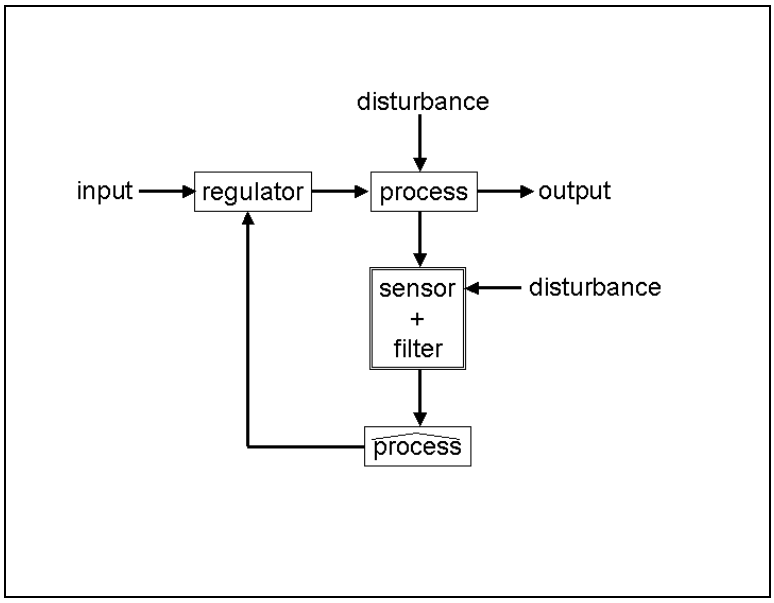

Figure 3.1 The position of the analyzers in process monitoring and control.

The system and measurement dynamics and uncertainties can be captured in the well-known linear, time invariant state space format as follows [32], [33], [42]

$$\dot{\mathbf{x}}(t) = \mathbf{A}_c \mathbf{x}(t) + \mathbf{b}_1 u(t) + \mathbf{b}_2 w(t) \tag{3.1a}$$

$$y(t) = \mathbf{c}' \mathbf{x}(t) + v(t) \tag{3.1b}$$

Where **x**(t) (n x 1) is the state of the system at time *t*, $\mathbf{A_c}$ (n x n) is the continuous time system matrix, $\mathbf{b}_i$ (n x 1) are input distribution vectors, *u*(t) is the deterministic input, and *w*(t) is the stochastic disturbance with distribution *N*(0,*q*(t)), where *q*(t) is the spectral density of *w*(t), *y*(t) is the measurement result, **c** (n x 1) is the output coupling vector, and *v*(t) is the stochastic measurement disturbance with distribution *N*(0,*r*(t)), where *r*(t) is the spectral density of *v*(t). For notational convenience we will only treat the theory for single channel inputs and measurements (SISO), the extension to the multiple inputs/outputs (MIMO) is however straightforward.

The discrete time solution for Eq. 3.1a – under zero order hold assumption for the inputs – is ($t = k.\Delta t$; $t+\Delta t = (k+1).\Delta t$)

$$\mathbf{x}_{k+1} = e^{\mathbf{A}_c \Delta t}\mathbf{x}_k + \int_t^{t+\Delta t} e^{\mathbf{A}_c (t+\Delta t-\tau)} d\tau \mathbf{b}_1 u_k + \int_t^{t+\Delta t} e^{\mathbf{A}_c (t+\Delta t-\tau)} d\tau \mathbf{b}_2 w_k = \mathbf{A}\mathbf{x}_k + \mathbf{B}\mathbf{b}_1 u_k + \mathbf{B}\mathbf{b}_2 w_k \tag{3.2a}$$

where integral **B** (n x n) is implicitly defined and w_k is the variance corresponding to the spectral density *w*(t) [32], [33], [42]. We further assume that measurements y_k are discrete observations (with sampling time Δt) from a system through the following equation

$$y_k = \mathbf{c}'\mathbf{x}_k + v_k \tag{3.2b}$$

where v_k is the stochastic measurement disturbance with distribution $N(0,r_k)$ and discrete time measurement variance r_k.

In this chapter we adopt the concept of the *standard plant* [36]. The idea of this concept is to incorporate all dynamics (both plant and analyzer) in one system matrix $\mathbf{A}_c$ in Eq. 3.1. Augmenting the original plant system matrix with the dynamics representing the behavior of the analyzers creates the *standard plant*. The augmented states transform the true process variable selected for measurement to a new, modified variable

filtered by the process analyzer dynamics. This 'virtual' variable gives the signal retrieved from the analyzer. This procedure has the advantage that all dynamics present in system Eq. 3.1 (plant, measurement and possibly control) are captured in one model, merging all operations in one system matrix $\mathbf{A}_c$.

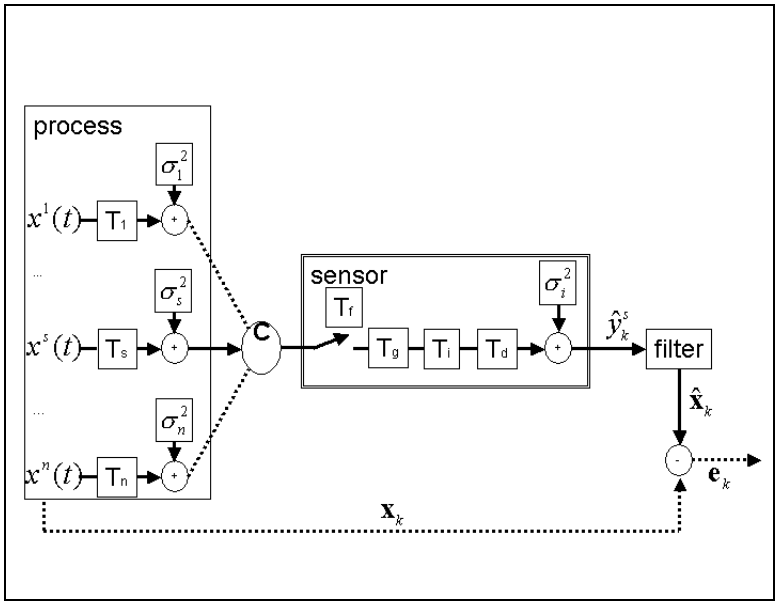

Figure 3.2 Sampling of one process variable in the process. The sample is 'processed' by the analyzer, and the result is used to estimate the entire system state **x**(t) via a filter. The goal of the in-process measurement is to minimize the estimation error **e**(t) over all time *t*.

Process analyzer model - Figure 3.2 zooms in on the process analyzer in a monitoring or control design. One of the state variables in the process is selected for measurement. This variable can e.g. be a concentration of one of the components. The variable under observation is in Figure 3.2 symbolized by element x^s(t) (x-signal or sampled variable) from the state vector **x**(t). The variable x^s(t) possesses certain dynamic behavior (symbolized by T_s) and variance/amplitude (σ_s^2) due to the process disturbances. These dynamics and variances are intrinsic properties of the process. In the remainder of the chapter we focus on the stochastic disturbance input to the process in Eq. 3.1a, assuming that the deterministic input component *u*(t) is completely known.

The analyzer 'processes' the selected process variable and yields an estimated value on discrete time points as measurement outcome y_k. This estimate is then fed to a filter that has two functions: invert the undesired signal processing by the analyzer, and estimate from this signal the

present state $\hat{\mathbf{x}}_k$ of the system under observation. This leads to an estimation error $\mathbf{e}_k = \hat{\mathbf{x}}_k - \mathbf{x}_k$, and the objective is to select the measurement and filter that minimize this estimation error. A small example in Appendix 3.B will help to illustrate the theory developed in this chapter [5].

To find the optimal in-process measurement configuration for estimating the state of a process we take six different aspects into consideration.
The first one is the selection of the process/state variable and location to be sampled. This selection is guided by the amount of information a variable contains on the dynamics of the process under investigation, the availability of a suitable in-process instrument for monitoring in 'real-time' that variable at that location, and the matching of the process dynamics and analyzer dynamics. The variable selection is achieved by defining the appropriate measurement vector **c** in Eq. 3.2b.

The second aspect is measurement uncertainty σ_i^2 (Fig. 3.2), present in all physical and analytical measurements. Uncertainty in the analyzer outcome is approximated by the true quantity $y_k(t) = \mathbf{c}'\mathbf{x}_k$ plus additive white noise v_k with known distribution, typically determined during the calibration procedure or supplied by the instrument vendor

$$\hat{y}_k = y_k + v_k \qquad v_k \sim N(0, \sigma_i^2) \tag{3.3}$$

which is similar in form as the system measurement Eq. 3.2b.

The second source of error is the sampling frequency of the instrument, the error introduced by making discrete observations on the continuous time process with continuous time disturbances. This analyzer characteristic is symbolized by the time interval between successive sample T_f (where the sample frequency is $1/T_f$, Fig. 3.2), and its impact on signal reconstruction is again illustrated in Figure 3.3. We assume equidistant samples where the basis for switching from continuous time in Eq. 3.1 to discrete time in Eq. 3.2 is the period Δt between two successive

measurements. This parameter thus determines the time-period over which stochastic disturbance *w*(t) in Eq. 3.1 is free to alter the system state before a new observation is done. The uncertainty about the state can only be reduced when this new measurement becomes available and a new state estimate is made.

For many instruments (e.g. spectrophotometers) there is a trade-off possible between the sample frequency and the measurement uncertainty in Eq. 3.2. If more time is taken per analysis, thereby increasing the signal-to-noise ratio, the measurement error can be reduced, at the cost of less frequent measurement outcomes.

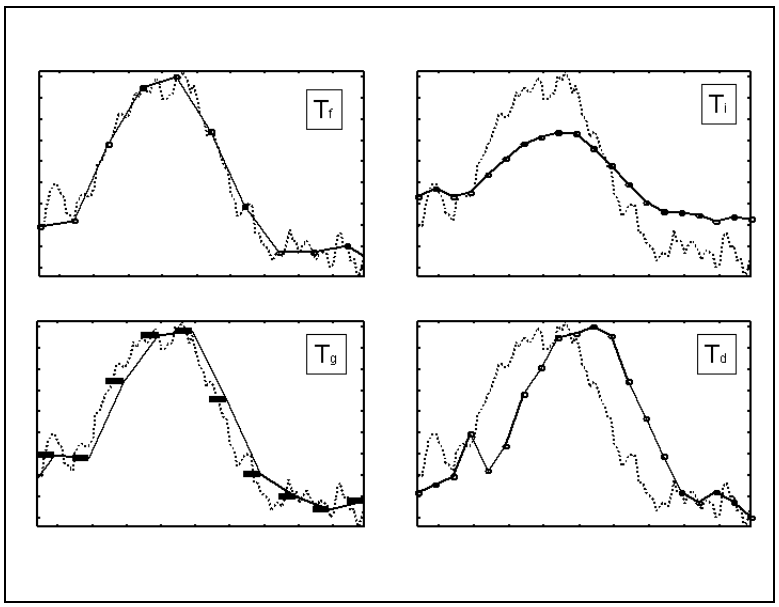

Figure 3.3 The effect of different process analyzer dynamics contributions on the observation of a variable for the outer world: T_f sampling frequency, T_g grab or sample, T_i sensor response correlation and T_d response delay. Markers indicate measurement points, (..) is the true signal and (-) is the sensor response.

The fourth phenomenon is introduced by sample size or grab size. This component to the analyzer dynamics is named T_g (Fig. 3.2). As an example one can think of a spectrophotometer averaging several spectra in a certain period of time to reduce the noise contribution in Eq. 3.2b. The mean spectrum with better signal-to-noise ratio can then e.g. be used to compute a concentration.

The expected value of a measurement taken over a short period of time is the average value over that time period. This expected value becomes available once the entire sample period has passed. Under the assumption that sampling or grab time is short compared to the dominant time

constants of the system we associate the measurement response with the mean time on this sampling time interval. Therefore we penalize the integration or sample time with a time delay of $T_g/2$ seconds. The effect of sample time or grab-size on signal reconstruction is illustrated in Figure 3.3. It is impossible to represent pure delays in the state space time domain notation in Eq. 3.1. A good approximation of pure delay for the problems presented in this chapter turns out to be a third order Padé approximation, shown here in the Laplace domain notation [38]

$$\hat{y}(s) = e^{-\frac{T_g}{2}s} y(s) + v(s) \approx \frac{-s^3 + \frac{24}{T_g}s^2 - \frac{120}{T_g^2}s + \frac{240}{T_g^3}}{s^3 + \frac{24}{T_g}s^2 + \frac{120}{T_g^2}s + \frac{240}{T_g^3}} y(s) + v(s) \qquad (3.4)$$

The concrete implementation of time delay in the state space time domain for the *standard plant* concept is illustrated by the example in Appendix 3.B.

The fifth component in process analyzer performance is the correlation between successive measurements. In many instruments there is significant carry over in the detector/signal response from one measurement to the next (e.g. pH Ion Selective Electrodes or Temperature Dependant Resistors), and this 'memory effect' can be modeled explicitly. In this chapter we assume exponentially first order correlation of the auto regressive form

$$\hat{y}_{k+1} = e^{-1/T_i}\hat{y}_k + \sqrt{1-\left(e^{-1/T_i}\right)^2} v_k \quad v_k \sim N(0, \sigma_i^2) \qquad (3.5)$$

where T_i is the correlation time between successive measurements (Fig. 3.2) and the uncertainty v_k is scaled to have equal magnitude as the uncertainty contribution in Eq. 3.3. The effect of sensor response correlation on signal reconstruction is illustrated in Figure 3.3. As can be seen it is effectively a convolution between the instrument dynamics and

the true underlying variable. The practical implementation is again shown in the example in Appendix 3.B.

The last component describing the performance of an in-process instrument is the delay time between sampling and the release of the result (T_d in Fig. 3.2). A frequently encountered example of an analyzer with a significant time delay is a gas chromatograph for concentration measurements, where the different components in a sample first have to be physically separated before the analysis results can be determined. We again use a Padé approximation - similar to the one for sample size in Eq. 3.4 - to approach pure time delay

$$\hat{y}(s) = e^{-T_d s} y(s) + v(s) \approx \frac{-s^3 + \frac{12}{T_d} s^2 - \frac{60}{T_d^2} s + \frac{120}{T_d^3}}{s^3 + \frac{12}{T_d} s^2 + \frac{60}{T_d^2} s + \frac{120}{T_d^3}} y(s) + v(s) \qquad (3.6)$$

To stress the importance of the dynamics of in-process analyzers Figure 3.4 shows the 'time-profile' of a measurement. Only after a period equal to the delay time T_d plus half the sample period T_g the results become available, while the sample frequency T_f determines how often a measurement outcome is retrieved. Optimal selection of instrument type and location must guarantee that sufficient information is left in the measurements to make a good 'real-time' estimate of the state of the system.

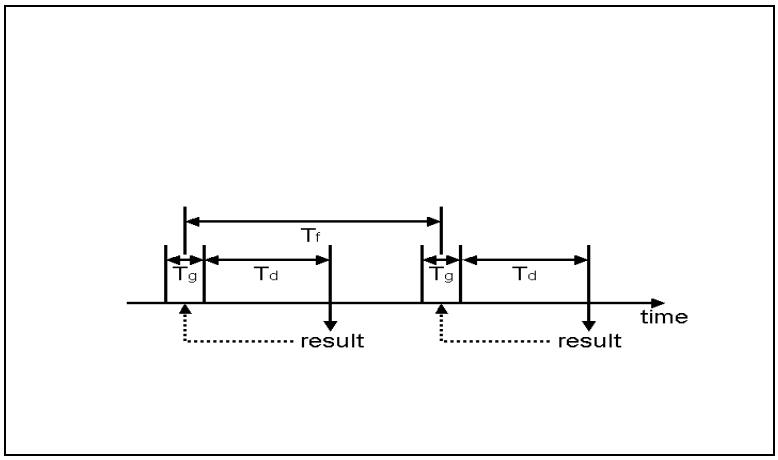

Figure 3.4 Time schedule for an in-process measurement. (↔) indicate the different time spans, (..) designate the time point a measurement result is connected with.

State estimation with a Kalman filter - The filter used for state estimation of the *standard plant* model – as depicted in Figure 3.1 and 3.2 - in this chapter is the well-known Kalman filter [32], [33], [42]. It consists of two parts:

i) the state estimation time update (known as *a priori* estimate $\hat{\mathbf{x}}_k^-$) between two successive measurements *k* and *k*+1, separated ∆t seconds

$$\hat{\mathbf{x}}_{k+1}^- = \mathbf{A}\hat{\mathbf{x}}_k^+ + \mathbf{B}\mathbf{b}_1 u_k \tag{3.7a}$$

$$\mathbf{P}_{k+1}^- = \mathbf{A}\mathbf{P}_k^+\mathbf{A}' + \mathbf{Q}_k \tag{3.7b}$$

ii) the state estimate measurement update/correction (known as *a posteriori* estimate $\hat{\mathbf{x}}_k^+$) using the measurement result at point *k*+1

$$\mathbf{k}_{k+1} = \mathbf{P}_{k+1}^-\mathbf{c}\left(\mathbf{c}'\mathbf{P}_{k+1}^-\mathbf{c} + r_k\right)^{-1} \tag{3.8a}$$

$$\hat{\mathbf{x}}_{k+1}^+ = \hat{\mathbf{x}}_{k+1}^- + \mathbf{k}_{k+1}\left(y_{k+1} - \mathbf{c}'\hat{\mathbf{x}}_{k+1}^-\right) \tag{3.8b}$$

$$\mathbf{P}_{k+1}^+ = (\mathbf{I} - \mathbf{k}_{k+1}\mathbf{c}')\mathbf{P}_{k+1}^- \tag{3.8c}$$

where $\mathbf{k}_{k+1}$ is the Kalman filter gain, $\mathbf{P}_{k+1}{}^+$ is the theoretical *a posteriori* estimation error covariance matrix, and $\mathbf{Q}_k$ is the positive semi-definite uncertainty distribution covariance matrix

$$\mathbf{Q}_k = \int_t^{t+\Delta t} e^{\mathbf{A}_c(t+\Delta t-\tau)}\mathbf{b}_2 q(\tau)\mathbf{b}_2' e^{\mathbf{A}_c'(t+\Delta t-\tau)} d\tau \tag{3.9}$$

The matrix $\mathbf{Q}_k$ represents the contribution of the system disturbance *w*(t) in Eq. 3.1 on the overall state estimation error in Eq. 3.7. Uncertainty *w*(t) - with a spectral density of *q*(t) - is 'injected' in the process with a system matrix $\mathbf{A}_c$. Uncertainty in Eq. 3.2a continuously builds up over the time period *t* to *t*+∆*t*, the time between two discrete measurements in Eq. 3.2b. At these discrete measurement time-points all uncertainty can – for the hypothetical case of perfect measurements - be removed, but not before these points.

The Kalman filter as presented in Equations 3.7 and 3.8 is an unbiased, minimum variance and consistent estimator for the linear (or linearized) system in Eq. 3.1. If the system is observable and controllable, and if $\mathbf{Q}_k$, r_k and $\mathbf{A}$ are bounded, the filter is asymptotically stable, meaning that all the eigenvalues of the matrix $\mathbf{A}$-$\mathbf{k}_k\mathbf{c}'$ fall within the unit circle.

Notice that in the approach taken in this chapter the role of $\mathbf{Q}_k$ - the constant term in the difference equation for the theoretical estimation error $\mathbf{P}_k$ in Eq. 3.7b - is somewhat different than the one encountered in many other studies [2], [24], [26], [28]-[30], [35], [Chap. 4]. Here, we give $\mathbf{Q}_k$ the role of describing the uncertainty propagation in the system for a period Δt between two measurements, since this is of importance for the optimal process analyzer location problem addressed in this research. Known uncertainties for the system parameters in $\mathbf{A}$ can also be accounted for by placing the appropriate values in the system uncertainty covariance matrix $\mathbf{Q}_k$. In many applications this is done by (post-run) analysis, 'tuning' the diagonal elements in $\mathbf{Q}_k$ to create a better fit between some reference values and the Kalman-predictions. In this chapter however we give guidelines for analyzer type and location selection in an early design stage of a process, which obviously excludes the use of post-run information. Known uncertainty in the system parameters can however be included in the system error matrix $\mathbf{Q}_k$ if available.

Instrument selection and location are optimized by minimizing a sensible norm of the expected estimation error $\mathbf{P}_k$ given by the algorithm in Equations 3.7 and 3.8. For linear time invariant systems this theoretical estimation error can be calculated *a priori* by implementing Equations 3.7b, 3.8a and 3.8c. This means that the optimal analyzer type and location can be determined without any form of process simulations.

Measurability factor - From Eq. 3.9 we notice that - for a stable system matrix $\mathbf{A}_c$ - there is an upper bound on the system uncertainty covariance matrix by $\mathbf{Q}_k$ for $\Delta t \rightarrow \infty$ (the covariance matrix of uncertainty propagation through the system). This value for $\mathbf{Q}_k$ corresponds with the maximum uncertainty in knowledge about the state of the process, corresponding to

the situation where no measurements what so ever are performed. When a analyzer/filter-combination is used to do an estimate, some of the uncertainty about the process state will be removed. The remaining uncertainty contribution after a measurement update is represented by the estimation error covariance matrix $\mathbf{P}_k$ in Eq. 3.8c. The performance of a analyzer/filter pair can be judge by the size of this uncertainty residual.
Using this upper bound we can define a performance index for a particular in-process measurement configuration (Appendix 3.A)

$$M^2 = \frac{trace(\mathbf{Q}_k) - trace(\mathbf{P}_k)}{trace(\mathbf{Q}_k)} \tag{3.10}$$

We will call the square root of this quantity the measurability factor. *M* can vary between 0 and 1, where 1 means perfect knowledge about the state of the system after a measurement is taken (all uncertainty has been removed by the measurement and state estimate), while 0 indicates that a particular measurement configuration supplies no information about the state of the process[3]. The best analyzer type and location is taken as the one maximizing the measurability factor *M*. If the system is unstable there is no upper bound on the error covariance matrix.
The criterion to judge the performance of the analyzer/filter combination is the trace of the estimation error covariance matrix $\mathbf{P}_k$ and the system uncertainty $\mathbf{Q}_k$. This norm corresponds to the sum of estimation error variances, thereby giving variances for all variables equal weight.
In this chapter we will estimate all process variables from one measurement, and place equal weight on all errors through the trace criterion in Eq. 3.10. If installing more analyzers is feasible or if appropriate information is available alternative (weighted) selection criteria can be introduced placing heavier penalties on mismatch for certain process variables. There is no problem in introducing these alternative criteria in the proposed procedure of optimal instrument selection and positioning.

[3] For an extremely poor choice of analyzer the trace of $\mathbf{P}_k$ could theoretically exceed the trace of $\mathbf{Q}_k$, giving a negative result for Eq. 3.10 and a negative value for the measurability factor *M*.

3.3 Tubular Reactor Model - The theory on analyzer selection developed in this chapter is illustrated with a simulation model of a fixed bed tubular reactor for the production of maleic anhydride by partial oxidation of benzene [5], [18], [19], [Chap. 2].

Three exothermic, irreversible gas phase reactions take place on a solid V_2O_5-MoO_3-P_2O_5 catalyst particles packed in a one-inch diameter tube

$$C_6H_6 + 4\ O_2 \xrightarrow[k_1]{} C_4H_2O_3 + CO + CO_2 + 2\ H_2O \qquad (3.11a)$$

$$C_6H_6 + 6\ O_2 \xrightarrow[k_2]{} 3\ CO + 3\ CO_2 + 3\ H_2O \qquad (3.11b)$$

$$C_4H_2O_3 + 2\ O_2 \xrightarrow[k_3]{} 2\ CO + 2\ CO_2 + H_2O \qquad (3.11c)$$

Reaction 3.11a is the desired path for the formation of maleic anhydride – the product – from benzene. Reactions 3.11b and 3.11c represent the undesired burning of reactant and product, respectively. The feed stream to the reactor is air mixed with approximately 0.9%(v/v) benzene. Because of the oxygen excess in the feed all reactions are assumed to be pseudo first order in the limiting reactant.

The two mass balances used in the model are molar flow benzene F_B (mol.s^{-1}) and molar flow maleic anhydride F_{MA} (mol.s^{-1}) in the fluid phase stream. The partial differential equations are given by Equations 3.12a and 3.12b (t denotes time; z indicates axial position in the reactor; v is linear gas velocity of 2.48m.s^{-1}; D_{eff} is effective mass diffusion coefficient)

$$\frac{\partial F_B(t,z)}{\partial t} = -v\frac{\partial F_B(t,z)}{\partial z} + D_{eff}\frac{\partial^2 F_B(t,z)}{\partial z^2} - k_1(t,z)F_B(t,z) - k_2(t,z)F_B(t,z) \qquad (3.12a)$$

$$\frac{\partial F_{MA}(t,z)}{\partial t} = -v\frac{\partial F_{MA}(t,z)}{\partial z} + D_{eff}\frac{\partial^2 F_{MA}(t,z)}{\partial z^2} + k_1(t,z)F_B(t,z) - k_3(t,z)F_{MA}(t,z) \qquad (3.12b)$$

Two heat balances are included in the simulation, namely the temperature of the fluid phase T_f (K) and the temperature of the stagnant solid phase catalyst T_s (K). The corresponding (partial) differential equations are shown in Equations 3.12c and 3.12d (k_{eff} is effective heat diffusion

coefficient; $U_{f\text{-}w}$ is the fluid phase-wall heat transfer coefficient; $U_{s\text{-}f}$ is the solid phase-fluid phase heat transfer coefficient; T_w is the reactor wall temperature; $c_s\Delta H_x$ is a reaction enthalpy coefficient)

$$\frac{\partial T_f(t,z)}{\partial t} = -v\frac{\partial T_f(t,z)}{\partial z} + k_{eff}\frac{\partial^2 T_f(t,z)}{\partial z^2} - U_{f-w}(T_f(t,z)-T_w) - U_{s-f}(T_s(t,z)-T_f(t,z)) \tag{3.12c}$$

$$\frac{dT_s(t,z)}{dt} = -U_{s-f}(T_s(t,z)-T_f(t,z)) + c_s\Delta H_1 k_1(t,z)F_B(t,z) + c_s\Delta H_2 k_2(t,z)F_B(t,z) + c_s\Delta H_3 k_3(t,z)F_{MA}(t,z) \tag{3.12d}$$

Figure 3.5 shows the steady-state concentration and temperature profiles over the reactor tube for three different benzene feeds. The boundary conditions used in the calculations are $F_B(t,0)$ = [feed] mol.s^{-1}, $F_{MA}(t,0)$ = 0 mol.s^{-1} and $T_f(t,0)$ = 733 K. Diffusion effects at the entrance and exit are neglected.

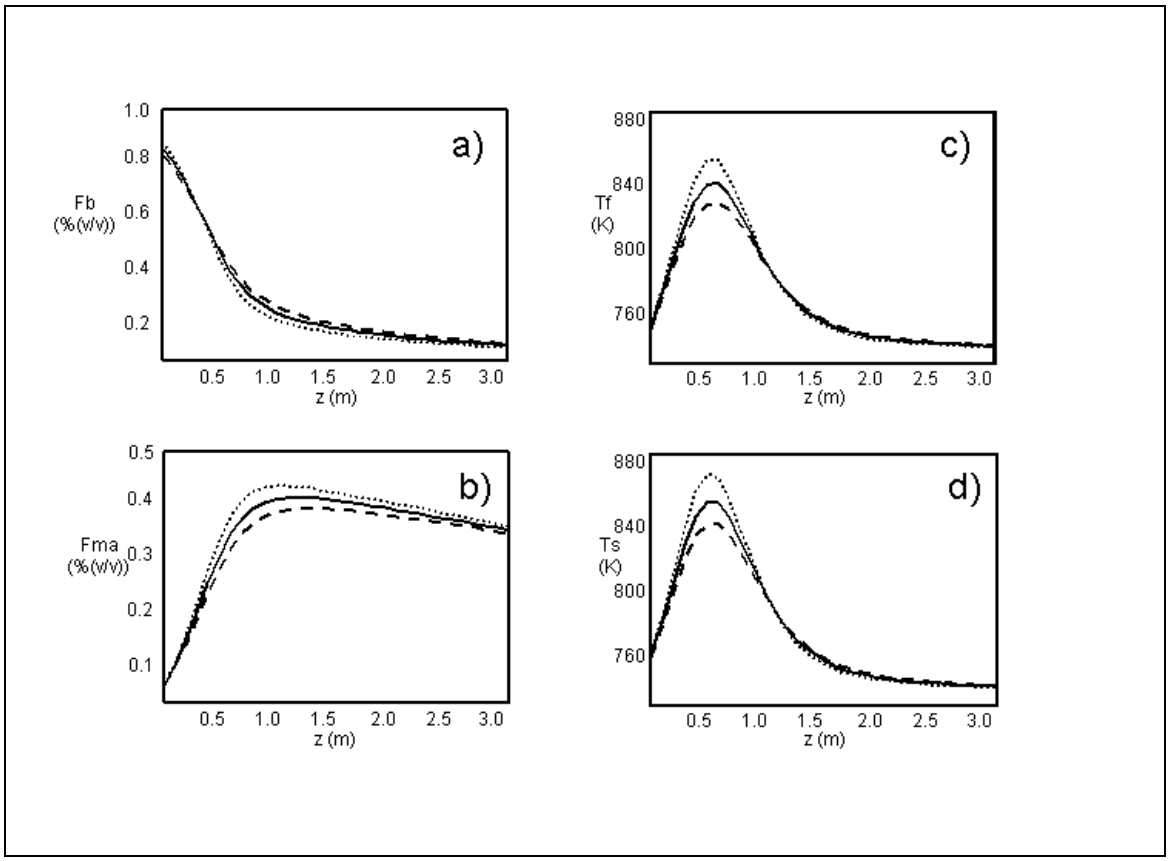

Figure 3.5 a) molar flow benzene b) molar flow maleic anhydride c) fluid phase temperature d) solid phase temperature; benzene feed 0.900 (-), 0.873 (..) and 0.927 %(v/v) (--).

The non-linear partial differential equation system in Eq. 3.12 is rewritten in a linear, finite dimensional state space reactor model [5]. The first step is to divide the reactor length into m equidistant segments indicated by z_i, where z_0 is the reactor entrance. For every grid-point z_i we define four (partial) differential equations from Eq. 3.12. In the next step, the first and second order differential terms in the partial differential equations on every grid-point are approximated by second order upwind and central difference terms. After this step, the original reactor model is transformed into a set of $n = 4 \times m$ ordinary differential equations, two mass and two heat balances on all m grid-point over the reactor length ('Method Of Lines' approximation).
The last step is to linearize all non-linear terms in the reactor model. This is done by a first order Taylor-series approximation.

After these modifications we have transformed the original reactor model into n linear time invariant ordinary differential equations. They can then be organized in a state space model as shown in Eq. 3.1a. The state vector is organized in an alternating fashion $\mathbf{x}(t) = [F_B(t,z_1), F_{MA}(t,z_1), T_f(t,z_1), T_s(t,z_1), F_B(t,z_2), \ldots, T_s(t,z_m)]'$. The band diagonal dynamic coefficients matrix $\mathbf{A}_c$ has appropriate constants connecting the n linear differential equations for successive grid points. In our reactor model both the deterministic input $u(t)$ and the stochastic input $w(t)$ is benzene concentration in the feed stream. This system for our reactor model is asymptotically stable.
To simulate analyzers in the reactor the system measurement equation 3.1b is used. All the components of the analyzer dynamics are included in the augmented system matrix $\mathbf{A}_c$ in accordance with the *standard plant* concept.

3.4 Results - To study the effect of process analyzer uncertainty and dynamics we introduce three kinds of measurements in our reactor simulation model presented in the previous paragraph [43], [44]. The first instrument is a fast but relatively inaccurate spectroscopic measurement of the benzene (B) or maleic anhydride (MA). The second analyzer is a fast gas chromatographic (GC) measurement of benzene or maleic anhydride. For this analyzer accuracy is increased at the cost of introducing delay time necessary to physical separate the different components in instrument. The third measurement is a thermal resistor sensor for the solid or fluid phase temperature in the reactor tube. This is an example of an instrument having significant correlation in the response. The specification of each instrument is specified in Table 3.1.

Analyzer	σ_I	T_g *)	T_i *)	T_f	T_d *)
(a) Spectrometer	B : 0.045%(v/v) MA: 0.030%(v/v)	-	-	0.05s	-
(b) GC	B : 0.014%(v/v) MA: 0.009%(v/v)	-	-	5.00s	5.00s
(c) Thermal resistor	1.5 K	-	3.0s	0.05s	-

Table 3.1

*) '-' means no significant contribution for the overall performance of this type of analyzer.

The disturbance on the system is a ten percent fluctuation of the nominal benzene feed flow of 0.9%(v/v). Using Equations 3.7, 3.8 and 3.9 the theoretical estimation errors for the different instruments are computed. The task of the Kalman filter is to estimate from the measurement outcome all state variables **x**(t) in the reactor tube in Eq. 3.13. The measurability factors for the three process analysers specified in Table 3.1 placed at different location in the reactor tube are shown in Figure 3.6.

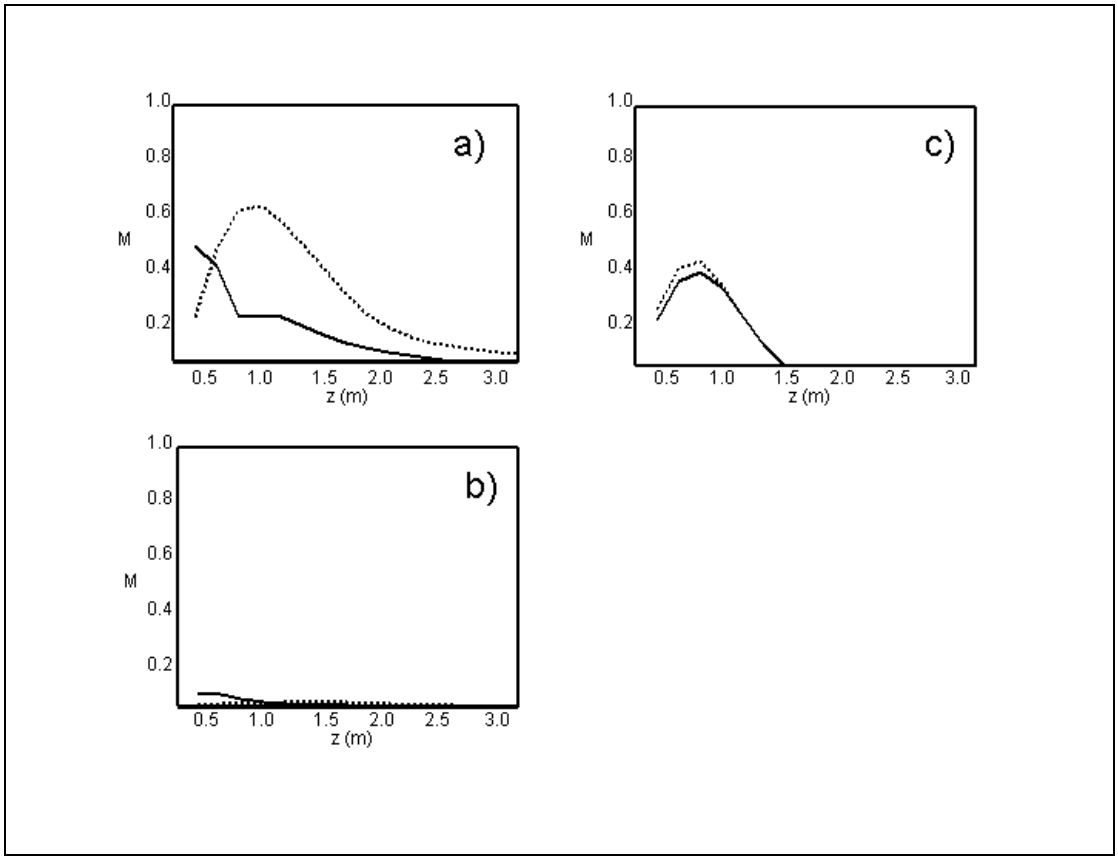

Figure 3.6 Measurability factor *M* for different analyzer configurations at different locations in reactor tube a) spectrometer for B (-) and MA (..); b) GC B (-) and MA (..); c) temperature fluid (-) and solid (..) phase.

From Figure 3.6 and Table 3.1 we learn that the best performance for monitoring the benzene/maleic anhydride reactor is achieved by analyzer (a) – the fast but less accurate spectroscopic analyzer - measuring maleic anhydride at z = 0.6-0.7m. Instrument (a) also gives a good performance for benzene concentration analysis near the entrance, which is close to the source of disturbance for the reactor model, namely fluctuation in the benzene feed. The second observation is that estimation of the reactor state using analyzer (b) performs poor for both benzene and maleic anhydride analysis. The delay time T_d of five seconds for this GC-analysis is simply to long for this process and the measurement thus contains hardly any information for real-time monitoring the system state. The third sensor (c) in the location z = 0.4-0.7 - sampling temperature of fluid or solid phase in the reactor tube - is a reasonable alternative for the use reactor state estimation, although not as good as the concentration measurement with analyzer (a).

If we look at Figure 3.6, together with the nominal reactor profiles plotted in Figure 3.5, we can draw some additional conclusions. The first one is that none of the instruments perform well in the last part of the reactor tube. Not much information on the dynamic behavior of the reactor system is available in the last half of the system, as is to be expected. A second observation is that the rather extreme 'hot-spot' plays a crucial role in the location. Temperature measurements are clearly dominated by its location, while the concentrations are indirectly influenced by the 'negative feedback' for the exothermic oxidation of benzene as can be observed in Figure 3.5a. Another observation is that all optimal positions have slightly moved towards the reactor entrance, as compared to deterministic selection criteria for optimal measurement location [5], [Chap. 2]. Two reasons can be identified: the interaction of analyzer and reactor dynamics, and the fact that the only disturbance for this particular example system was selected to be the uncertainty in the benzene feed at the reactor entrance. If alternative disturbances, possibly taking place at different positions in the reactor tube, where to be included in the process model the optimal measurement location might be altered.

3.5 Conclusions - In this chapter we have shown that the dynamic behavior of a process analyzer plays an important role in selection of the optimal in-process measurement type and location. Six contributions that are needed to specify the in-process analyzer performance have been identified: analyzer location, uncertainty σ_i^2, sample frequency T_f, sample/grab size T_g, response correlation T_i and delay time T_d. Other important components in the success or failure of the process state estimation problem are the dynamics T_s and amplitude σ_s^2 of the process variable selected for measurement.

In our case study – partial oxidation of benzene to maleic anhydride in a tubular reactor – the best analyzer is a fast spectroscopic measurement of the product and, to a lesser extent, the reactant. Gas chromatographic measurement of neither reactant nor product performed well, due to the relative large delay time associated with this instrument. Temperature measurement of fluid and solid phase also performed well in the 'hot-spot' region of the reactor tube.

The approach as formulated in this chapter – including all process analyzer relevant dynamics in the so called *standard plant*, and using the theoretical estimation error to compute the measurability factor – can serve to optimize new in-process measurement implementations. This optimization for analyzer type and position can be done in an early ('drawing board') stage of the process design cycle. By using analyzer specifications, retrieved e.g. from instrument vendors, analytical chemistry departments or earlier experiences, and a model of the process the theory developed in this chapter makes it possible to determine the feasibility of process state estimation and monitoring/control tasks. The measurability factor *M* is a convenient scalar number to compare different in-process measurement configurations. The tools formulated in this chapter can be used to investigate the potential of in-process measurements.

3.A Appendix - In this Appendix we will give an introduction to the ideas as presented by P.M.E.M van der Grinten on optimization of measurements and control schemes [3], [37]. We have changed some of the notation used in the original work in order to create a closer parallel with the work presented here.

Controlling is intervening in a situation on the basis of measurements [3]. Three possible sources for lack controller performance can be identified in this definition. I) The measurement may be in error due to sensor inaccuracies and sluggishness. II) The intervention may lose its effectiveness through over-determinacy or dynamically unfavorable regulator behavior. III) The static and dynamic characteristics of the system under control are insufficiently known. If a measurement is used for control, the accuracy and speed with which the result becomes available are of equal importance. If time is lost in the measurement, or sampling intervals are long, the systems status may have changed without this appearing in the sensor response. Intervention made on such a basis can never be fully correct.

Three dynamic operations are identified for the measured signal (denoted $w(t)$): the sample time or frequency T_f, the averaging or grab-size time

T_g, and the delay time T_d, needed to condition and process the sample (Fig. 3.4). A measurement error v(t) is superimposed on the result.
In many practical applications a reconstruction filter is used to minimize error e(t) between the sensor outcome and the true value. In evaluating the efficiency of the estimator only variations in the measured quantity w(t) and the measuring error v(t) are considered (systematic errors are not included). The definition 3.A1 is used to determine optimum efficiency

$$m^2 = \frac{\sigma_w^2 - \sigma_e^2}{\sigma_w^2} \qquad (3.A1)$$

where m denotes the measurability factor ('meetbaarheidsfactor'), indicating what part of the signal is actually measured under optimal conditions (m = 1 is perfect reconstruction; m = 0 means no information at all).
Completely analogous we can define an efficiency factor for the control structure, again focusing on the changes of the variable about their nominal value. Variable w(t) now represents the equivalent disturbance (summed effect of all disturbances on the process) in the point immediately before the measurement location. The goal of stabilizing control is to minimize the resulting error output e(t). The controller efficiency is now derived as

$$r^2 = \frac{\sigma_w^2 - \sigma_e^2}{\sigma_w^2} \qquad (3.A2)$$

where controllability factor ('regelbaarheidsfactor') r indicates the extent to which disturbances can be suppressed. Notice that r can never exceed m. This means that besides e.g. sluggishness of the controller itself, the sensor performance can dominate the overall control performance.

Dynamics of stationary signal or time series w(t) can be characterized by their auto-correlation function, which for many physical systems can be approximated by Markov processes

$$\varphi_{ww}(\tau) = E\left[w(t)w(t+\tau)\right] \approx \sigma_w^2 e^{-\tau/T_w} \qquad \varphi_{ww}(0) = \sigma_w^2 \tag{3.A3}$$

Equation 3.A3 can be seen as a prediction curve, characterized by the variance/amplitude σ_w^2 and the correlation time T_w. The latter can be estimated already during the design stage by computing the largest time constant of the expected disturbances.

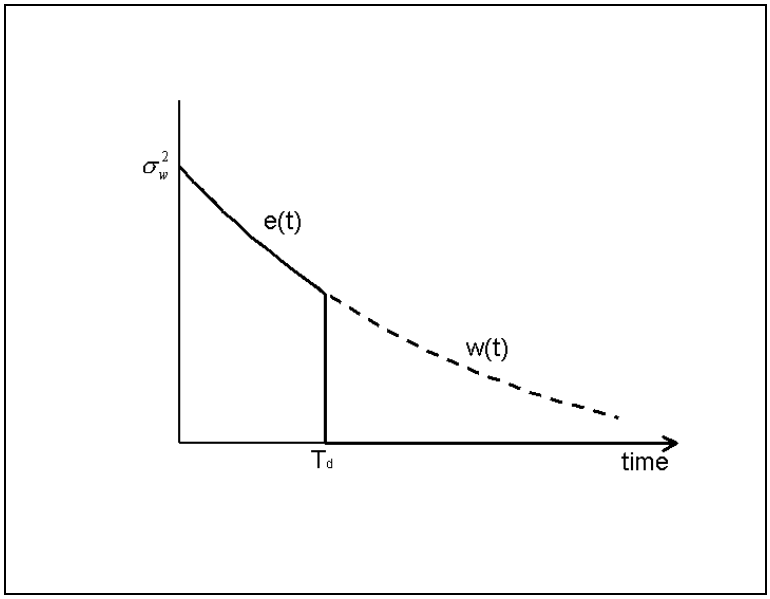

Figure 3A.1 The role of delay time on the controller performance.

To achieve good control the overall delay time (sum of sensor and controller delay) must be smaller than the disturbance time constant: $T_d < T_w$. This is illustrated in Figure 3.A1 for the case of optimal control. A disturbance w(t) will emerge as output error e(t) until time equals $t = T_d$, after which the error is compensated for by the controller. From this observation and Eq. 3.A2 a controllability factor due to delay time is deduced

$$r_d = e^{-T_d/T_w} \tag{3.A4a}$$

For all other contributions to the overall measurement and control uncertainty similar equations can be derived. These are often simplifications of more complicated, statistically more thorough

descriptions. Here we present only the final results. For details on derivations, more complicated auto-correlation functions and process disturbances we refer to van der Grinten [3].
The contribution of sampling frequency is given by

$$m_f = e^{-T_f/2T_w} \tag{3.A4b}$$

The factor $\frac{1}{2}T_f$ stems from the notion that information at the moment of sampling is complete, but immediately before the next sample the information is obsolete by a time equal to T_f. Similar reasoning leads to an equation for the sample size error

$$m_g = e^{-T_g/2T_w} \tag{3.A4c}$$

Formulas can be derived for the measurement error with sensor error correlation T_v and the inverse controller response with inversion time T_{in}

$$m_n \approx 1 - \frac{\sigma_v}{\sigma_w}\sqrt{\frac{T_v}{T_w}} \tag{3.A4d}$$

$$r_{in} = \frac{1 - T_{in}/T_w}{1 + T_{in}/T_w} \tag{3.A4e}$$

The overall controllability factor can now be determined from the different contributions by the following equation

$$r_{tot} = mr = m_g m_f m_n m_d r_d r_{in} \tag{3.A4f}$$

Equation 3.A4f serves two purposes. The value of the overall controllability factor r_{tot} must be close to 1. As a rule of thumb values larger than 0.8 indicate good measurement/controller couples, while values below 0.5 indicate that control schemes are of little use. Equation 3.A4f gives us a quantity to directly compare various sensor/controller set-ups. The second advantage is that the overall uncertainty can be split

up in separate contributions that can be optimized individually, with the aim of identifying (and ultimately removing) the bottleneck from a control structure or sensor implementation.
We would like to emphasize again that a more complete (English) treatment on the material as presented in this Appendix can be found in van der Grinten [3].

3.B Appendix - The autonomous system in Eq. 3.B1 serves as an example to study some of the influence of analyzer location and dynamics defined in the main text [5]

$$\dot{\mathbf{x}}(t) = \mathbf{A}_c\mathbf{x}(t) + \mathbf{b}_2 w(t) = \begin{bmatrix} -1 & 1 & 1.5 \\ 1 & -2 & 1 \\ 0 & 1 & -3 \end{bmatrix} \cdot \begin{bmatrix} x_1(t) \\ x_2(t) \\ x_3(t) \end{bmatrix} + \begin{bmatrix} 1 \\ 0 \\ 0 \end{bmatrix} \cdot w(t) \qquad \text{(3.B1)}$$

$$\mathbf{x}(0) = \begin{bmatrix} 1 & 1 & 1 \end{bmatrix}' \qquad q(t) = 0.1$$

As can be seen from Eq. 3.B1 disturbances *w*(t) are 'injected' on the first state and are distributed over the other two states through the system dynamics in $\mathbf{A}_c$. The autonomous solution for the system plus the auto-correlation's $\phi(x_i x_i)$ and cross-correlation's $\phi(w_i x_i)$ for a white noise feed pattern with distribution N(0,0.1) is shown in Figure 3.B1. The dynamics of state x_1(t) and x_2(t) show a clear system delay time for input uncertainty *w*(t).

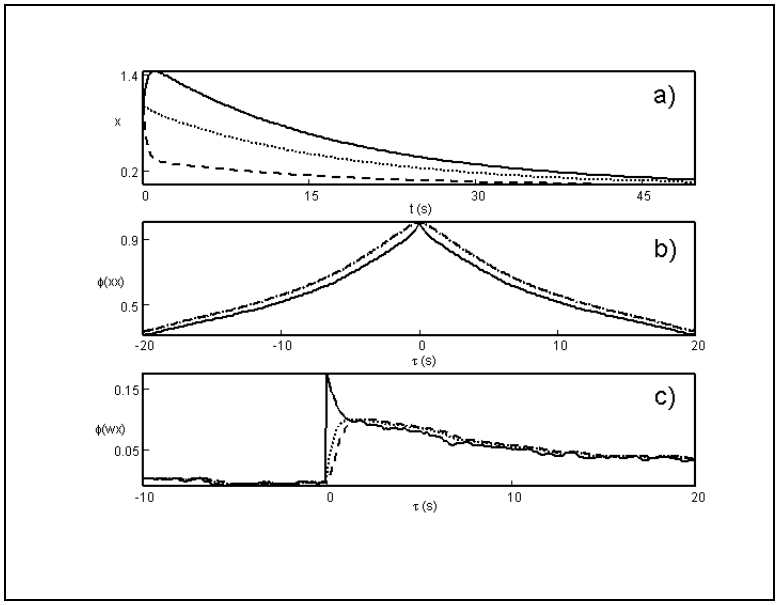

Figure 3B.1 (a) Autonomous response, (b) auto- (c) and cross-correlation's for the three states in system (B.1): x_1 (-), x_2 (..) and x_3 (--) (σ_{x1} = 0.17, σ_{x2} = 0.10 and σ_{x3} = 0.03).

On this system we define three 'instruments' with the specifications as shown in Table 3.B1.

Analyzer	σ_i^2	T_g *)	T_i *)	T_f *)	T_d *)
B_a	1.0	-	-	0.1s	-
B_b	0.1	-	-	5.0s	5.0s
B_c	0.5	-	2.0s	0.1s	-

Table 3.B1

*) '-' means no significant contribution on the overall performance of this analyzer.

The specifications of the instruments imply the following characteristic features: B_a is a moderately accurate instrument with a high sampling frequency, B_b is a very accurate analyzer, but suffering from a large delay time (typically equal to the analysis time), and B_c is a representative of many physical measurements with a moderate accuracy and a significant memory effect.

Implementation of B_a is straightforward using the appropriate values in equations as presented in the theory section: sampling time T_f forms the basis for going from the continuous system in Eq. 3.B1 to discrete observation, while σ_i^2 specifies the uncertainty in the measurement responses.

To implement the time delay of B_b, measuring e.g. the first state, the original system $\mathbf{A}_c$ has to be augmented with three virtual states x_4(t)-x_6(t) in accordance with Eq. 3.6 creating the *standard plant*

$$\dot{\mathbf{x}}(t) = \mathbf{A}_c\mathbf{x}(t) + \mathbf{b}_2 w(t) = \begin{bmatrix} -1 & 1 & 1.5 & 0 & 0 & 0 \\ 1 & -2 & 1 & 0 & 0 & 0 \\ 0 & 1 & -3 & 0 & 0 & 0 \\ 1 & 0 & 0 & -2.4 & -2.4 & -0.96 \\ 0 & 0 & 0 & 1 & 0 & 0 \\ 0 & 0 & 0 & 0 & 1 & 0 \end{bmatrix} \cdot \begin{bmatrix} x_1(t) \\ x_2(t) \\ x_3(t) \\ x_4(t) \\ x_5(t) \\ x_6(t) \end{bmatrix} + \begin{bmatrix} 1 \\ 0 \\ 0 \\ 0 \\ 0 \\ 0 \end{bmatrix} \cdot w(t)$$

$$y(t) = \mathbf{c}'\mathbf{x} + v(t) = \begin{bmatrix} -1 & 0 & 0 & 4.8 & 0 & 1.92 \end{bmatrix}\mathbf{x} + v(t)$$

(3.B2)

In Eq. 3.B2 the parameters for the augmented part of the system form a companion canonical state space representation of the Padé approximation for time delay in Eq. 3.6.

To model the signal correlation in B_c, sampling e.g. state number two, system B1 has to be augmented by one state x_4(t) in accordance with Eq. 3.5

$$\dot{\mathbf{x}}(t) = \mathbf{A}_c\mathbf{x}(t) + \mathbf{b}_2 w(t) = \begin{bmatrix} -1 & 1 & 1.5 & 0 \\ 1 & -2 & 1 & 0 \\ 0 & 1 & -3 & 0 \\ 0 & 1/2 & 0 & -1/2 \end{bmatrix} \cdot \begin{bmatrix} x_1(t) \\ x_2(t) \\ x_3(t) \\ x_4(t) \end{bmatrix} + \begin{bmatrix} 1 \\ 0 \\ 0 \\ 0 \end{bmatrix} \cdot w(t) \qquad \text{(3.B3)}$$

$$y(t) = \mathbf{c}'\mathbf{x} + \sqrt{1-(e^{-1/T_i})^2} = \begin{bmatrix} 0 & 0 & 0 & 1 \end{bmatrix}\mathbf{x} + 0.8v(t)$$

For these three analyzer types the uncertainty propagation from Eq. 3.9 is determined and the expected estimation error $\mathbf{P}_k$ is computed from Equations 3.7 and 3.8. The measurability factor Eq. 3.10 for these the three analyzers in Table 3.B1 for the system 3.B1 are given in Table 3.B2

Analyzer	x_1	x_2	X_3
B_a	0.8	0.7	0.3
B_b	0.4	0.3	0.1
B_c	0.7	0.6	0.4

Table 3.B2

The table shows that measuring the first state is favorable for every instrument [5]. It also shows that the best overall match between system and analyzer dynamics for state estimation is between B_a and the first state. The last conclusion from this example is that if only state x_3 is available, B_c is to be preferred.

4. Selection and Positioning: a Case Study

Selection of Optimal Process Analyzers for Plant-Wide Monitoring

Abstract - In this chapter the effect of process analyzer location and performance on plant-wide process monitoring is investigated. A fundamental problem in process analytical chemistry is the incomparability of different instrument characteristics. A fast but imprecise instrument is incomparable to a slow but precise instrument. Theory is developed to overcome this problem by using an abstract definition of a process analyzer. This definition allows us to put all instrument characteristics for a particular monitoring task on an equal footing. This results in a measurability factor *M* that expresses monitoring performance of any process measurement by combining instrument characteristics like precision, sampling rate, grab-size, response correlation and delay time. Both the choice of location and the performance characteristics of different process analyzers can be evaluated using the measurability factor. The unifying nature of the measurability factor allows for a rational decision between completely different process analyzers and locations [45].

The theory is illustrated and validated with an experiment. A tubular reactor for free radical bulk polymerization of styrene is monitored by in-line short-wave near-infrared spectroscopy at different positions. Alternatively, product samples are collected for at-line near-infrared analysis. Both analyzers measure styrene monomer concentration. The analysis results are used to predict conversion as well as number and weight average molecular mass of the polystyrene reactor product. The theoretical measurability factors for this case study correspond well with the experimental findings.

4.1 Introduction - An ever-increasing number of process analyzers are implemented in the chemical industry. At the same time the diversity in techniques suitable for harsh process conditions - e.g. Chromatography, (Near)Infrared-, Raman- or (low field) nuclear magnetic resonance spectroscopy, mass spectrometry, flow injection analysis, ultrasonic analysis, to name just a few - grows steadily [34]. The implementation and operation of analytical in-process[4] measurements is, however, still relatively expensive. The cost of purchase and maintenance often limits the number of analyzers that can be implemented for monitoring and/or control purposes to one or a few key-components. This naturally leads to the following questions: what is the added value of process analyzers as compared to more conventional, interferential measuring devices like temperature-, pressure- or flow-sensors, what is the better choice from the wide selection of process analyzers, and what is the best location to place this limited number of instruments? All these questions are related and can only be answered adequately by looking at the process under observation [2]-[6], [45].

The 'information content' of measured process variables is a function of the underlying process dynamics, the external process disturbances and of the process analyzer measuring these variables. The dynamic behavior of various important process variables e.g. reactant versus product can be quite distinct. An important objective is thus to sample the process variable with the most information in its measured signal, at the most informative position in the process (e.g. reactor inlet versus outlet). The characteristics of a process analyzer - e.g. slow but precise GC-analysis versus fast but relative imprecise spectroscopic-measurements - determine which technique is best suited for the analysis task at hand.

To assess the performance of process analyzers we identify six characteristics, the so-called *process analyzer dynamics* [6], [Chap. 3]. The first characteristic is the process variable selected for measurement and the location at which it is sampled. The second contribution is instrument precision: the uncertainty or error encountered in every

[4] The expression 'in-process' is an idiom for all at-line, on-line, in-line and non-invasive measurement techniques suited for 'real-time' monitoring and/or control of a process.

measurement. The third contribution is the sampling rate, the effect of making discrete measurements on a continuous process. The fourth contribution is 'grab-size' error: the information loss introduced by collecting a sample of sufficient size. The fifth contribution is response correlation. This phenomenon is often observed in 'physical' measurements like ion-selective electrodes, pH or conductivity, where instrument responses are correlated over time (a 'memory' effect of preceding measurement responses). The sixth contribution is analysis or delay time: the time passed between collecting the sample and getting the analysis result. Obvious examples are separation based composition analyzers that require some time to handle a sample before the result becomes available. These six characteristics must be taken into account when assessing the performance of different in-process implementations. Additional characteristics could be considered, but these six are sufficient to model most present-day process analyzers.

In this chapter we make use of a so-called Kalman state vector observer to estimate process variables from in-process measurements. The process state vector is a collection of all the important process variables such as concentrations of the different components or moments of the polymer product mass distribution. The process state vector's time trajectory thus shows the behavior of the process in time by showing the trajectory of all important process variables in it. Many of the process state vector elements, e.g. the mass distribution, cannot be measured directly. The input to the Kalman state observer is the measurement result from the process analyzer, measuring e.g. the monomer concentration. The output of the state observer is an estimate of the complete state vector. It contains both filtered results of the measured process variables (the monomer concentration) and estimated values for the unmeasured process variables (the mass distribution). To make an estimate of unmeasured process variables the state observer uses a fundamental process model based on e.g. mass balances of the different reacting species.

The Kalman observer also provides an expected estimation error in the form of a theoretical covariance uncertainty matrix of the estimated state vector. The optimal analyzer type and location for a process is selected by

minimizing this state vector estimation error. More details on the Kalman state observer can be found in Appendix 4.A. To quantify the performance of a process analyzer implementation and state vector observer we define the measurability factor *M*, ranging from zero to one, where one indicates perfect process state vector reconstruction. Perfect reconstruction in this context means that the process variables in the estimated state vector coincide with the true process variables for every point in time.

The theory on process analyzer selection and positioning is tested on experiments with a bench-scale continuous tubular reactor for free-radical bulk polymerization of styrene to polystyrene [46], [47]. At different locations along the reactor tube in-line short-wave near-infrared (SW-NIR) spectroscopic styrene concentration measurements can be performed. At the same time samples are collected at the reactor outlet for at-line near-infrared (NIR) spectroscopic styrene concentration analysis. In combination with a Kalman state observer, the different spectroscopic measurements can be used to predict molar mass distribution of the polystyrene product (M_n and M_w) at the reactor exit. The molar mass average predictions will be verified by off-line size exclusion chromatography (SEC).

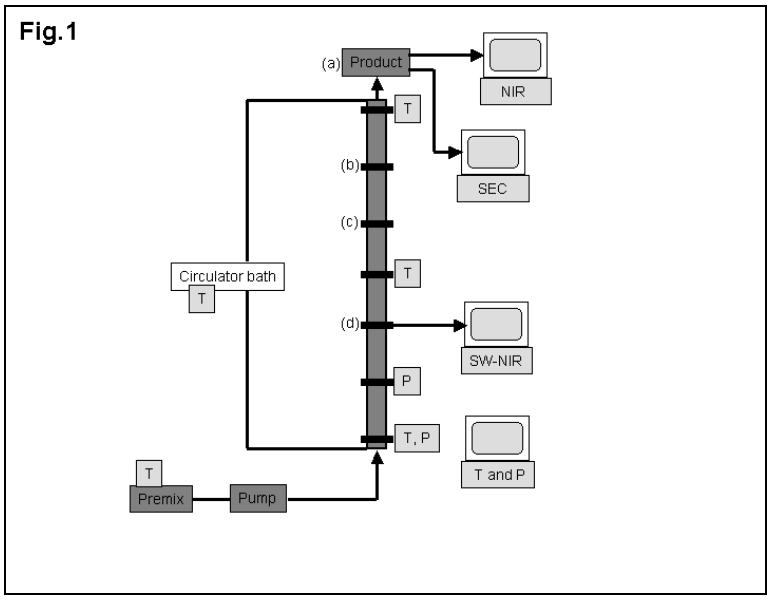

Figure 4.1 Overview of the bench scale polystyrene tubular reactor setup. The characters (a)-(d) mark different process analyzer locations used in the experimental section.

4.2 Theory - The theory will be explained using the styrene polymerization case study as a leading example. A schematic drawing of the tubular polymerization reactor is shown in Figure 4.1. Two types of spectroscopic in-process analyzers are available: in-line SW-NIR at one of seven locations along the reactor tube, and at-line NIR on product samples. Styrene concentration is the measured process variable for both techniques. From this measurement, the process state vector containing all relevant process variables - initiator concentration $C_i(t)$, monomer concentration $C_m(t)$ and molecular mass distribution moments $M_n(t)$ and $M_w(t)$ - is determined by a state vector observer. Details of the measurement scheme are illustrated in Figure 4.2. Process variable $C_m(t)$ is measured in-line somewhere along the reactor tube or at-line on product samples. At every sample location the $C_m(t)$-signal shows a distinct dynamic behavior (symbolized by T_m) and variance/amplitude (σ^2_m) as a function of the process dynamics and the external process disturbances. The analyzer with its distinct analyzer characteristics 'processes' the sampled variable $C_m(t)$ and gives an estimated $\hat{C}_m(t)$ as measurement outcome. This analysis result is then fed to a process state observer that has the following task: invert the undesired signal processing by the analyzer and estimate the state vector (containing both measured and unmeasured process variables) for the reactor system.

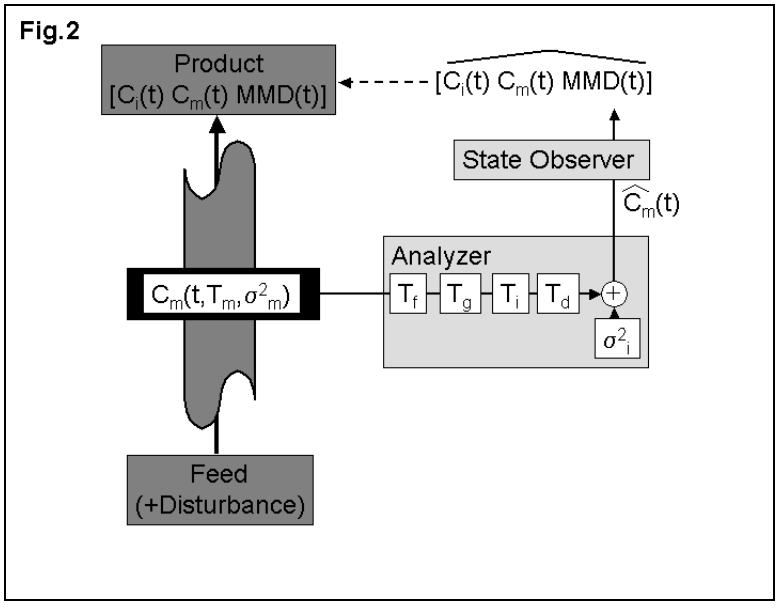

Figure 4.2 A detailed look on monitoring with a process analyzer.

To find the optimal in-process measurement configuration we take six different aspects into consideration, loosely called the *process analyzer dynamics* [6]. The first aspect is the process variable selected for measurement and the location at which this process variable is sampled. This selection is guided by the amount of information a variable contains on the overall dynamics of the process and the availability of a suitable in-process instrument for monitoring in 'real-time' this variable at that particular location. Process engineers and analytical chemists should make a first selection of potential candidate analyzers and locations for a specific monitoring task. The methods we propose can then make a rational selection from this set. In our case study the choice is limited to in-line SW-NIR or at-line NIR, measuring monomer concentration $C_m(t)$. Alternative measurement schemes could be developed for spectroscopic initiator measurements or on-line Size Exclusion Chromatography. However, the low initiator concentrations in free radical polymerization and the relative long analysis times required for SEC, a requirement incompatible with the relative fast dynamics in our reactor system, immediately classify them as unattractive alternatives for this system.
The second contribution of instrument characteristic is process analyzer precision σ_i^2. Uncertainty in the instrument outcome will be approximated by the true concentration $C(t)$ plus additive white noise $v(t)$ with known distribution, typically determined during the calibration procedure or supplied by an instrument vendor:

$$\hat{C}(t) = C(t) + v(t) \qquad v(t) \sim N(0, \sigma_i^2) \tag{4.1}$$

The third source of error is the sampling rate of the instrument, specified by the time interval between successive samples T_f (where the sample frequency is $1/T_f$). In-process analyzers typically make discrete observations on continuous process. The state of the process - altered by external disturbances - can only be determined when a new analysis result comes in. Hence, the uncertainty can only be reduced when a new measurement becomes available and a new state vector estimate is

performed. For many instruments (e.g. spectrophotometers) there is a trade-off possible between the sampling frequency $1/T_f$ and precision σ_i^2. Spending more time per analysis to increase the signal-to-noise ratio will automatically lead to a lower sampling rate (further details are given in Appendix 4.A).

The fourth analyzer characteristic is grab-size T_g. If a sample is collected over a short period of time, e.g. to gather enough material for physical experiments or to get sufficient detector signal for spectroscopy, the expected value of the measurement will be the average value over that same time period. Hence, variability during that period goes undetected. This average value becomes available once the entire grab has passed. If this grab-size is relatively short we can associate the analysis result with the true value at time equal to half the grab time interval. Therefore, in our *process analyzer dynamics* we penalize grab-size with a time delay of half the grab time T_g:

$$\hat{C}(t) = C(t - 0.5T_g) + v(t - 0.5T_g) \qquad (4.2)$$

In words equation (4.2) would read: the estimate of process variable *C* we retrieve at time *t* is really an estimate of this variable $0.5T_g$ time units ago. As a consequence, information on the continuously changing *C*-signal is already $0.5T_g$ time units 'old' before we get it. The same reasoning holds for precision *v*(t).

The fifth contribution to process analyzer performance is response correlation T_i. In many instruments there is significant carry-over in the detector response from one measurement to the next (e.g. pH ion selective electrodes or some temperature dependent resistors). This carry over can be approximated by an exponentially first order correlation of the auto regressive form.

$$\hat{C}(t) = (1 - e^{-1/T_i})C(t) + e^{-1/T_i}C(t - T_f) + v'(t) \qquad (4.3)$$

The noise *v'*(t) is scaled to have equal magnitude as the uncertainty in equation (4.1). The final estimate is written as an exponentially weighted

sum of present and previous values of the sampled variables; where the weights are determined by the response correlation time constant T_i between successive measurements. When T_i is very small, say zero, then the term containing T_f vanishes and the effect of the correlation time is cancelled.

The last component describing the performance of in-process instrumentation is the analysis or delay time T_d between taking the sample and obtaining the analysis result.

$$\hat{C}(t) = C(t - T_d) + v(t - T_d) \tag{4.4}$$

In words, information on the continuously changing *C*-signal is already T_d time units 'old' before we get it. An example of an analyzer with a significant time delay is in-process chromatography where the components first have to be physically separated before the final analysis results becomes available.

The six contributions to *process analyzer dynamics* - the process variable and location selected for measurement plus the five instrument characteristics - as formulated above give us a more abstract definition of in-process analyzers. It enables us to compare completely different measurement techniques – e.g. GC versus NIR-spectroscopy - on a theoretical level, comparing their individual merits on conceptual grounds. The goal of all analyzer/observer combinations is the same: to estimate the process state vector, which holds the process variables as considered important. Optimal selection of instrument type and location must guarantee that sufficient information is obtained from a measurement to make a good 'real-time' estimate of the state vector.

In this chapter we use the Kalman observer to estimate the process state. This observer is an unbiased, minimum variance and consistent estimator for the process state of a linearized system [32], [33], [42]. Further details on reactor dynamics and the observer are given in Appendix 4.A.

To assess the performance of different process analyzers we have developed the measurability factor *M* [3], [6]. For a stable process such as the tubular polymerization reactor in our case study, *M* will be a scalar

between zero and one, where one indicates perfect process state vector estimation. A stable process perturbed from normal operation conditions by external process disturbances – e.g. variations in initiator concentration of the feed stream in our example - will operate within a limited range surrounding these normal operating conditions. We can express this variation in the form of a process covariance matrix **Q**. In our reactor tube **Q** thus gives the range or boundaries of the composition of the reactor product stream over time due to expected disturbances in the reactor feed. Task of the process analyzer and observer is to estimate the exact position of the process state vector - with all the important process variables - within this operating range surrounding the normal trajectory. Moreover, this estimate should be available for every point in time. Because of the *process analyzer dynamics* this state estimate will, however, never be perfect. We can express the estimation error or uncertainty due to analyzer characteristics in the form of a covariance matrix **P**. From the covariance matrices **Q** and **P** we can compute the measurability factor *M*.

$$M = \frac{trace(\mathbf{Q}) - trace(\mathbf{P})}{trace(\mathbf{Q})} \tag{4.5}$$

The 'trace' is the sum of diagonal elements of the covariance matrices and serves as a norm for the matrix involved. In our case study this is equal to summing (expected) variances for all the relevant process variables in the reactor state vector. *Trace(***Q***)* is the unknown process variance caused by external process disturbances, and *trace(***P***)* is the prediction error after measurement and state vector estimation. The numerator part of equation (4.5), *trace(***Q***)* - *trace(***P***)*, is thus the removed unknown process variance. The measurability factor *M* in equation (4.5) thus approaches one when the *trace(***P***)* approaches zero. For an extremely poor choice of a process analyzer, the covariance matrix **P** after state vector estimation could be larger than the initial process uncertainty in **Q**. In this (hypothetical) case the measurability factor will get a negative value, which means that the in-process measurements serve no purpose, and our 'best guess' for the process state vector is: somewhere in the operating range surrounding

the normal trajectory. The measurability factor in equation (4.5) thus shows how much of our initial uncertainty in knowledge of the process state vector is removed by the process analyzer and observer. The theory in this chapter can be generalized to evaluating different combinations of multiple process analyzers for one estimation task.

4.3 Experimental Section - A bench scale tubular reactor is constructed for the operation of a free radical bulk polymerization of styrene in continuous mode. A drawing of the instrumentation is shown in Figure 4.1. The heart of the setup is a vertically placed stainless steel tube (1.1m length; 10mm i.d.) with seven gageable tube fitting union crosses. Teflon connectors can assemble different sensors in these crosses. Three thermocouples and two pressure sensors are inserted at different locations. Quarts windows for the in-line SW-NIR spectrometer are mounted in similar Teflon parts. By positioning windows on opposite sites in one cross piece an in-line 'cuvette' is created that can be sampled by the spectrometer (effective path length ±8mm).

The temperature inside the reactor tube is regulated by a circulator water bath and six cross-wise connected aluminum pipes placed along the inner reactor tube. The system is isolated to minimize heat loss. The temperature of the circulator bath is logged. A feed vessel and HPLC-pump supply a continuous stream of styrene and AIBN initiator to the reactor entrance (flux = 2 $mL.min^{-1}$; average residence time 42min). The temperature of the premix is logged.

Product samples are collected from the reactor outlet in grabs of three minutes every ten minutes. The styrene concentration is determined by at-line NIR spectroscopy. M_n and M_w for the polymer molar mass distribution in the product stream are determined off-line by SEC [48]. Multivariable calibration was used for both spectroscopic techniques. The preprocessing and calibration results are shown in Table 4.1. Using the theory of *process analyzer dynamics* the performance of the two instruments can be characterized as shown in Table 4.2.

	NIR	Visual/SW-NIR
Integration	90 seconds (30 scans) 3499-10000cm^{-1} 2cm^{-1} (resolution)	15 seconds (± 150 scans) 400-1000nm 1nm interval (resolution)
Savitzky-Golay filter [49]	37-points second derivative second order polynomial	31-points fourth derivative fourth order polynomial
Spectral range used in PLS1	5618-6390cm^{-1}	860-890nm
PLS1-model [51] (Partial Least Squares)	Data mean centered 3 Latent Variables	Data mean centered 4 Latent Variables
Conversion uncertainty	0.2%(m/m) ($RMSEP_{cv}$)	0.4%(m/m) ($RMSEP_{cv}$)

Table 4.1

The process disturbance is a ±25% uncertainty from the normal 0.04mol.L^{-1} initiator concentration of the reactor feed. The range of this process disturbance is used to compute the measurability factor *M* for different process analyzers and state observers. During the experiments this process disturbance was realized by switching between three premix vessels with different (known) initiator concentrations.

	NIR	SW-NIR
σ_i	0.2%	0.4%
T_f	600s	35s
T_g	180s	15s
T_i	---	---
T_d	420s	20s

Table 4.2

4.4 Results and Discussion - The objective of in-process measurements in our case study is to estimate the styrene conversion and polystyrene molar mass distribution of the reactor polymer product. The best position for the in-line SW-NIR and the performance of the at-line NIR can be determined from the measurability factor *M*. This factor can be computed using the dynamic reactor model and expected process disturbances as formulated in Appendix 4.A, together with the process analyzer

characteristics as specified in Table 4.2. The result is shown as the solid curve in Figure 4.3. From this figure we observe that the better location for in-line SW-NIR analysis is in the second half of the reactor tube ($z \approx$ 0.6-1.0m). In-line SW-NIR measurements for the first part of the reactor tube ($z <$ 0.40m) are incapable of picking up process disturbances and estimating the reactor product composition, resulting in a low score for the measurability factor *M* in this segment. The slower but more precise at-line NIR measurement on product samples is slightly better than the optimal in-line SW-NIR implementation.

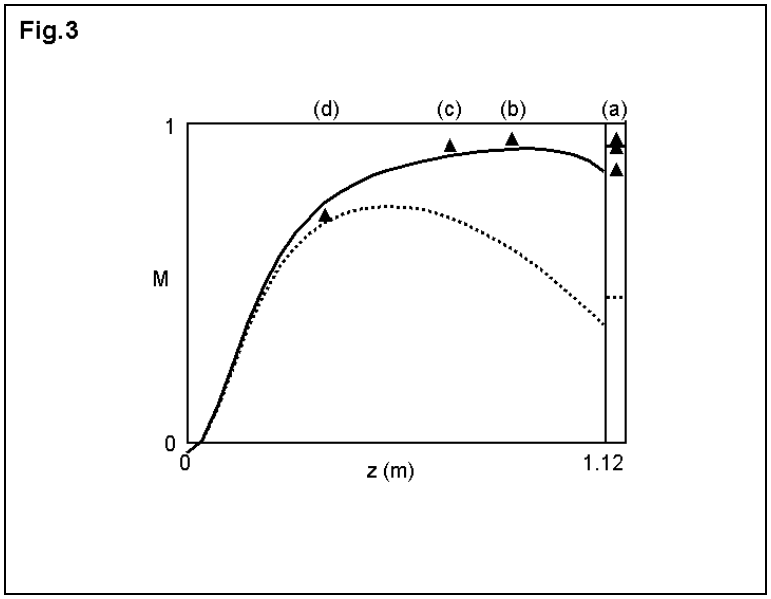

Figure 4.3 Theoretical measurability factor *M* as a function of in-line SW-NIR on position *z* in the reactor tube. Optimized for reactor product composition ('—') or entire tube contents ('..'). The bar after z = 1.12m gives the theoretical measurability factor for at-line NIR on reactor outlet samples. Triangles mark the *practical measurability factors* for three different experiments.

To verify our theoretical measurability we have conducted three experiments for different SW-NIR positions: z = 0.88, 0.72 and 0.40m. In Figure 4.4 the estimated styrene conversion in collected product samples are plotted as a function of time. Also shown are reference values for product samples and the target value for normal operation conditions. From this figure we can calculate a 'practical' measurability factor. The variance between the normal and the reference values represent the range of process variance in the product caused by the disturbances, in our case initiator concentration changes in the feed stream. The difference between references and observer estimates quantify the residual

uncertainty after making a reactor state vector estimate. From these two variances a practical measurability factor, similar to the one given in equation (4.5), can be computed. It shows how well we can estimate styrene conversion in the reactor product using a particular measurement. The practical measurability factors are shown as triangles in Figure 4.3. Although there is some variation in the outcomes, as evident from the triplicates for at-line NIR-analysis, the results for the theoretical and the practical measurability factor correspond well. The two computed moments of the polymer product molar mass distributions (M_n and M_w) are shown in Figure 4.5, together with the SEC reference values and normal values. Due to the 'stiffness' of the styrene polymerization dynamics the relative small changes in feed initiator concentration have only minor effects on the MMD [46], [47], [49].

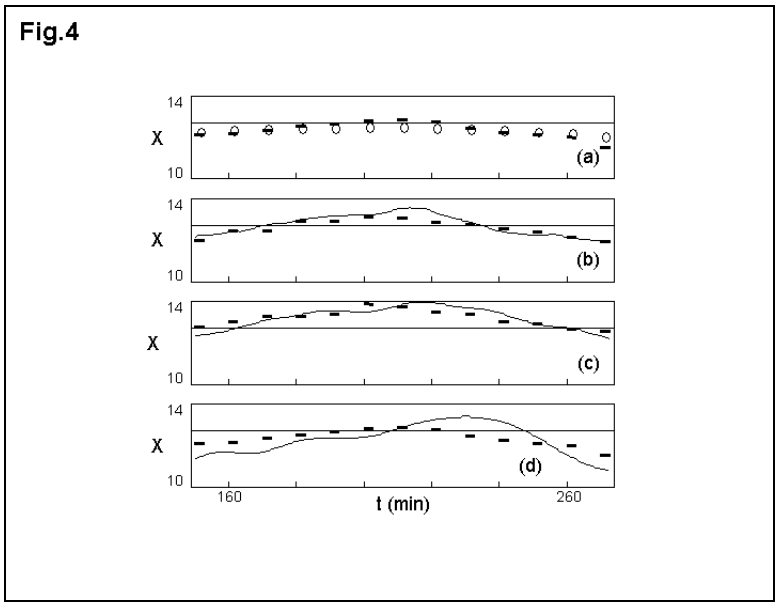

Figure 4.4 Estimated degree of styrene monomer conversion X (%) in reactor product. Bars are the reference values; horizontal line corresponds to normal operation. Predictions from (a) at-line NIR ('o'; results shown for one experiment) and in-line SW-NIR ('—') on position (b) z = 0.88m, (c) z = 0.72m and (d) z = 0.40m.

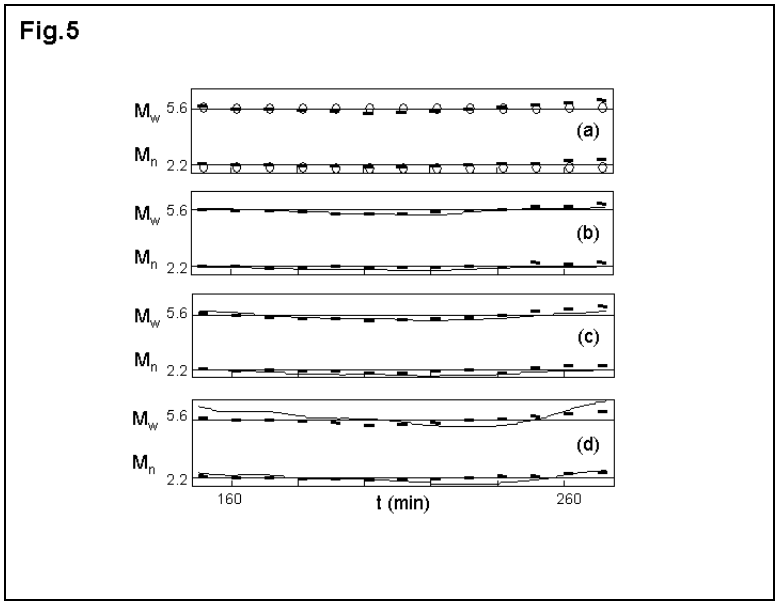

Figure 4.5 Estimated M_n and M_w (x10^4 g.mol^{-1}) for reactor polymer product. Bars are the reference values; horizontal line corresponds to normal operation. Predictions from (a) at-line NIR ('o'; results shown for one experiment) and in-line SW-NIR ('—') on position (b) z = 0.88m, (c) z = 0.72m and (d) z = 0.40m.

4.5 Extensions - So far our objective was defined as estimating the composition of the reactor product. To illustrate the versatility of the theory we will briefly describe a different monitoring task. Suppose that the objective for this process analyzer and state vector observer combination is to estimate all relevant process variables for the entire reactor tube length. The purpose could e.g. be model predictive control, anticipating process regulation on the (estimated) reactor state vector [50]. The broken line in Figure 4.3 shows the measurability factor M for this analyzer/observer objective. The outcome illustrates that different monitoring objectives can lead to completely different results: the theoretical measurability factor is overall lower (the estimator task is more complex), the best location for in-line SW-NIR shifts towards the reactor inlet and the at-line NIR is ineffective for this job.

The optimization method of process analyzer selection and positioning presented in this chapter can be utilized already in an early process design stage. From a dynamic process or unit operation model, an expected (range of) process disturbance(s) and process analyzer characteristics, the theoretical measurability factors M can be computed without actually collecting any experimental data. To elucidate this point we refer back to the theory section where it was stated that concentration of the monomer, as target for in-process analysis is preferred over initiator concentration or

molecular mass distribution moments. To reach an acceptable *M*-value of e.g. 0.8 for our monitoring objective on the reactor output stream one needs either a very precise method for initiator concentration or an exceptionally fast (less than 20 minutes analysis time) technique for determining polymer mass distribution. Both requirements are difficult to fulfill. Hence, without investigating specific instrument a priori the required *process analyzer dynamics* tell us that monomer concentration is the best or most affordable candidate for monitoring in this process.

4.6 Conclusions - In this chapter we have developed and applied the theory of optimal process analyzer selection and positioning on spectroscopic concentration measurements in a bench scale tubular reactor for free radical bulk polymerization of styrene to polystyrene. The performance of different in-process instruments and state vector observers is evaluated as a function of the *process analyzer dynamics*. Both the choice of location and the performance characteristics of different instruments can be assessed using the measurability factor *M*. The theoretical performance for predicting product composition by both in-line SW-NIR and at-line NIR analysis is shown to correspond well with the experimental results. It is shown that in selecting an analyzer and sample position the dynamics of the measured process variable and its information content regarding other (unmeasured) process variables is important. It is also shown to be a function of the dynamics of the instruments and the monitoring objective.
Through the measurability decision criterion we hope to formulate a guideline to counteract the more or less ad-hoc practice for present process analyzer selection and positioning. It is the task of the (process) analytical chemist (together with system and control engineers) to provide sensible input for this optimization procedure.

4.A Appendix - In this study we estimate the process state vector of a tubular reactor for the initiator driven, free-radical bulk polymerization of styrene [46], [47] using a Kalman state observer [32], [33], [42]. To implement the observer, mass balances in the form of partial differential equations are required for initiator concentration C_i, styrene monomer C_m,

the first three moments for chain length distribution of growing (λ) and terminated polymer (μ). Equation (4.A1) is a mathematical model of the tubular reactor in our case study (t is time; z is axial position in the reactor tube) [48].

$$\frac{\partial C_i}{\partial t} = -v\frac{\partial C_i}{\partial z} - k_d C_i \tag{4.A1a}$$

$$\frac{\partial C_m}{\partial t} = -v\frac{\partial C_m}{\partial z} - k_p C_m \lambda_0 \tag{4.A1b}$$

$$\frac{\partial \lambda_0}{\partial t} = -v\frac{\partial \lambda_0}{\partial z} - k_t \lambda_0^2 + k_{sp} C_m^2 + 2fk_d C_i \tag{4.A1c}$$

$$\frac{\partial \lambda_1}{\partial t} = -v\frac{\partial \lambda_1}{\partial z} - k_t \lambda_0 \lambda_1 + k_{sp} C_m^2 + 2fk_d C_i + k_p C_m \lambda_0 - k_{trm} C_m (\lambda_1 - \lambda_0) \tag{4.A1d}$$

$$\frac{\partial \lambda_2}{\partial t} = -v\frac{\partial \lambda_2}{\partial z} - k_t \lambda_0 \lambda_2 + k_{sp} C_m^2 + 2fk_d C_i + k_p C_m (2\lambda_1 + \lambda_0) - k_{trm} C_m (\lambda_2 - \lambda_0) \tag{4.A1e}$$

$$\frac{\partial \mu_0}{\partial t} = -v\frac{\partial \mu_0}{\partial z} + (1 - 0.5 z_t) k_t \lambda_0^2 + k_{trm} C_m \lambda_0 \tag{4.A1f}$$

$$\frac{\partial \mu_1}{\partial t} = -v\frac{\partial \mu_1}{\partial z} + k_t \lambda_0 \lambda_1 + k_{trm} C_m \lambda_1 \tag{4.A1g}$$

$$\frac{\partial \mu_2}{\partial t} = -v\frac{\partial \mu_2}{\partial z} + k_t \lambda_0 \lambda_2 + k_t z_t \lambda_1^2 + k_{trm} C_m \lambda_2 \tag{4.A1h}$$

From (4.A1) the number M_n and weight average molar masses M_w can be computed (M_m = 104.15 g.mol^{-1}).

$$M_n \approx M_m \frac{\mu_1}{\mu_0} \qquad M_w \approx M_m \frac{\mu_2}{\mu_1} \tag{4.A2}$$

To implement the Kalman observer, the model in (4.A1) is rewritten in a discrete time, linear, time invariant state space format of the following form ($\mathbf{u}_k$ are the deterministic reactor feed streams, C_i and C_m; $w_k \sim N(0,q)$ is the stochastic component or uncertainty in the feed stream C_i; y_k is the conversion measurement at discrete time point k, where measurements are preformed every Δt seconds (the time between successive discrete observations); $v_k \sim N(0,r)$ is the analysis error) [5], [6].

$$\mathbf{x}_k = \mathbf{A}\mathbf{x}_{k-1} + \mathbf{B}_1\mathbf{u}_{k-1} + \mathbf{b}_2 w_{k-1} \qquad y_k = \mathbf{c}'\mathbf{x}_k + v_k \tag{4.A3}$$

In (4.A3) the system matrix **A** contains all the dynamics and kinetics from model (4.A1), and the input distribution $\mathbf{B}_1$ and $\mathbf{b}_2$ are the connection between deterministic and stochastic process input and the system, respectively. Measurement vector **c** selects the sampled process variable y_k from state vector $\mathbf{x}_k$.

The mass balances for C_i, C_m and λ_0 can be separated from the last five equations in (4.A1). This separation is possible because there is no backwards coupling between the last five equations and the first three. State vector $\mathbf{x}_k$ holds values for these first three process variables on equidistant grid-points over the reactor tube length. The values for the five remaining mass balances on every grid-point are determined numerically using the estimated state vectors as boundary conditions. The *process analyzer dynamics* as formulated in the theory section can be incorporated in the system by appropriately augmenting matrix **A** and state vector $\mathbf{x}_k$ [6].

The implementation of the Kalman state observer consists of two parts:

i) the state estimation time update (known as *a priori* estimate or '-', the state transition between two discrete measurements)

$$\hat{\mathbf{x}}_k^- = \mathbf{A}\hat{\mathbf{x}}_{k-1}^+ + \mathbf{B}_1\mathbf{u}_{k-1} \qquad \mathbf{P}_k^- = \mathbf{A}\mathbf{P}_{k-1}^-\mathbf{A}' + \mathbf{Q}^{\Delta t} \tag{4.A4}$$

ii) the state estimate measurement update (known as *a posteriori* estimate or '+', correcting the state estimate when measurement y_k becomes available)

$$\begin{aligned} &\hat{\mathbf{x}}_k^+ = \hat{\mathbf{x}}_k^- + \mathbf{k}_k\left(y_k - \mathbf{c}'\hat{\mathbf{x}}_k^-\right) \qquad \mathbf{P}_k^+ = (\mathbf{I} - \mathbf{k}_k\mathbf{c}')\mathbf{P}_k^- \\ &\mathbf{k}_k = \mathbf{P}_k^-\mathbf{c}(\mathbf{c}'\mathbf{P}_k^-\mathbf{c} + r)^{-1} \end{aligned} \tag{4.A5}$$

Where $\mathbf{k}_k$ is the observer gain, $\mathbf{P}_k$ is the theoretical estimation error covariance matrix, and $\mathbf{Q}^{\Delta t}$ is the uncertainty distribution covariance matrix. The matrix $\mathbf{Q}^{\Delta t}$ holds the contribution of the process disturbance w_k on the overall state estimation error, build up over the time period Δt

between two process measurements. For a stable system matrix **A** there is an upper bound on the system uncertainty covariance matrix by $\mathbf{Q}^{\Delta t}$ for $\Delta t \rightarrow \infty$. This $\mathbf{Q}^{\infty}$ corresponds to the maximum uncertainty in knowledge about the state of the process for the situation where no in-process measurements are implemented.
For linear time invariant systems the theoretical estimation error $\mathbf{P}_k$ can be calculated *a priori* by solving the associated equations in (4.A4) and (4.A5). When an analyzer/observer-combination is used to make an estimate, part of the uncertainty about the process state will be removed. Estimation error covariance matrix $\mathbf{P}_k$ then gives the process state uncertainty that remains. A suitable norm of the estimation covariance matrix $\mathbf{P}_k$ can thus guide the selection of optimal process analyzer and type and position. The matrix trace-norm – sum of all variances on the diagonal – is an appropriate choice here.

4.B Appendix - In this appendix we will briefly study the influence of the last component in the optimal process analyzer location problem: system parameter uncertainty. The first influence in location optimization was a purely deterministic one [5]: the dynamics of the system determine where in the process the analyzer will pick up the best/most information to estimate the system states. The next step was to define a particular process input disturbance and specify the measurement uncertainty in the form of *process analyzer dynamics* [6]. The outcome of this theory has been confirmed by experimental work in the main body of this chapter. In this appendix some theory is presented for the situation of uncertainty in the system parameters of the tubular reactor model for the polymerization of styrene. Three different types of parameter uncertainties and/or errors in process settings are introduced to illustrate their influence on process analyzer location: reactor contents temperature, reactor contents flux and initiator efficiency (see Table 4.B1). The motivations for selecting these three specific disturbances are as follows. In the main part of this chapter it is shown that the kinetic parameters for the polymerization reaction are estimated by so-called gain scheduling [52], using three thermo-couples in the reactor tube as inputs. The first disturbance - temperature - can thus be seen as a bias in these (primary) measurements and/or in our

knowledge of the reaction kinetics model. The second uncertainty - flux - symbolizes malfunctioning of the process instrumentation, which would be the pump in this case. Uncertainty in initiator efficiency is a representative of chemical change symbolizing e.g. pollution of the feed stream or a change in the feedstock. All system parameter uncertainties are assumed additive effects to the feed premix input disturbance used in the main text (first row in Table 4.B1).

Process Variable	Nominal Value	Uncertainty (σ)	Subplot
Initiator feed concentration	0.040mol.L^{-1}	0.010mol.L^{-1}	(a)
Reactor temperature	343.15K	0.10K	(b)
Material flux	2.04mL.min^{-1}	0.03mL.min^{-1}	(c)
Initiator efficiency*)	0.35-3.0X	0.01	(d)

*) X is degree of conversion **Table 4.B1**

The decision to cover the last component in optimal process analyzer positioning (system parameter uncertainty) in this appendix instead of the main body of this chapter is motivated by theory for linear(ized) systems. From Ito stochastic calculus we can make the following observation (in a rather informal notation; deterministic input neglected for convenience; see e.g. Jazwinski [33] for a detailed treatment):

$$\begin{aligned} &\dot{\mathbf{x}}(t) = (\mathbf{A} + \Delta\mathbf{A})\mathbf{x}(t) + \mathbf{b}w(t) \quad \mathbf{b}w(t) \sim N(0, \Sigma_p) \\ &\Rightarrow \dot{\mathbf{x}}(t) = \mathbf{A}\mathbf{x}(t) + \tilde{\mathbf{b}}w(t) \quad \tilde{\mathbf{b}}w(t) \sim N(0, \tilde{\Sigma}_p) \end{aligned} \tag{4.B1}$$

In (4.B1) the uncertainty in the system parameters is symbolized by matrix $\Delta\mathbf{A}$ (see (4.A3)). The equation shows that uncertainty in the parameters can be expressed by a modified input uncertainty $\tilde{\mathbf{b}}w(t) \sim N(0, \tilde{\Sigma}_p)$. Using the new state equation, all the theory used in the main text on e.g. (extended) Kalman state observers and the measurability factor remains valid. The new process covariance matrices $\tilde{\Sigma}_p$ in (4.B1) are found through error propagation.

The uncertainties as specified in Table 4.B1 and the reactor model in (4.A1) are used to generate a hundred new tubular profiles. From these

profiles a reactor profile covariance matrix is computed. This new profile is added to the covariance structure due to feed premix uncertainty. This new covariance matrix is used in equations (4.A4), (4.A5) and (4.5) to compute the measurability factors for the new situation. In this appendix we will limit the selection of process analyzers to in-line SW-NIR at different positions along the tube.

It must be pointed out that the uncertainty in state estimation due to parameter uncertainty as used in this appendix is rather conservative (almost a 'worst-case-scenario'). In real implementations the theoretical covariance matrix found by the error propagation method can be significantly reduced, still leading to good state estimations. E.g. process uncertainty in reactor temperature, and hence in the kinetic parameters, due to a day-night rhythm would in our case be modeled as random noise over a long time period. In more advanced applications an adaptive scheme can be used to eliminate the systematic errors over shorter periods (e.g. day- versus nighttime), very likely improving the tracking performance of the observer by working with a more realistic error covariance by a 'adaptive' scheme [32], [53].

Figure 4.B1 shows the results for in-line SW-NIR product and state estimation under influence of the different parameter uncertainties. The result for only initiator feed uncertainty as used in the main text is repeated in plot (a). From the results in the figure we observe two things. The first one is that the overall measurability profiles are lower when additional uncertainty is introduced. This is to be expected since the estimation task becomes considerably more difficult. Besides the estimation error as a function of the *process analyzer dynamics* an additional error propagates through the state estimation procedure, increasing the expected estimation error in (4.A5).

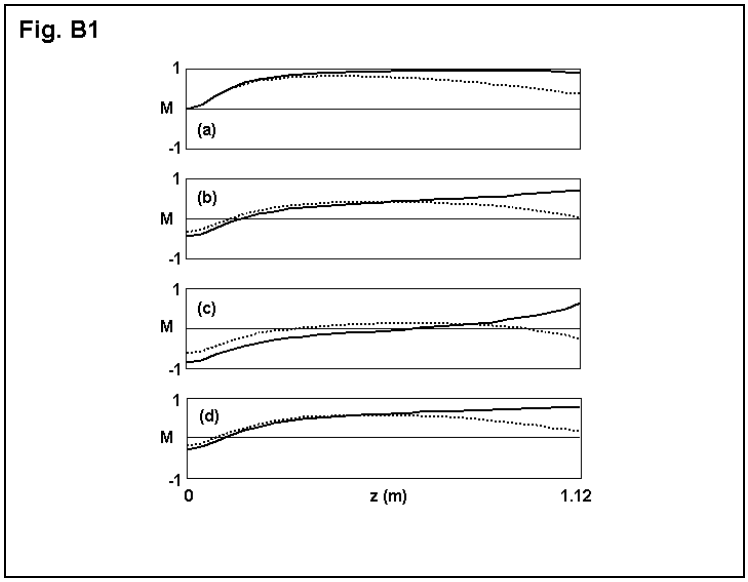

Fig. 4.B1 Measurability factor *M* as a function of in-line SW-NIR on position *z* in the reactor tube. Optimized for product composition ('—') or entire tube contents ('..'); see Table 4.B1 and text for details on subplots (a)-(d).

The second observation is that system parameter uncertainty can also change the shape of the measurability profile. In the case of estimation reactor product composition (solid lines) the optimum tends to shift downstream towards the reactor outlet. The additional parameter uncertainty makes in-process measurement at e.g. halfway the reactor tube inadequate for the product state estimation task. Keeping in mind the two contributions in the state observer – 'measurement update' and 'time update' (4.A4)-(4.A5) – we come to the following conclusion. The parameter uncertainties in this appendix mainly affect the latter: the use of the dynamic process model to propagate the system state through time. Estimating e.g. the product composition at the reactor outlet (solid lines) from a measurement halfway in the tube is not feasible. The error that results using these measurements in combination with the relative poor dynamic model to extrapolate the state estimate to the product/reactor outlet is too large. For process analyzers close to the reactor exit we do not have this problem, and the figure shows that the measurability factor stays nearly the same for this position.

When estimating the entire tube contents (broken lines) we find a similar shape for all disturbances with a change in absolute value of the measurability factor curve. In this situation the measurement results have to be extrapolated towards reactor entrance and exit. For this reason the estimation error due to parameter uncertainty now acts as a 'offset',

leading to systematic worst state observer performance as a function of the error in dynamic system model.

5. Selection and Positioning: Batch Processes

Some observations on NIR Process Analyzer in combination with a State Observer in a Batch Styrene Polymerization Reactor

5.1 Introduction - In this chapter we will focus our attention on a batch process for the polymerization of styrene to polystyrene. One question we will answer is that of optimal process analyzer implementation/operation. The difference with previous chapters is that a batch processes has no spatial dimension (we assume a batch to be a well stirred vessel). Therefore, the question of optimal analyzer operation is redefined for temporal problems: what point in the process is the best time to collect a sample/perform a measurement.

In this chapter we will also illustrate some ideas on the process analyzer and state observer combination for predictive process monitoring using data from a bench scale styrene/polystyrene reactor. The conclusion from this part of the chapter is that the combination of a good process model and a high quality in-process measurement (side-loop NIR for styrene conversion, in this case study) can have enormous potential for process monitoring and control[*)].

We will use simulations on a batch process to answer the question of sampling optimization. In this chapter we will also explain some of the underlying theory on systems and observers used in previous chapters. The reason for withholding this part until now is the considerable reduction of the model complexity for batch process compared to distributed parameter systems (DPS) as e.g. a tubular reactor. The first can be modeled with eight variables (or even as little as two in the reducing assumptions used in this chapter), while in the latter systems the large number of process variables required can easily obscure the understanding of the system and state observer. The 'price to pay' is the non-linearity of batch operations. Where the DPS's in the previous chapters were well approximated by a linear system, leading to good state estimations and simple computations for e.g. uncertainties, the batch

[*)] Batch polymerization data used in this chapter was kindly supplied by Henk Lousberg, University of Amsterdam.

system used in this chapter require extensive simulations to determine error propagation of external disturbances and process analyzer dynamics.

5.2 Styrene Polymerization System - In this chapter we use a batch system model for initiator driven, free-radical bulk polymerization of styrene [46]. Mass balances in the form of differential equations are required for initiator concentration C_i, styrene monomer C_m, the first three moments for chain length distribution of growing (λ) and terminated polymer chains (μ). Equation (5.1) shows the mathematical model of the batch reactor [48].

$$\frac{dC_i(t)}{dt} = -k_d C_i(t) \tag{5.1a}$$

$$\frac{dC_m(t)}{dt} = -k_p C_m(t)\lambda_0(t) \tag{5.1b}$$

$$\frac{d\lambda_0(t)}{dt} = -k_t\lambda_0^2(t) + k_{sp}C_m^2(t) + 2fk_d C_i(t)$$
$$\Rightarrow \lambda_0(t) = \sqrt{\frac{2fk_d C_i(t)}{k_t}} \tag{5.1c}$$

$$\frac{d\lambda_1(t)}{dt} = -k_t\lambda_0(t)\lambda_1(t) + k_{sp}C_m^2(t) + 2fk_d C_i(t) + k_p C_m(t)\lambda_0(t) - k_{trm}C_m(t)(\lambda_1(t) - \lambda_0(t))$$
$$\Rightarrow \lambda_1(t) = \frac{2fk_d C_i(t) + k_p C_m(t)\lambda_0(t)}{k_t\lambda_0(t) + k_{trm}C_m(t)} \tag{5.1d}$$

$$\frac{d\lambda_2(t)}{dt} = -k_t\lambda_0(t)\lambda_2(t) + k_{sp}C_m^2(t) + 2fk_d C_i(t) + k_p C_m(t)(2\lambda_1(t) + \lambda_0(t)) - k_{trm}C_m(t)(\lambda_2(t) - \lambda_0(t))$$
$$\Rightarrow \lambda_2(t) = \frac{2fk_d C_i(t) + 2k_p C_m(t)\lambda_1(t) + (k_p + k_{trm})C_m(t)\lambda_0(t)}{k_t\lambda_0(t) + k_{trm}C_m(t)}$$

(5.1e)

$$\frac{d\mu_0(t)}{dt} = (1 - 0.5z_t)k_t\lambda_0^2(t) + k_{trm}C_m(t)\lambda_0(t) \tag{5.1f}$$

$$\frac{d\mu_1(t)}{dt} = k_t\lambda_0(t)\lambda_1(t) + k_{trm}C_m(t)\lambda_1(t) \tag{5.1g}$$

$$\frac{d\mu_2(t)}{dt} = k_t\lambda_0(t)\lambda_2(t) + k_t z_t\lambda_1^2(t) + k_{trm}C_m(t)\lambda_2(t) \tag{5.1h}$$

From (5.1) the number M_n and weight average molar masses M_w can be computed (M_m = 104.15 g.mol^{-1}).

$$M_n(t) \approx M_m \frac{\mu_1(t)}{\mu_0(t)} \qquad M_w(t) \approx M_m \frac{\mu_2(t)}{\mu_1(t)} \tag{5.2}$$

The nominal operation conditions for this system will be set as follows: batch temperature T = 75°C (all temperature dependent constants are determined via gain scheduling [52]), initiator concentration at time zero C_i = 0.015mol.l^{-1} and batch termination at 180 minutes. The external disturbance to the process is an uncertainty in initiator charge of σ_{Ci} = 0.001mol.l^{-1}. Figure 5.1 shows the time profiles for initiator, degree of conversion and polymer molar mass distribution (MMD) for the normal batch operation and disturbances of $\pm 3\sigma_{Ci}$.

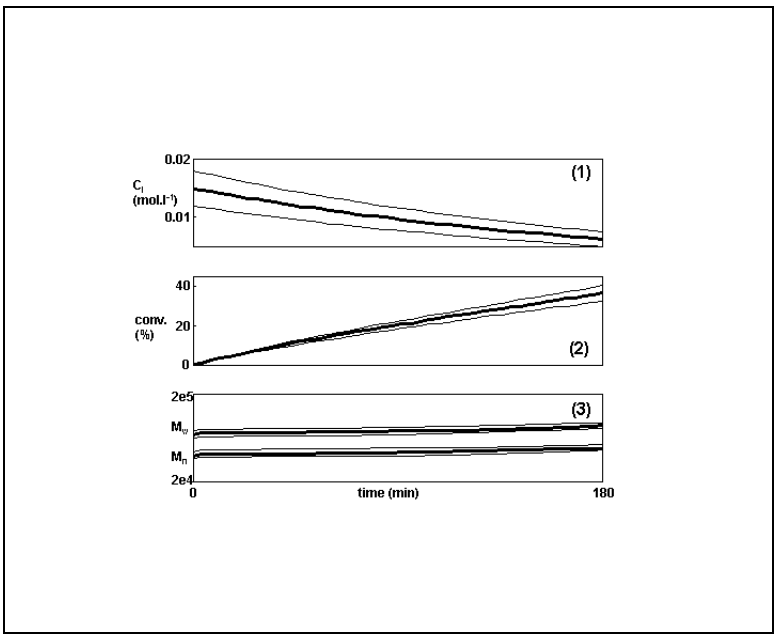

Figure 5.1 Simulated batch time profiles for nominal operation (solid line) and $\pm 3\sigma_{Ci}$ disturbances (thin lines); 1) initiator concentration; 2) styrene degree of conversion; 3) $\log_{10} M_n$ and M_w moments of polystyrene MMD.

Based on chemical and physical inside of the reaction mechanisms, the so-called Quasi Steady State- (QSSA) and Long Chain Assumption (LCA) [48], the system can be split up into three parts. Equations (5.1a-b) – the two mass balances of most importance for the monitoring objective presented below – can be separated from the moments for growing and terminated polymer chains. A way to determine batch time trajectories is to solve (5.1c-e) analytically, while the later three (5.1f-h) can be determined using the outcomes of (5.1a-e) as inputs. An alternative way to interpret this observation is to say that the system is 'stiff' or 'singular perturbed': the three different parts of the system operate in a different time modes. The C_i-C_m balances operate on a time scale of seconds, while growing polymer chains for this system exist no longer than milliseconds

(and in the alternative formulation in (5.1) are defined to change instantaneously) [46]. The MMD terms have an accumulative nature, and are thus expected to be effective on a much longer time scale for this process with a nominal runtime of 180 minutes. To illustrate this observation the non-linear system in (5.1) has been linearised around different, equidistant points on the nominal batch run time-axis. The eigenvalues of this linearised system are plotted in Figure 5.2. The three eigenvalues associated with (5.1c-e) are zero for every time point and not shown in the figure. Although they are connected through the system, and can as such not be assigned individually, the three 'fast' eigenvalues are more closely related to the MMD in (5.1f-h), while the two intermediate ones are associated with (5.1a-b).

In the remainder of this work we will always assume the reduced system (5.1a-b) to be the dynamic ('real-time') part of the model, while the other variables can be determined at convenience.

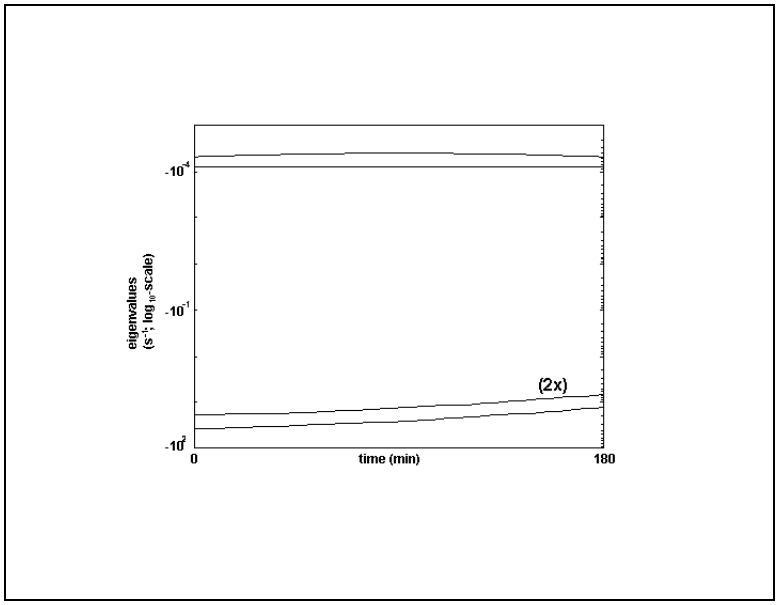

Figure 5.2
Eigenvalues for linearized styrene polymerization process model on equidistant time point in a batch run.

5.3 Extended Kalman State Observer - In this chapter we use the well-established extended Kalman observer to estimate the state for every point in time of the polystyrene batch reactor from NIR measurements on styrene concentration [32], [33], [42]. In this paragraph we will give a short description of state observers, the (extended) Kalman observer and the way we implemented and used the observer to monitor the polymerization process. To simplify notation we first introduce the state-

vector $\mathbf{x}$ = [C_i(t) C_m(t)]' for our batch reactor containing the two variables - initiator and monomer concentration - of interest in our estimation problem. Combining the state-vector concept with equations (5.1) we can construct the state-space equation for our reactor system.

$$\dot{\mathbf{x}}(t) = \begin{bmatrix} \dot{C}_i(t) \\ \dot{C}_m(t) \end{bmatrix} = \begin{bmatrix} -k_d C_i(t) \\ -k_p C_m(t)\sqrt{2fk_d/k_t}\sqrt{C_i(t)} \end{bmatrix} + \begin{bmatrix} w_i(t) \\ w_m(t) \end{bmatrix} = a_c(\mathbf{x}(t)) + \mathbf{w}(t) \quad (5.3)$$

Equation (5.3) is the non-linear system for describing the transitional behavior of our batch reactor. The term $\mathbf{w}(t) \sim N(0,\mathbf{Q}(t))$ in (5.3) is the (stochastic) uncertainty for the state elements, assumed to be zero mean, normally distributed with process noise covariance $\mathbf{Q}(t)$. The latter uncertainty is a summation of both external disturbance acting upon the reactor system and 'internal' disturbances (e.g. errors in our knowledge of the reactor kinetic, errors introduced by numerical approximations in the state observer, etc.). The reaction rate constants in (5.3) are computed from temperature measurements inside the reactor vessel, a gain scheduling approach to linearization of the Arrhenius equations in (5.1) [52].

NIR-measurements on monomer concentration are determined every minute. To use these measurements in the state observer we rewrite the system (5.3) into equation (5.4) on a discrete time-scale t_k - t_{k+1} of 60 seconds.

$$\mathbf{x}_{k+1} = a_d(\mathbf{x}_k) + \mathbf{w}_k \quad \mathbf{w}_k \sim N(0,\mathbf{Q}_k) \qquad C_m(k) = \mathbf{c}'\mathbf{x}_k + v_k \quad v_k \sim N(0,r_k) \quad (5.4)$$

In equation (5.4) the measurement vector $\mathbf{c}$ = [0 1]' samples the measured variable - concentration monomer in our case - from the state-vector. We assume that the estimated concentration is corrupted by a zero mean, normally distributed noise with variance r_k.

The non-linear system in equation (5.4) can be linearized around a known state $\mathbf{x}_k$ by computing a first order Taylor approximation for the function a_d [49].

$$\mathbf{A}_k = \frac{\partial a_d(\mathbf{x})}{\partial \mathbf{x}}\Big|_{\mathbf{x}=\mathbf{x}_k} = \begin{bmatrix} -k_d & 0 \\ k_p C_m(k)\sqrt{2fk_d/k_t}\,0.5C_i(k)^{-0.5} & -k_p\sqrt{2fk_d/k_t}\sqrt{C_i(k)} \end{bmatrix} \tag{5.5}$$

From this local approximation we can determine a linear state-space model applicable around state-vector $\mathbf{x}_k$.

$$\mathbf{x}_{k+1} = \mathbf{A}_k\mathbf{x}_k + \mathbf{w}_k \qquad C_m(k) = \mathbf{c}'\mathbf{x}_k + v_k \tag{5.6}$$

The observer as implemented in this chapter has no knowledge of the true, underlying system. The only direct information about our process state is the measurement of $C_m(k)$. Our best estimate of the true system state $\mathbf{x}_k$ will have a form equal to (5.6).

$$\hat{\mathbf{x}}_{k+1} = \mathbf{A}_k\hat{\mathbf{x}}_k \qquad \hat{C}_m(k) = \mathbf{c}'\hat{\mathbf{x}}_k \tag{5.7}$$

Subtracting (5.7) from (5.6), using the assumption $E(\mathbf{w}_k) = E(v_k) = 0$ and specifying the state estimation error $\mathbf{e}_k = \mathbf{x}_k - \hat{\mathbf{x}}_k$.

$$\mathbf{e}_{k+1} = \mathbf{A}_k\mathbf{e}_k \qquad C_m(k) - \hat{C}_m(k) = \mathbf{c}'\mathbf{e}_k \tag{5.8}$$

The state observer is based on (5.8) correcting the state estimation error by the weighted difference between estimated and measured monomer concentration [54], [55].

$$\mathbf{e}_{k+1} = \mathbf{A}_k\mathbf{e}_k - \mathbf{k}(C_m(k) - \hat{C}_m(k)) = (\mathbf{A}_k - \mathbf{k}\mathbf{c}')\mathbf{e}_k \tag{5.9}$$

From (5.9) we conclude that the estimation error $\mathbf{e}_k$ will vanish if the observer equation is stable. This stability is realized if all eigenvalues or observer poles of the matrix ($\mathbf{A}_k$ - $\mathbf{k}\mathbf{c}'$) are positioned inside the unit circle [54]. If the system is observable, which is the case for our reduced reactor model (5.3), any desired transient behavior of the observer can be achieved by selecting the appropriate gains $\mathbf{k}$ (so-called observer pole-

placement). If the system is detectable only the observable part of the observer can be 'tuned' in this way.

Based on equations (5.3)-(5.6) we construct an extended Kalman observer, comparable to the state estimator in equation (5.9), consisting of the following two steps:

i) the state estimation time update (*a priori*)

$$\begin{aligned}\hat{\mathbf{x}}_{k+1}^{-} &= a_d(\hat{\mathbf{x}}_k^{+}) \\ \mathbf{P}_{k+1}^{-} &= \mathbf{A}_k \mathbf{P}_k^{-} \mathbf{A'}_k + \mathbf{Q}_k\end{aligned} \tag{5.10}$$

ii) the state estimate measurement update/correction (*a posteriori*)

$$\begin{aligned}\mathbf{k}_{k+1} &= \mathbf{P}_{k+1}^{-}\mathbf{c}(\mathbf{c'}\mathbf{P}_{k+1}^{-}\mathbf{c} + r_k)^{-1} \\ \hat{\mathbf{x}}_{k+1}^{+} &= \hat{\mathbf{x}}_{k+1}^{-} + \mathbf{k}_{k+1}\left(C_m(k+1) - \mathbf{c'}\hat{\mathbf{x}}_{k+1}^{-}\right) \\ \mathbf{P}_{k+1}^{+} &= (\mathbf{I} - \mathbf{k}_{k+1}\mathbf{c'})\mathbf{P}_{k+1}^{-}\end{aligned} \tag{5.11}$$

where $\mathbf{k}_{k+1}$ is the Kalman filter gain, $\mathbf{P}_{k+1}^{+}$ is the theoretical estimation error covariance matrix and $C_m(k+1)$ is the NIR-measurement outcome for time $k+1$. From the state estimates - under LCA and QSSA - we can determine the moments of living polymer analytically via equation (5.1c-e) and moments of the death polymer by solving equation (5.1f-h) numerically.

For a detectable system the observer poles in equation (5.9) for the Kalman are assured to be stable. Furthermore, the Kalman observer implemented in (5.10)-(5.11) is an unbiased, minimum variance and consistent estimator for the process state of the linearised system [32], [33], [42]. From the equations the performance of the state observer can be seen as governed by the (relative ratio of) covariance matrices r_k and $\mathbf{Q}_k$ for measurement and system uncertainty, respectively. The first can easily be obtained from the calibration stage of the NIR-spectrometer measurements: r_k = [0.026mol.L^{-1}]^2. System uncertainty $\mathbf{Q}_k$ however is often considered a tuning parameter, establishing a desirable performance of the state observer. The experiments presented in this chapter consist of eight styrene polymerization batches: six 'on-spec' batches run at

different temperatures and initiator concentrations, and two 'off-spec' batches with deliberately induced disturbances (see result section). We have used the first six batches to 'calibrate' the Kalman observer to a desirable response, resulting in the following system uncertainty matrix.

$$\mathbf{Q}_k = \begin{bmatrix} 1.0 \cdot 10^{-7} & 0 \\ 0 & r_k \end{bmatrix} \tag{5.12}$$

The Results section of this chapter will demonstrate that the speed and accuracy of the in-line NIR-analysis allows us to place great confidence in the measurement part of the observer equation. Note that the Kalman observer is just one choice for observer pole placement. For other monitoring or control tasks different choices might be better suited [52], [56].

In the remainder chapter we will use the Kalman observer both as filter, where we improve the current state estimate by using the measurements up to that point, and as predictor. In the latter we propagate both the state and the estimation error in (5.10) towards the batch termination time. For prediction we obviously not correct our estimates through a measurement update (5.11) since no future measurements are available. This prediction will turn out to be a powerful monitoring mechanism to detect e.g. unexpected batch behavior due to external disturbances or small deviations from expected initial conditions in the batch charge.

5.4 Optimal Sampling Time-point in a Batch Run - In this paragraph we will develop a method to determine the best time to sample the polymerization process described in the first part of this chapter. We limit the theory to one specific example: the only process analyzer considered is on-line NIR-spectroscopy for degree of conversion. We assume measurement uncertainty σ_i = 0.3% to be the only 'process analyzer dynamics' contribution of importance, neglecting e.g. delay time. This corresponds to the analyzer performance for the real batch data used in this chapter. The disturbance to the process is an uncertainty in initiator charge as explained before. The motivation for selecting initiator charge

as external disturbance stems from the experiments with the real batch data, as will become clear later on. We are interested in estimating degree conversion during the batch run, determined by a state observer and the NIR-measurement result. Two analyzer/observer objectives will be investigated: how well can we determine initiator concentration and degree of conversion over the entire batch run (180min) using one (or two) NIR measurements, and how well can we estimate initiator concentration and degree of conversion at batch termination (at time = 180min) from one (or two) measurements. Note that this 'single shot' is an extreme form of the extended Kalman filter. At one point during a batch run we perform a measurement, the system is linearized around that point, and our estimate of the batch trajectory is improved from that single measurement.

The first step is to determine total process uncertainty for initiator and monomer. A total of 2000 batches where simulated using the nominal operating conditions and a normally distributed initiator concentration $N(0.015,0.001)$. From these results the uncertainty in knowledge can be determined and expressed as an average squared error deviation between nominal and simulated batch run ($\mathbf{Q}_{\text{true}}$; the $\pm 3\sigma_{Ci}$ uncertainty lines Figure 5.1 give a good impression of this simulated system uncertainty). This error interval would form our best guess if no measurements were performed. The next step is to determine gains for the state observer (5.9). Again 2000 simulations with measurement errors were used for this purpose, where the average Kalman gain over batch time – shown in Figure 5.3 – is determined. The last step is to simulate in-process measurements in a batch run and compute the remaining uncertainty, this time expressed as the average squared error between estimated and simulated batch run ($\mathbf{Q}_{\text{error}}$). From these two uncertainties we compute the measurability factor:

$$M = \frac{trace(\mathbf{Q}_{true}) - trace(\mathbf{Q}_{error})}{trace(\mathbf{Q}_{true})} \qquad (5.13)$$

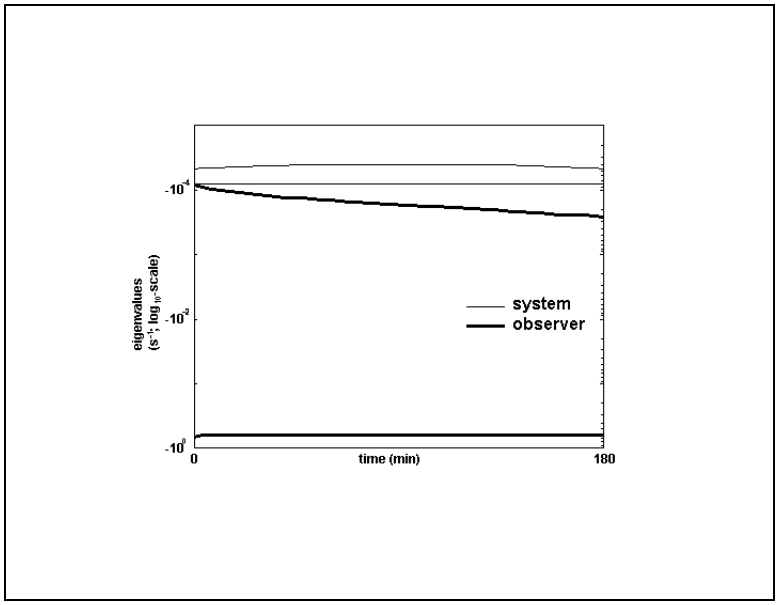

Figure 5.3 System (thin line) and observer poles (solid line) for the nominal styrene polymerization batch.

The results of these simulations for one single measurement are shown in Figure 5.4. In the upper left plot of this figure we see that the best time-point when estimating over the entire batch run is slightly past half the termination time. If we are only interested in the process state at batch termination we can expect reliable results (M > 0.8) after approximately 120min. To illustrate the sensitivity in relation with process conditions the same computations are performed for initiator concentration C_i = 0.010mol.L^{-1} and temperature T = 70°C; see Figure 5.4. From this figure we see that the measurability for T = 70°C is slightly lower. This is due to the lower degree of conversion for these process conditions in relation to the estimation error for NIR-analysis.

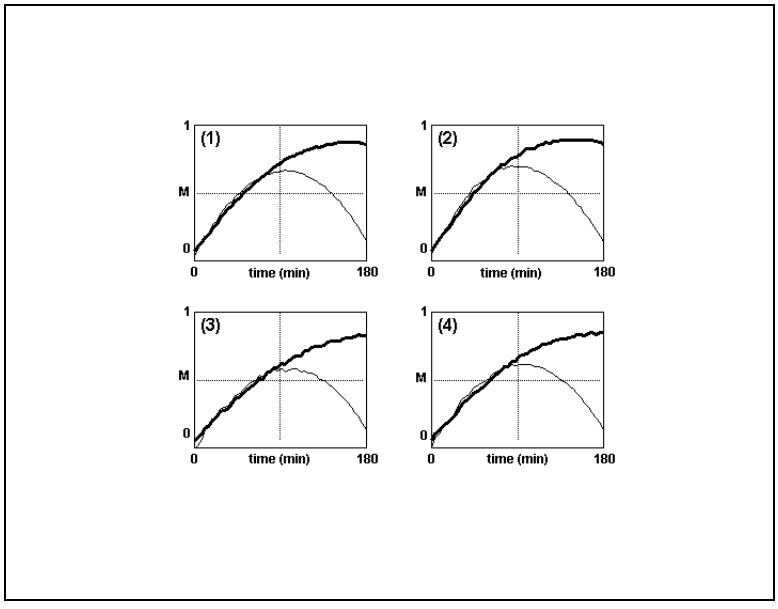

Figure 5.4
Measurability factor for entire batch run (thin line) and batch termination (solid line). 1) C_i = 0.015mol.L^{-1}, T = 75°C; 2) C_i = 0.010mol.L^{-1}, T = 75°C; 3) C_i = 0.015mol.L^{-1}, T = 70°C; 4) C_i = 0.010mol.L^{-1}, T = 70°C

Figure 5.5 and 5.6 show similar results when allowing two measurements during a batch run. The two figures are obviously symmetric on the 'forbidden line' where time on the x- and y-axis is the same. The overall performance of the measurability improves considerably. The optimal time sample time-points when allowing for two measurements when estimating the entire batch are found in the area 90-130 minutes (half-batch time). When estimating process values for batch termination the best results remain those based on measurements performed after approximately 120 minutes. Notice however that reliable results ($M > 0.8$) can already be retrieved from two measurements within 90 minutes batch-time.

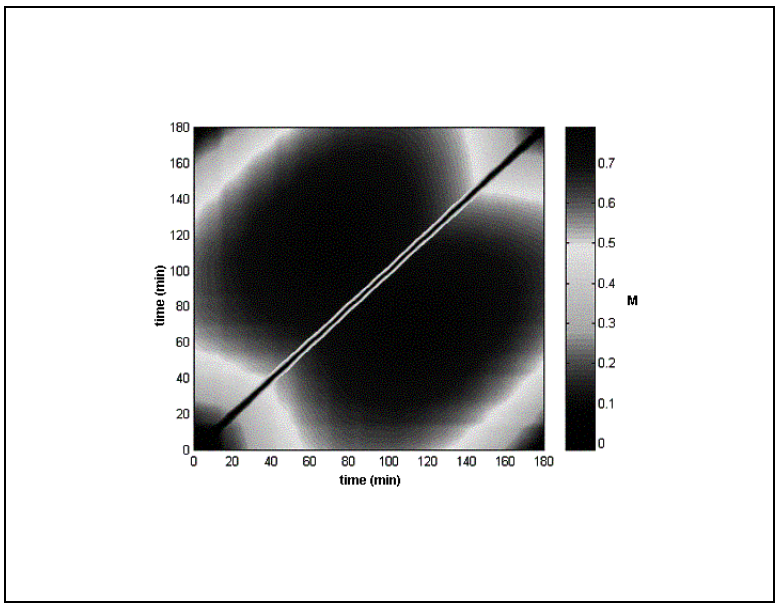

Figure 5.5 Two measurements measurability landscape for entire batch run.

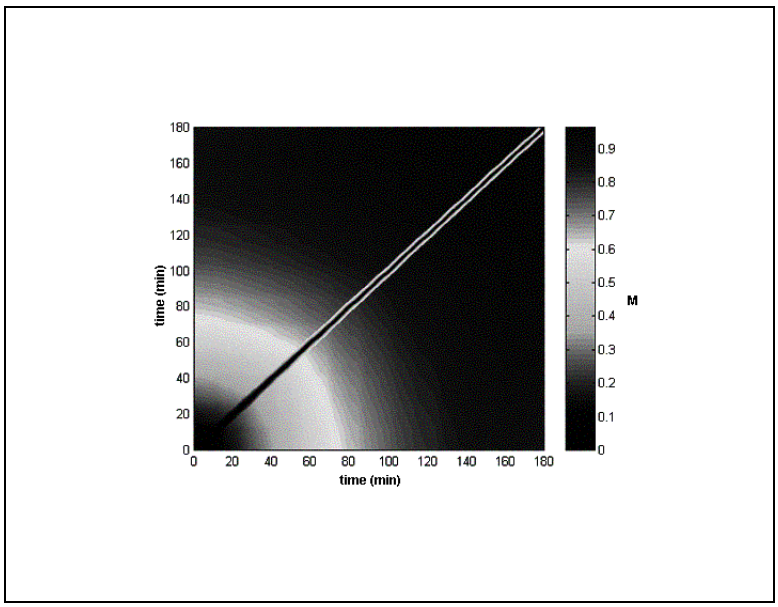

Figure 5.6 Two measurements measurability landscape for batch termination.

The experimental data available from the polystyrene batch system is unfortunately not collected to conform the theory as presented in this paragraph. It turns out that the very limited amount of data is not suitable to establish a direct link with concepts explained in this paragraph. Instead we will present some potential applications for 'hard models' in combination with in-process analyzers in the remainder of this chapter.

5.5 Results for 'Predictive Batch Monitoring' - The data presented in this chapter is taken from of eight styrene polymerization batches experiments. Six on-spec runs we performed with different reactor temperatures between 70-80°C and initiator concentrations between 0.005-0.030mol.L^{-1}. The results on two of these on-specs A and B will be presented in this section. Two more batch-experiments - C and D - where performed introducing (deliberate) process disturbances. The experimental settings of the four runs are given in Table 5.1. The measured temperature profiles of the four batch runs are shown in Figure 5.7.

Batch	temp. (°C)	C_I (mol.L^{-1})	run length (min.)	Disturbance At t = 60min.
A	75	0.0150	180	---
B	80	0.0300	60	---
C	70	0.0050	180	temp. step 70 → 80°C
D	70	0.0009	180	init. impulse of 0.0400mol.L^{-1}

Table 5.1

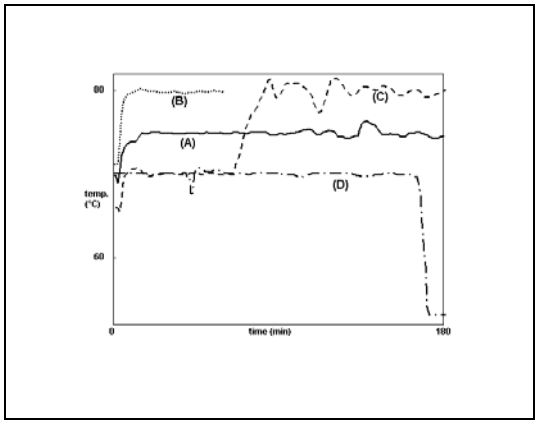

Figure 5.7 Temperature records of the four batch-runs A-D.

The results for on-spec batch A are shown in Figure 5.8. In the upper left plot shows estimated styrene conversion using equations (5.10)-(5.11) as a function of time together with the conversion determined by the XSEC reference method on fifteen samples [8]. The upper right plot shows the computed MMD-parameters $\log_{10}$ M_n and M_w together with the reference values determined by SEC-analysis. The lower-left plot in Figure 5.8 shows the predicted conversion for batch termination plus the one standard deviation uncertainty boundaries of the estimation error determined by equation (5.10). Conversion at batch termination is predicted every time a NIR-measurement is done (once a minute). The target value for conversion on batch termination is also plotted, which in our case is just the conversion after 180 minutes determined from the reference method. The lower right plot shows the predicted $\log_{10}$ M_n and M_w for batch termination together with the target values, again selected to be the last reference measurements of the reactor contents. Although the gain in (5.11) for the extended Kalman observers is computed anew for every measurement update, it remains almost constant at **k** = [-0.004 0.6]' for the entire 180 minutes. Using this gain vector the observer poles in (5.9) stay well within the stable region, as is to be expected from Kalman observer theory.

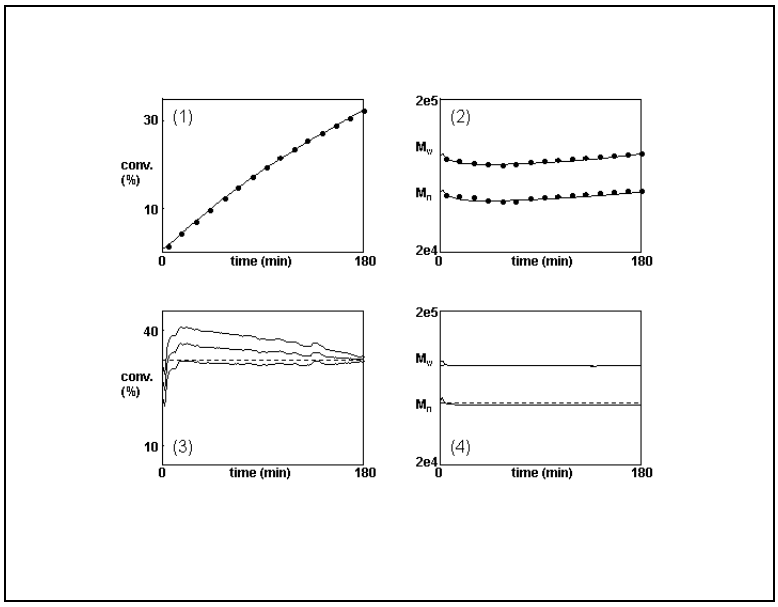

Figure 5.8 Results for batch A; 1) estimated conversion ('-') and reference values ('•'); 2) estimated $\log_{10}$ M_n and M_w ('-') and reference values ('•'); 3) predicted conversion for batch termination plus $\pm 1\sigma$ boundaries ('-') and target value ('- -'); 4) predicted $\log_{10}$ M_n and M_w for batch termination ('-') and target value ('- -').

Figure 5.9 shows the comparable plots for on-spec batch B, the main difference being that this batch is terminated after 60 minutes. The observer gain for this batch remains almost constant for the entire 60 run time at **k** = [-0.002 0.6]'.

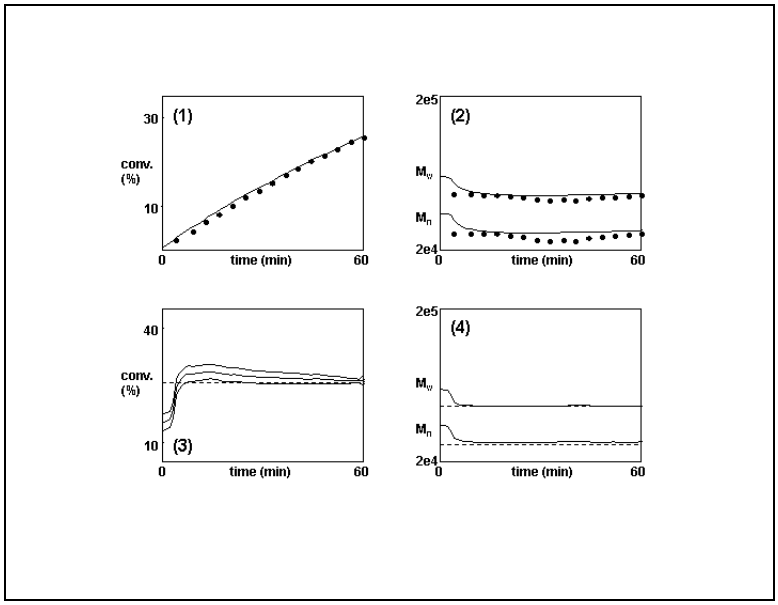

Figure 5.9 Results for batch B; see Figure 5.8.

The results for off-spec batch C are plotted in Figure 5.10. One clearly recognizes the (sluggish) change in batch operation induced at 60 minutes in the batch run. The observer gain before the disturbance has an average size of **k** = [-0.002 0.6]'. When the new operating regime has settled the observer gain has converged to **k** = [-0.005 0.6]'.

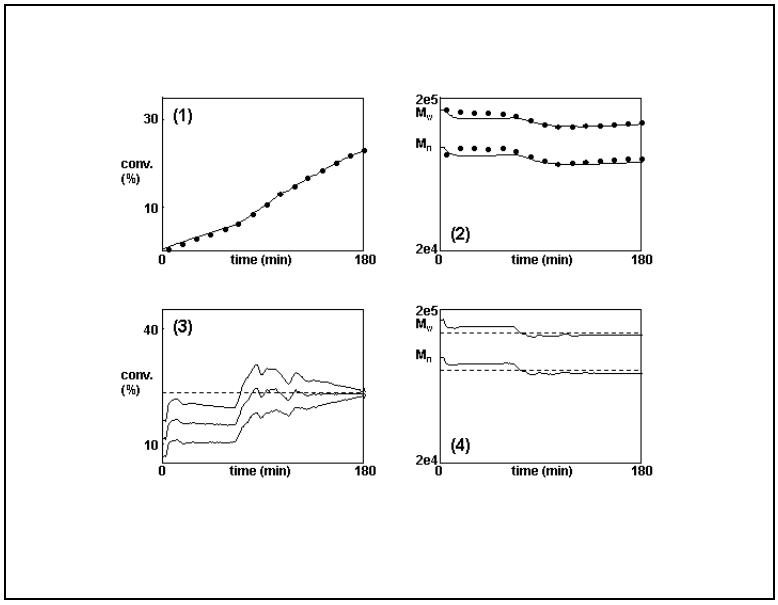

Figure 5.10 Results for batch C; see Figure 5.8.

The results for off-spec batch D are plotted in Figure 5.11 (beware of the different y-axis scaling). To handle the severe initiator disturbance for this

batch run the initiator uncertainty in equation (5.12) is increased to σ^2_{Ci} = 200x10^{-7} mol^2.L^{-2}, keeping the monomer uncertainty constant at r_k. This way we reduce our confidence in the system model, thereby favoring the measurement update part in the in the Kalman filter equations (5.10) and (5.11). The first 60 minutes of the results are rather noisy. This is a consequence of the high observer gains (**k** = [-0.085 0.7]') and the low signal for conversion measurements (only a 2.5% conversion after 60 minutes). After the disturbance the observer estimates converge towards the correct process state, but a considerate bias remains present.

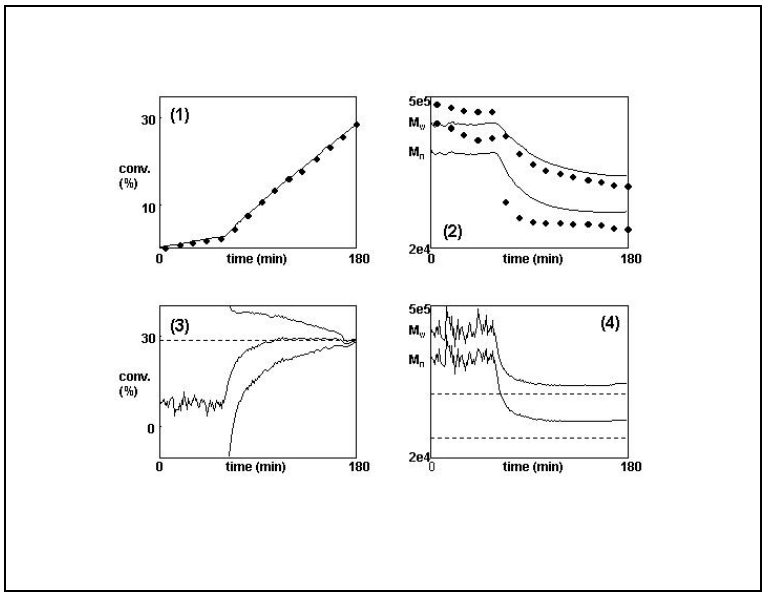

Figure 5.11 Results for batch D; see Figure 5.8.

The results in Figure 5.11 treat the initiator change in batch D as a disturbance. This enormous system upset seems rather unrealistic in actual production processes. We therefore show some additional results where the initiator pulse is considered a control action. The state observer is fed with information of the approximate magnitude of the regulator action. This estimation task is comparable with the batch charge error for on-spec batches, and the original system uncertainty matrix $\mathbf{Q}_k$ from (5.12) can be used. The results are shown in Figure 5.12. The control action at 60 minutes is clearly visible in both the estimations and predictions. The observer gain before the initiator pulse is on average **k** = [-0.005 0.6]'. After settling the new observer gain is approximately **k** = [-0.002 0.6]'. Under the more realistic assumptions the estimations for batch D improve notably.

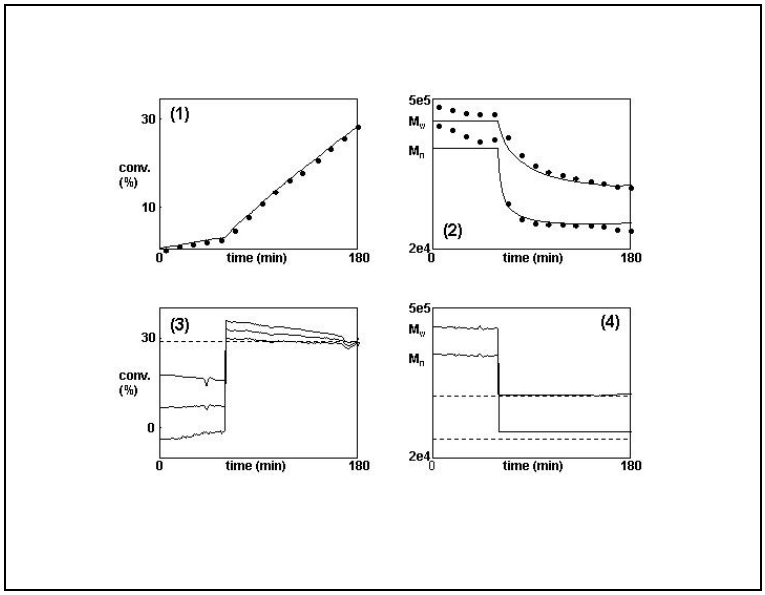

Figure 5.12 Results for batch D; see Figure 5.8.

The information as presented in Figure 5.8-5.12 is of course not available during a process run. To illustrate the potential of state observers Figure 5.13 gives three 'snap-shots' of an on-line monitoring chart for batch run D. Estimated and predicted conversion for time points 55, 65 and 120 minutes are plotted together with the one standard deviation boundaries for the prediction part and the reference value at batch termination. From these plots we see that shortly after the new process conditions are introduced (at time = 60 minutes) we get a good impression of the rest of our run and the expected process state at batch termination.

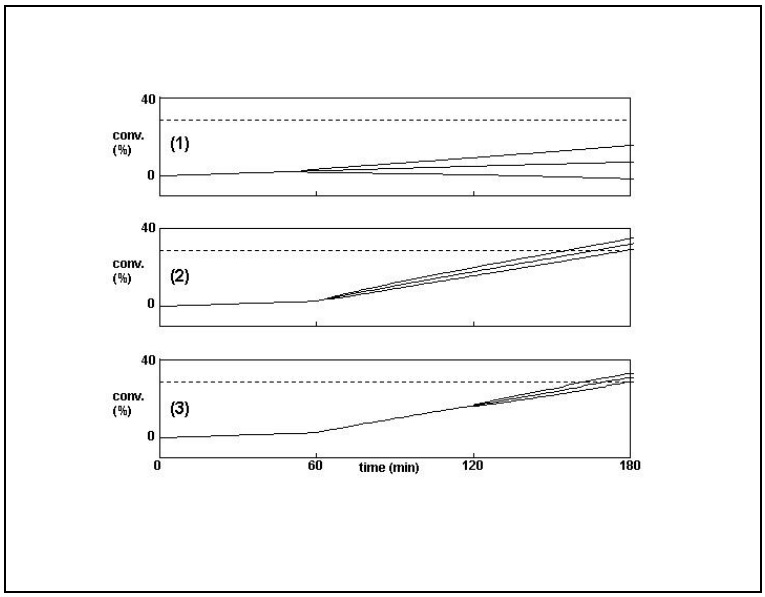

Figure 5.13 Monitoring chart for batch D; estimated conversion and predicted $\pm 1\sigma$ boundaries for conversion at termination ('-') and reference values ('- -') for (1) 55, (2) 65 and (3) 120 minutes.

5.6 Conclusions - In this chapter we present the application of an extended Kalman observer for monitoring the state of a styrene to polystyrene batch reactor [32], [33], [42]. Through both the Long Chain- and Quasi Steady State Assumption we are able to significantly reduce the original dynamic reactor model in (5.1) into a dynamic model for the initiator and monomer concentration and analytical and numerical solutions for the moments of living and death polymer moments. The fast and accurate in-process Near Infrared spectroscopic measurements for degree of conversion, together with temperature readings on the reactor contents, form a reliable measurement scheme to implement the dynamic state observer. Using six on-spec batches - of which two examples are included in the results - the system uncertainty is estimated.

We briefly show how simulations can function to find the optimal sampling time(s) in a batch process. The results do illustrate the possibility of optimizing in-process measurement schemes for a batch processes. This optimization strategy forms an alternative for the tactics presented in previous chapters. In the earlier work we used statistical error propagation in the optimization procedures, while in this chapter exhaustive simulation of the nonlinear system are used to find optima.

First focusing our attention on the on-spec batches A and B in Figures 5.8-5.9, we observe that both state estimation and prediction perform really well. Estimated trajectories show good correspondence with the reference XSEC and SEC values. From the prediction we see that there is a small deviation in the beginning of each batch. This is due to a small uncertainty in the batch initiator charge. The expected values (the batch recipe) are used as initial conditions to start up the dynamic state observer. In the measurement update part of the observer a mismatch between expected and measured process state is detected, and a combination of fast and accurate in-process measurements assures a rapid convergence towards the true process state. Combining this with a reliable process model guarantees a good prediction of the MMD moments.

Similar conclusions can be drawn for the off-spec batches C and D presented in Figure 5.10-5.12. Conversion can be estimated fairly accurate, and the computed moments M_n and M_w are in good agreement with the reference values. The small deviation in the beginning of batch D

is due to disagreement between the process conditions at that stage (extremely low initiator concentration) and the polymerization model used in this chapter. The monitoring charts in Figure 5.13 illustrate the potential use of state estimator and predictor for process monitoring.

References

[1] J.B.Callis, D.L.Illman and B.R.Kowalski 'Process Analytical Chemistry' Anal. Chem. 59(1987)624A-637A

[2] Th.J.Harris, J.F.MacGregor and J.D.Wright 'Optimal sensor location with application to a packed bed tubular reactor' AIChE Journal 26(1980)910-916

[3] P.M.E.M.van der Grinten 'Uncertainty in measurement and control' Statistica Neerlandica 22(1968)43-63

[4] C.Didden and J.Duisings 'On-line measurements of a liquid reactor feed with a mass spectrometer' Process Control and Quality 3(1992)263-271

[5] F.W.J.van den Berg,H.F.M.Boelens, H.C.J.Hoefsloot and A.K.Smilde 'Selection of optimal sensor position in a tubular reactor using robust degrees of observability criteria' Chemical Engineering Science 55(2000)827-837

[6] F.W.J.van den Berg, H.C.J.Hoefsloot, H.F.M.Boelens and A.K.Smilde 'Process Analyzer Location and Performance Assessment for Optimal Process Monitoring in a Tubular Reactor' AIChE Journal(2000) accepted for publication

[7] F.W.J.van den Berg, H.C.J.Hoefsloot and A.K.Smilde 'Selection of optimal process analyzers for monitoring' (2001) submitted for publication

[8] H.H.A.Lousberg, H.F.M.Boelens, H.C.J.Hoefsloot, P.Schoenmakers and A.K.Smilde 'Development and validation of a fast size exclusion chromatography method for the at-line determination of the conversion of a polymerization reaction' Journal of Polymer Analysis and Characterization (2001) in press

[9] Th.E.Fortmann and K.L.Hitz 'An Introduction to Linear Control Systems' Dekker New York (1977)

[10] C.D.Johnson 'Optimization of a Certain Quality of Complete Controllability and Observability for Linear Dynamical Systems' Transactions of the ASME 91(1969)228-237

[11] P.C.Müller and H.I.Weber 'Analysis and Optimization of Certain Qualities of Controllability and Observability for Linear Dynamical Systems' Automatica 8(1972)237-246

[12] M.Healey and D.J.Mackinnon (1975) 'A quantitative measure of observability for a linear system' Int. Journal of Control (1975)421-426

[13] M.Morari and G.Stephanopoulos 'Part III: Optimal Selection of Secondary Measurements within the Framework of State Estimation in the Presence of Persistent Unknown Disturbances' AIChE Journal 26(1980)247-259

[14] A.J.Ericsson-Jackson, P.M.Bainum and H.G.Xing 'Actuator/Sensor Placement Using Degree of Controllability and Observability for Digitally Controlled Orbiting Platforms' The Journal of the Astronautical Sciences 45(1997)73-89

[15] D.Dochain, N.Tali-Maanar and J.P.Babary 'On modelling, monitoring and control of fixed bed bioreactors' Computers and Chemical Engineering 21(1997)1255-1266
[16] H.H.Rosenbrock 'State-Space and Multivariable Theory' Nelson London (1970)
[17] S.Skogestadt and I.Postlethwaite 'Multivariable feedback control' Wiley Chichester (1996)
[18] K.Wohlfahrt and G.Emig 'Compare Maleic Anhydride routes. Hydrocarbon Processing' June(1980)83-90
[19] J.F.Ramirez and P.H.Calderbank 'The Oxidation of Benzene in Packed Catalyst Beds' The Chemical Engineering Journal 14(1977)49-58
[20] J.C.Willems and S.K.Mitter 'Controllability, Observability, Pole Allocation and State Reconstruction' IEEE Transactions on Automatic Control 6(1977)582-595
[21] K.Ogata 'State Space Analysis of Control Systems' Prentice Hall EngleWood Cliffs (1967)
[22] A.C.Atkinson and A.N.Donev 'Optimum experimental designs' Oxford Sciences Publications (1992)
[23] G.H.Golub, S.Nash and C.Van Loan 'A Hessenberg-Schur Method for the Problem AX + BX = C' IEEE Transaction on Automatic Control AC-24(1979)909-913
[24] S.Kumar and J.H.Seinfeld 'Optimal Location of Measurements in Tubular Reactors' Chemical Engineering Science 33(1978)1507-1516
[25] S.Kumar and J.H.Seinfeld 'Optimal Location of Measurements for Distributed Parameter Systems' IEEE Transactions on Automatic Control AC-23(1978)690-698
[26] L.C.Windes, A.Cinar and W.H.Ray 'Dynamic Estimation of Temperature and Concentration Profiles in a Packed Bed Reactor' Chemical Engineering Sciences 44(1989)2087-2106
[27] T.K.Yu and J.H.Seinfeld 'Observability and optimal measurement location in linear distributed parameter systems' Int. Journal of Control (1973)785-799
[28] G.Colantuoni and L.Padmanabhan 'Optimal Sensor Locations for Tubular-Flow Reactor Systems' Chemical Engineering Sciences 32(1977)1035-1049
[29] W.H.Chen and J.H.Seinfeld 'Optimal location of process measurements' Int. Journal of Control (1975)1003-1014
[30] S.E.Aidarous, M.R.Gevers and M.J.Installé 'Optimal sensors allocation strategies for a class of stochastic distributed systems' Int. Journal of Control, (1975)197-213

[31] L.Padmanabhan and G.Colantouni 'Sequential estimation in distributed systems' Int. Journal of Control (1974)973-986
[32] M.S.Grewal and A.P.Andrews 'Kalman Filtering, Theory and Practice' Prentice Hall Englewood Cliffs (1993)
[33] A.H.Jazwinski 'Stochastic Process and Filtering Theory' Academic Press San Diego (1970)
[34] J.Workman, D.Veltkamp, S.Doherty, B.Anderson, K.Creasy, M.Koch, J.Tatera, A.Robinson, L.Bond, L.Burgess, G.Bokerman, A.Ullman, G.Darsey, F.Mozayeri, J.Bamberger and M.Stautberg-Greenwood 'Process Analytical Chemistry' Analytical Chemistry 12(1999)121R-180R
[35] J.Alvarez, J.A.Romagnoli and G.Stephanopoulos 'Variable Measurement Structures for the Control of a Tubular Reactor' Chemical Engineering Sciences 36(1981)1695
[36] P.van Overschee and B.de Moor 'Subspace Identification for Linear Systems' Kluwer Academic Publishers Norwell Massachusetts (1996)
[37] P.M.E.M.van der Grinten and J.M.H.Lenoir 'Statistische Procesbeheersing' Spectrum Utrecht The Netherlands (1973)
[38] G.Stephanopoulos 'Chemical Process Control' Prentice Hall Englewood Cliffs (1984)
[39] F.A.Leemans 'Selection of an Optimal Analytical Technique for Process Control' Analytical Chemistry 11(1971)36A
[40] J.E.Rijnsdorp 'The Contribution of Quality Aspects to Process Control' Analytica Chimica Acta 190(1986)33
[41] M.Darouach and M.Zasadzinski 'Data Reconciliation in Generalized Linear Dynamic Systems' AIChE Journal 37(1991)193
[42] A.Gelb 'Applied Optimal Estimation' The M.I.T. Press Cambridge (1974)
[43] A.S.Skoog 'Principles of Instrumental Analysis' Sauders College Publishing Philadelphia (1985)
[44] R.Pallás-Areny and J.G.Webster 'Sensors and Signal Conditioning' Wiley New York (1991)
[45] A.K.Smilde, F.W.J.van den Berg and H.C.J.Hoefsloot 'Theory of Process Analytical Chemistry' submitted for publication (2001)
[46] R.J.Young and P.A.Lovell 'Introduction to Polymers' Chapman & Hall London (1991)
[47] N.A.Dotson, R.Galvan, R.L.Laurence and M.Tirrell 'Polymerization Process Modeling' VCH Publishers New York (1996)

[48] H.H.A.Lousberg, P.J.Hamersma, P.D.Iedema and E.Ruitenberg 'Determination of Kinetic Parameters from Styrene Bulk Polymerization with Continuous and Batch Experiments' submitted for publication (2000)
[49] W.H.Press, S.A.Teukolsky, W.T.Vetterling and B.P.Flannery, 'Numerical recipes in FORTRAN: the art of scientific computing' Cambridge University Press Cambridge (1992)
[50] M.Morari and J.H.Lee 'Model predictive control: past, present and future' Computers and Chemical Engineering 23(1999)667-682
[51] H.Martens and T.Næs 'Multivariate Calibration' Wiley (1989)
[52] K.J.Åström and B.Wittenmark 'Adaptive Control' Addison Wesley (1995)
[53] J.Valappil and Ch.Georgakis 'Systematic Estimation of State Noise Statistics for Extended Kalman Filters' AIChE Journal 46(2000)292-308
[54] R.T.Stefani, C.J.Savant, B.Shahian and G.H.Hostetter 'Design of Feedback Control Systems' Saunders College Publishing (1994)
[55] N.S.Nise 'Control System Engineering' The Benjamin/Cummigs Publishing Company (1995)
[56] I.R.Petersen and A.V.Savkin 'Robust Kalman Filtering for Signals and Systems with Large Uncertainties' Birkhäuser (1999)

Samenvatting

Dit proefschrift handelt over de optimalisatie van selectie en positionering van zogenaamde *procesanalysatoren*. Onder procesanalysatoren verstaan we instrumenten, voor de uitvoering van analytisch chemische metingen, die binnen of dichtbij een productieproces zijn gesitueerd. In dit aspect onderscheiden procesmetingen zich van andere metingen in een productie omgeving, b.v. metingen voor kwaliteitgarantie, welke vaak (met aanzienlijke vertraging) in een centraal laboratorium worden uitgevoerd.
Vanwegen hun grote regelmaat en snelle beschikbaarheid kunnen de analytisch chemische procesmetingen gebruikt worden voor het monitoren en eventueel regelen van het procesverloop. Ze vormen hierin een belangrijke aanvulling op meer conventionele signalen in de meet- en regeltechniek (temperatuur, druk, stroming, enz.). Een aanzienlijk nadeel met betrekking tot procesanalysatoren is de relatief hoge kosten voor aanschaf en onderhoud. Dit laatste aspect maakt het noodzakelijk om de maximale hoeveelheid informatie uit een meetsignaal te halen. Het onderzoek gepresenteerd in dit proefschrift geeft aanwijzingen hoe deze optimalisatie bereikt kan worden.

Figuur 1

De eerste keuze waar een procesanalytisch chemicus (met ondersteuning van een chemisch technicus) voor staat is: welke variabele uit de overweldigende hoeveelheid variabelen gaan we meten (zie Figuur 1)? Welke component, op welke plaats in de fabriek moeten we meten om zoveel mogelijk en zo snel mogelijk informatie over de toestand van het proces te verkrijgen? Het antwoord op deze vragen kan worden gevonden in de *procesdynamica*, en dit is het onderwerp van **hoofdstuk 2**. In dit hoofdstuk worden aan de hand van een

rekenvoorbeeld een aantal *deterministische* selectiecriteria voor het beste meetsignaal en bemonsterlocatie onderzocht.
Naast de procesdynamica zijn ook het type procesverstoring en de karakteristieken van het meetinstrument belangrijk voor selectie van procesanalysatoren en meetlocaties. In **hoofdstuk 3** wordt, wederom aan de hand van een rekenvoorbeeld, een *stochastisch* selectiecriterium ingevoerd: *de meetbaarheidfactor*. Met behulp van deze factor kunnen de prestaties van verschillende instrumenten, op verschillende locaties binnen een proces, kwantitatief worden vergeleken. Voor het berekenen van de meetbaarheidfactor wordt er een abstracte definitie van het meetinstrument geïntroduceerd, de zogenaamde *procesanalysator dynamica*, gebaseerd op vijf contributies: meetnauwkeurigheid, meetfrequentie, bemonsteringstijd, meetsignaal correlatie en analysetijd. De meetbaarheidfactor biedt bijvoorbeeld de mogelijkheid tot bestuderen en vergelijken van verschillende meetconfiguraties in rekenmodellen en computersimulaties voor een nieuw proces, zonder dat metingen daadwerkelijk worden uitgevoerd of een (proef)fabriek is gebouwd.
Om de theorie over procesanalysator selectie en positionering te kunnen verifiëren is een proefopstelling gebouwd. In een laboratoriumschaal buisreactor werd Polystyreen gemaakt uit Styreen, waarbij verschillende spectroscopische meetinstrumenten in en om de reactorbuis konden worden geplaatst. De resultaten voor deze experimenten – beschreven in **hoofdstuk 4** – bevestigen het verband tussen theorie en (laboratorium)praktijk.
Al het werk zoals hiervoor beschreven is toegespitst op continue processen. In het laatste deel – **hoofdstuk 5** – wordt een batchproces bestudeerd, wederom polymerisatie van Styreen. In deze nieuwe situatie luidt de vraag op welk tijdstip in het batchtraject geeft een meeting de meeste informatie. Getoond wordt hoe de theorie omtrent meetbaarheidfactor kan worden benut op zoek naar het antwoord. Verder worden in dit hoofdstuk een aantal aspecten rondom het praktisch gebruik van zogenaamde *toestandschatters* in batchprocessen besproken.

Nawoord

Op deze plaats wil ik graag mijn dank uiten aan mijn (co)promotors Age en Huub voor voldoende inspiratie en speelruimte voor een bevredigend promotieonderzoek. Florian, Renger en Sabina wil ik bedanken voor de *ge*moedelijke werksfeer, Hans voor de vele prettige discussies over bijna evenveel onderwerpen en alle verdere PAC collega's - Ad, Erik, Henk-Jan, Johan, Marlon, Ricard, Steve - voor een buitengewoon aangename tijd.
Verder wil ik mijn dank betuigen aan alle mensen binnen het Instituut voor Technische Scheikunde die gedurende de werkzaamheden aan de Universiteit van Amsterdam mijn pad hebben gekruist.